STATE-DEPENDENT INFORMATION PROCESSING IN THE RAT VIBRISSA PATHWAY

A Dissertation

Presented to

The Academic Faculty

by

He J.V. Zheng

In Partial Fulfillment

of the Requirements for the Degree

Doctor of Philosophy in the

Department of Biomedical Engineering

Georgia Institute of Technology

December 2015

STATE-DEPENDENT INFORMATION PROCESSING IN THE RAT VIBRISSA PATHWAY

Approved by:

Dr. Garrett Stanley, Advisor
Department of Biomedical Engineering
Georgia Institute of Technology
& Emory University

Dr. Dieter Jaeger
Department of Biology
Emory University

Dr. Robert Liu
Department of Biology
Emory University

Dr. Christopher Rozell
Deptartment of Electrical and Computer Engineering
Georgia Institute of Technology

Dr. Anna Roe
Department of Psychology
Vanderbilt University

Date Approved: August 5, 2015

To my parents

ACKNOWLEDGEMENTS

I would like to thank my adviser, Garrett Stanley, for his guidance and patience. I am grateful for all that I have received. I have learned a lot and I am a different person.

Many thanks to the committee members Drs Robert Liu, Dieter Jaeger, Chris Rozell, and Anna Roe for helping me and making time out of busy schedules for this thesis.

I would like to thank all my lab mates for all the help and support. Special thanks to Clarissa Whitmire for giving me an enormous amount of help and support; to Doug Ollerenshaw for the collaboration on the behavior work presented in this thesis and resulted in a joint Neuron publication; to Chris Waiblinger for performing all the awake experiments while I worked on this thesis; to Alex Ortiz for performing many surgeries.

TABLE OF CONTENTS

ACKNOWLEDGEMENTS ..... **IV**

LIST OF FIGURES ..... **VIII**

SUMMARY ..... **X**

CHAPTER 1 INTRODUCTION **1**

1.1 An overview of brain state **1**

1.2 Sensory adaptation and bottom-up modulation on brain state **6**

1.3 Intrinsic brain state and its relationship to sensory evoked response **8**

1.4 Top-down control of brain state **10**

1.5 Experimental approach **11**

1.5.1 The rat vibrissa pathway **11**

1.5.2 Voltage-sensitive imaging **13**

1.5.3 Detectability and discriminability as a model for information processing **14**

1.6 Organization of the thesis **15**

CHAPTER 2 SENSORY ADAPTATION, A BOTTOM-UP MODULATION OF BRAIN STATE **16**

2.1 Introduction **16**

2.2 Methods **19**

2.2.1 Surgery **19**

2.2.2 Staining **20**

2.2.3 Optical imaging **20**

2.2.4 Vibrissa stimulation **21**

2.2.5 Barrel mapping **21**

2.2.6 Data analysis **22**

2.2.7 Ideal observer analysis **22**

2.3 Results **24**

2.3.1 Adaptation spatially constrains the cortical response 24
2.3.2 Adaptation degrades stimulus detectability for an ideal observer 26
2.3.3 Adaptation enhances stimulus discriminability for an ideal observer ... 28
2.3.4 Adaptation degrades stimulus detectability for awake, behaving animals 30
2.3.5 Adaptation improves spatial discriminability in awake, behaving animals 33
2.3.6 Adaptation of the thalamocortical circuit of awake, behaving animals 35
2.4 Discussion 37
CHAPTER 3 SENSORY ADAPTATION ENCOMPASSES A CONTINUUM OF BRAIN STATES 42
3.1 Introduction 43
3.2 Methods 45
3.2.1 Surgery 45
3.2.2 Staining 46
3.2.3 Optical imaging 46
3.2.4 Vibrissa stimulation 46
3.2.5 Data analysis 48
3.2.6 Adaptation intensity 48
3.2.7 Ideal observer analysis 49
3.3 Results 54
3.3.1 Frequency and velocity of adapting stimuli differentially shape cortical response 54
3.3.2 Adaptation degrades detectability of the stimulus 60
3.3.3 Moderate extent of adaptation enhances discriminability of the stimulus 64
3.4 Discussion 71
CHAPTER 4 THE INTRINSIC BRAIN STATES 77
4.1 Introduction 77
4.2 Methods 79
4.2.1 Surgery 79
4.2.2 Electrophysiology 80
4.2.3 Vibrissa stimulation 81

4.2.4 Data analysis 82
4.3 Results 85
4.3.1 Brain state modulates sensory-evoked activity 86
4.3.2 Brain state modulates the information encoded about the stimulus 93
4.4 Discussion 96
CHAPTER 5 CONCLUSION AND FUTURE WORK 101
5.1 Sensory adaptation induces bottom-up modulation on brain state 101
5.2 Information theory and sensory stimulus decoding 103
5.3 The diverse mechanisms regulating the brain state 105
5.4 The interaction of modulating processes 107
5.5 The nature of brain state 108
5.6 Future work 109
REFERENCES 111

LIST OF FIGURES

Figure 1.1 An illustration of two states. ..6

Figure 1.2 Voltage-sensitive dye imaging of the rat barrel cortex *in vivo*. 12

Figure 1.3 A cartoon illustration of the effect of mean and variance on separability of two response distributions. 15

Figure 2.1 Adaptation spatially constrains the cortical response. 25

Figure 2.2 Ideal observer analysis - adaptation degrades detection. 27

Figure 2.3 Ideal observer analysis - adaptation improves spatial discriminability. 29

Figure 2.4 Behavioral detection thresholds are increased with adaptation (*courtesy of DRO*). 31

Figure 2.5 The spatial discrimination performance of the animals is improved with adaptation (*courtesy of DRO*). 34

Figure 2.6 Adaptation of thalamic VPm cells in the awake animal (*courtesy of DRO*).35

Figure 3.1 Cortical responses to separate deflections on two adjacent whiskers. 55

Figure 3.2 Cortical response decreased in both magnitude and area with stronger adapting stimulus energy. 58

Figure 3.3 Detectability of the stimulus was degraded with adaptation. 61

Figure 3.4 Ideal observer analysis of spatial discrimination. 66

Figure 3.5 Discrimination performance peaked at intermediate adaptation intensity. 68

Figure 4.1 Experiment setup. 86

Figure 4.2 The degree of cortical synchrony modulates stimulus-evoked activity. 89

Figure 4.3 The UP/DOWN states modulate stimulus-evoked activity. 93

Figure 4.4 The detectability and discriminability of the stimulus are state-dependent. 94

LIST OF SYMBOLS AND ABBREVIATIONS

LFP	Local field potential
LRT	The likelihood ratio test
ROC	Receiver operating characteristic
S1	The primary somatosensory cortex
TC	Thalamocortical
vM1	The vibrissal portion of primary motor cortex
VPm	The ventral posteromedial nucleus of the thalamus
VSD	Voltage-sensitive dye

SUMMARY

To navigate the world, we must efficiently extract relevant information from complex sensory inputs to form perceptions and make decisions on a moment-to-moment basis. The efficient encoding of sensory information necessarily relies on the ability of the pathway to dynamically interpret the sensory input according to the context under which external stimuli are processed. Internally, this context is represented by the state of the brain, which can be modulated by bottom-up processes such as sensory adaptation, intrinsic mechanisms such as neuromodulators, and top-down processes such as arousal.

This thesis examines the modulation of brain state induced via bottom-up sensory adaptation and the intrinsic brain states, the relationship between brain state and sensory-evoked activity, and the potential implications of brain state modulation for the perception of the stimulus.

Using voltage-sensitive dye imaging in anesthetized rats and the paradigm of detection / spatial discrimination task by the ideal observer, I quantified, in the adapted state, how the cortical response to a stimulus in the vibrissa pathway was shaped and how the information for detecting and spatially discriminating the stimulus was differentially optimized. Cortical activation and detection / discrimination tradeoff were quantified in relation to the degree of adaptation, which was modulated continuously by the frequency and velocity of the adapting stimulus. Finally, I investigated the intrinsic brain states

reflected in the spontaneous cortical activity and how it modulated sensory evoked response.

This thesis investigates the regulation of brain state via bottom-up sensory adaptation and intrinsic mechanisms, providing a glimpse into a high-dimensional continuum of cortical dynamics.

CHAPTER 1 INTRODUCTION

1.1 An overview of brain state

A fundamental pursuit of neuroscience is to understand how external stimuli are encoded in the brain and how the information about the stimuli is extracted to form sensory perception. An interesting and challenging aspect of this problem is that the brain is not simply a machine that transforms an input stimulus to an output. One piece of evidence for the highly dynamical nature of the brain is the high trial-to-trial variability of response to the same stimulus under well-controlled experimental conditions in the primary sensory cortex, relative to the lower response variability in earlier stages of the pathway (Adams et al., 1997; Arabzadeh et al., 2005; Lottem and Azouz, 2011; Scholvinck et al., 2015). This cortical variability arises, at least partially, from the internal state of the brain, which encompasses a variety of properties of the neural system that affect multiple aspects of sensory encoding. Brain state can refer to spontaneous spiking and membrane potential fluctuations in individual cells, synaptic plasticity, network dynamics such as the excitation-inhibition balance, and the correlation and synchrony among a subset of cells (Buonomano and Maass, 2009; Harris and Thiele, 2011). Brain state provides the context under which the stimulus is encoded, and determines what information about the stimulus is being conveyed, which ultimately influences the animal's perception and behavior.

Given the wide-spread effects and diverse properties of brain state, it is likely a high-dimensional space where multiple mechanisms can be dynamically combined and fine-tuned depending on the task of the sensory system, posing an extremely complicated and challenging problem for neuroscientists. Nonetheless, the state of the brain is at least partially reflected in the spontaneous activity. Studies of spontaneous oscillations have

been fruitful and provided a glimpse into the brain state space. The mammalian cortex exhibits a wide range of frequency oscillations, ranging from 0.05 to 500 Hz, and the power of EEG or local field potential (LFP) linearly decreases with frequency on a logarithmic scale (Buzsaki and Draguhn, 2004; Freeman et al., 2000). These bands of oscillations have been shown to be associated with specific brain states and can either compete or interact with each other, locally or globally (Buzsaki and Draguhn, 2004; Csicsvari et al., 2003; Engel et al., 2001; Klimesch, 1999; Kopell et al., 1999; Steriade, 2001). For example, delta (0-4 Hz), alpha (8-12 Hz), and beta (13-25 Hz) waves in the EEG are observed in different stages and depths of sleep and general anesthesia (Brown et al., 2010). Alpha and theta rhythms are implicated in cognitive and memory performance (Klimesch, 1999). Gamma rhythm (30-80 Hz) has been an intense subject of research in recent studies. Although the mechanism of Gamma has been proposed and that it is generally thought to be most prominent during alertness and attention (McCormick et al., 2015; Kopell et al., 1999; Börgers et al., 2008), the relationship between Gamma and cortical state is still debated. For example, gamma increases in rodents during active behavior (Harris and Thiele, 2011; Niell and Stryker, 2010), but selective attention can either decrease or increase Gamma power in primates (Chalk et al., 2010; Fries et al., 2001; Harris and Thiele, 2011; Khayat et al., 2010).

Particularly well studied brain states are the “synchronized” and “de-synchronized” states. It was discovered that during slow wave sleep, the EEG displays characteristic low frequency, high amplitude oscillations, while alert wakefulness displays high frequency, low amplitude EEG (Moruzzi and Magoun, 1949; Steriade et al., 1993). These two states, respectively termed “synchronized” and “de-synchronized” states, represent the extreme ends of the arousal spectrum. Following these early studies, much effort has been poured into this area and started to paint a broadly consistent picture where these two states are shown to be indicative of cortical dynamics and behavioral states. Specifically, the de-

synchronized state is signified by cortical de-synchronization (Curto et al., 2009; Hirata and Castro-Alamancos, 2010; Poulet and Petersen, 2008), high-frequency, small-amplitude fluctuations in the cortical EEG or LFP, associated with thalamic depolarization and tonic firing (Castro-Alamancos and Oldford, 2002; Hirata and Castro-Alamancos, 2010; Poulet et al., 2012), thalamocortical synaptic depression (Castro-Alamancos and Oldford, 2002), suppressed cortical representation of an external stimulus (Castro-Alamancos, 2002; Poulet et al., 2012; Otazu et al., 2009), and active behavior such as arousal and active whisking in rodents (Castro-Alamancos, 2004; Crochet and Petersen, 2006; Poulet et al., 2012). In contrast, in the synchronized state, the low frequency, high amplitude cortical oscillations are associated with thalamic hyperpolarization, cortical synchronization, stronger cortical response to the stimulus in terms of the amplitude of field potential (Castro-Alamancos, 2002) and single cell membrane potential (Crochet and Petersen, 2006), and quiescent behavior or lack of arousal (Castro-Alamancos, 2004; Crochet and Petersen, 2006; Poulet et al., 2012). Figure 1.1 illustrates these states. Studies have also independently shown the suppression of cortical activity to a stimulus when the animal is alert or actively sensing (Fanselow and Nicolelis, 1999; Otazu et al., 2009) or when the thalamus is firing tonically (Crick, 1984; Sherman, 2001a; Swadlow and Gusev, 2001).

Many mechanisms have been shown to be able to influence the brain state. They can be broadly classified into intrinsic, bottom-up or top-down mechanisms. Under anesthesia, the cortex is mostly under the synchronized state, but can show spontaneous de-synchronized states (Clement et al., 2008; Curto et al., 2009). During sleep, intrinsic neuromodulatory mechanisms switch the brain from slow-wave sleep with low-frequency, synchronized EEG to REM sleep with high-frequency, de-synchronized EEG (Brown et al., 2010). Neuromodulators, particularly acetylcholine from the brainstem *laterodorsal tegmentum* (reticular formation) (Castro-Alamancos and Gulati, 2014;

Castro-Alamancos and Oldford, 2002; Steriade et al., 1990; Williams et al., 1994) and norepinephrine (Constantinople and Bruno, 2011) can produce a de-synchronized state and facilitate wakefulness. Bottom-up drive from external stimuli can also induce state change (Ferezou et al., 2007; Hasenstaub et al., 2007), and sensory adaptation can substantially change the thalamic synchrony and the cortical encoding of a stimulus (Temereanca et al., 2008; Wang et al., 2010). Tonic glutamatergic drive from the thalamus has been shown to be sufficient to de-synchronize the cortex (Harris and Thiele, 2011; Hirata and Castro-Alamancos, 2010). Top-down influences like active whisking behavior, arousal, and corticocortical input (such as vM1 activation) can all produce de-synchronized state and suppressed cortical response (Fanselow and Nicolelis, 1999; Otazu et al., 2009; Poulet et al., 2012; Zagha et al., 2013). More complex cognitive functions like attention have been shown to enhance cortical correlation (Kohn et al., 2009) and may increase or decrease high-frequency gamma oscillation, depending on the cortical area and the type of task (Chalk et al., 2010; Fries et al., 2001; Harris and Thiele, 2011; Khayat et al., 2010).

Even though there is an emergence from the literature that the two seemingly bimodal synchronized and de-synchronized states of the cortex encompass a set of broadly consistent cortical dynamics and behavior (see Figure 1.1), it is important to note that there is a growing body of evidence that the brain state is likely a high dimensional continuum, not discrete states that can be fully captured by the frequency of spontaneous activity (Harris and Thiele, 2011). The synchronized and de-synchronized states were originally thought to exist only in sleep and wakefulness, respectively. However, more recent studies have shown the slow frequency EEG or LFP or synchronized cortical activity in quiet wakefulness, suggesting a continuum of arousal states (Castro-Alamancos, 2004; Crochet and Petersen, 2006; Ferezou et al., 2007; Greenberg et al., 2008; Harris and Thiele, 2011; Poulet and Petersen, 2008; Zagha and McCormick, 2014;

Zagha et al., 2013). Further evidence points to more dynamic effects and mechanisms of brain state. As mentioned above, although attention decreases low-frequency content, it could either increase or decrease gamma power, and could enhance or reduce correlation and synchrony (Cohen and Maunsell, 2009; Kohn et al., 2009), depending on the cortical area and the task (Chalk et al., 2010; Fries et al., 2001; Harris and Thiele, 2011; Khayat et al., 2010). Stimulation of dorsal Raphe nuclei in rats decreases both low frequency and gamma power (Puig et al., 2010). The activities of different classes of interneurons have been shown to depend on the behavioral correlates of the desynchronized state (Harris and Thiele, 2011). For example, in desynchronized states corresponding to locomotion (Niell and Stryker, 2010), difficult discrimination tasks (Chen et al., 2008), or increased thalamic drive, fast-spiking neurons increase their firing rate (Hirata and Castro-Alamancos, 2010); but the opposite effect ensues in actively whisking rodents, where fast-spiking neurons decrease firing rate and non-fast spiking neurons increase their rate (Gentet et al., 2010). These results suggest that although there are common effects and mechanisms in brain states broadly classified using its frequency content, the cortical properties can be dynamically combined and tuned depending on the specific behavior and cognitive function.

In a broader view, the effect of state modulation can be local or global. Attention has been shown to reduce the low frequency LFP at a local level. In general, slow oscillations tend to affect a larger network, often in travelling waves across the cortex, possibly facilitating the integration of information across multiple cortical areas (Buzsaki and Draguhn, 2004; Csicsvari et al., 2003; Ferezou et al., 2006, 2007; Harris and Thiele, 2011; Luczak et al., 2007; Petersen et al., 2003b; Steriade, 2001). Brain state also exists in and regulates other areas outside of the neocortex. Theta rhythm in the hippocampus (different from theta rhythm in the neocortex) for instance, is associated with mobile and exploratory behaviors in rodents (Vanderwolf, 1969). Taken together, the brain state is

likely a multidimensional continuum where multiple cortical, thalamic/sub-cortical, and neuromodulatory mechanisms interact dynamically and provide the context for the encoding of external stimuli.

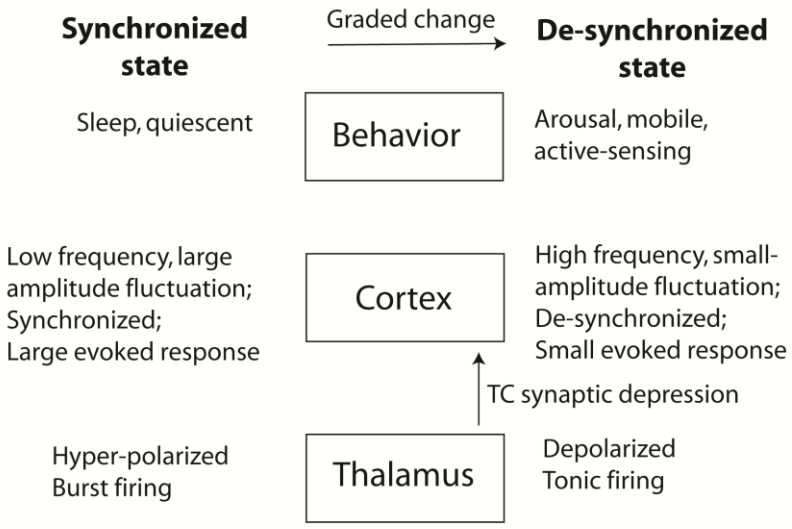

Figure 1.1 An illustration of two states.
The de-synchronized state is characterized by fast but small cortical fluctuations, accompanied by thalamic tonic firing, suppressed cortical response to external stimuli, and typically associated with alertness and active behavior such as active whisking. In contrast, the synchronized state is characterized by slow but large cortical fluctuations, associated with thalamic burst firing, relatively strong cortical response to external stimuli, and typically associated with quiescence or sleep. However, these two states signify the two extremes of the brain state spectrum, which is likely a continuum.

1.2 Sensory adaptation and bottom-up modulation on brain state

One major form of brain state modulation through bottom-up input is rapid sensory adaptation. Our sensory systems are constantly inundated with a flood of stimuli every waking hour, yet we efficiently extract relevant information to form perceptions and make decisions. The efficient encoding of sensory information necessarily relies on the ability of the pathway to dynamically shift its operating regime. When presented with repetitive and persistent stimuli, neurons, particularly cortical neurons, decrease their

firing rate on the time scale of hundreds of milliseconds (Webber and Stanley, 2006). This cross-modal and ubiquitous property, known as rapid sensory adaptation, is not simply the fatigue of the system, but rather induces a state with significant changes in neurophysiology, behavior, and stimulus encoding.

Adaptation has been shown to fundamentally change the encoding of the stimulus and the information conveyed (Ahissar et al., 2000; Chung et al., 2002; Clifford et al., 2007; Ego-Stengel et al., 2005; Fairhall et al., 2001; Higley and Contreras, 2006; Khatri et al., 2009; Maravall et al., 2007; Wang et al., 2010). In particular, adaptation switches the pathway from conveying information for detecting novel features in the environment, to conveying information for discerning fine details (Lesica and Stanley, 2004; Moore, 2004; Wang et al., 2010), reminiscent of the "searchlight hypothesis" where detection mode was proposed for a state with thalamic bursting and a discrimination mode was speculated for a state with thalamic tonic firing (Crick, 1984; Sherman, 2001ab; Swadlow and Gusev, 2001). In rodent somatosensation, it has also been speculated that the repetitive stimulation of the whisker (i.e. sensory adaptation) may resemble the function of active whisking and thus primes the cortex for stimulus discrimination, while a still whisker in a quiescent state without sensory adaptation may be primed for detecting a stimulus (Moore, 2004).

Specific to spatial discrimination in somatosensation, human psychophysical studies have shown that adaptation heightens spatial acuity in tactile discrimination tasks (Goble and Hollins, 1993; Tannan et al., 2006; Vierck and Jones, 1970). Electrophysiological studies qualitatively show a spatially constrained cortical representation of repetitive stimuli in addition to suppressed magnitude in cortical response. This spatial constraint has been proposed as a potential mechanism for enhanced acuity (von Békésy, 1967; Lee and Whitsel, 1992; Moore, 2004; Moore et al., 1999; Sheth et al., 1998). However, animals

form perceptions and make decisions on a moment-to-moment basis. As previously mentioned, the cortical response to the same stimulus is variable. Adaptation has also been shown to change the trial-to-trial covariability (noise correlation) in cortical activity (Adibi et al., 2013). Thus, the trial-averaged representation shown in these studies is not sufficient to convey the information about the stimulus relevant to real-time behavior (Averbeck et al., 2006). Furthermore, given that the brain state exhibits a multitude of mechanisms and effects, it is insufficient to infer the perceptual consequence of a stimulus simply based on the average size of cortical response. In Chapters 2 and 3, I examine the variability and correlation change following adaptation and explicitly test on single-trial basis, the hypothesis of detection and *spatial* discrimination trade-off during sensory adaptation.

1.3 Intrinsic brain state and its relationship to sensory evoked response

The relationship between spontaneous activity and sensory-evoked response in the cortex is complex and dynamic. Interpreting the stimulus under the context of the spontaneous activity has generally been predictive of the sensory evoked response. For example, pre-stimulus activity has been shown to interact negatively with tasked-evoked activity in human fMRI (He, 2013); the spontaneous activity measured with VSD can at least partially explain the variability in the evoked response (Arieli et al., 1996); baseline fMRI activity has been shown to predict somatosensory perception in humans (Boly et al., 2007); the frequency content and synchrony in the spontaneous activity can predict sensory evoked response in anesthetized rats (Curto et al., 2009).

In particular regard to the synchronized and de-synchronized cortical states, it has been proposed that in the synchronized state, cortical cells alternate between depolarization termed UP state, and hyperpolarization (or silence) termed DOWN state. In the DOWN

state, an excitatory input engages a recurrent network and transitions the cortex into UP state. The occurrence of UP states could be stochastic (or at least the mechanisms for the timing of UP state is not yet clear) because the transition into UP states is triggered by an excitatory volley that can occur spontaneously (McCormick et al., 2015). Over time, refractory mechanisms build up and eventually the network is unable to maintain activity and falls silent (McCormick et al., 2015). During DOWN state, a sensory stimulus evokes a larger cortical response than in UP state (Li et al., 2009; Petersen et al., 2003b). Therefore, in addition to the frequency of the spontaneous activity, the sensory evoked response also depends on the phase of spontaneous activity.

Under anesthesia, the cortex is largely in the synchronized state, but can spontaneously transition into the de-synchronized state (Clement et al., 2008; Curto et al., 2009). Along with increased thalamic tonic firing, neuromodulators are another major influence on brain state. Acetylcholine (ACh) from the brainstem *laterodorsal tegmentum* (reticular formation) (Castro-Alamancos and Oldford, 2002; Steriade et al., 1990; Williams et al., 1994) and norepinephrine (Constantinople and Bruno, 2011) facilitate wakefulness and can thus produce the de-synchronized state. Multiple neuromodulatory systems and metabotropic glutamate receptors are thought to suppress low frequency fluctuations by promoting tonic firing in pyramidal cells, reducing intracortical recurrent excitatory synaptic strength, and depolarizing layer 5 pyramidal cells, which are currently thought to be the origin of the fluctuations (Harris and Thiele, 2011). These mechanisms help suppress the bursts and recurrent excitation that leads to fluctuation of UP and DOWN states in the synchronized state (Harris and Thiele, 2011).

In chapter 4, under controlled anesthesia and without behavioral influences, I examine the intrinsic brain states and the sensory evoked response under these states in the primary sensory cortex.

1.4 Top-down control of brain state

A final major category of influence on brain state is top-down modulation from behavior, cognitive functions, or inputs from other cortical areas, natural or artificial. A prominent behavioral influence is the level of arousal, which was indicated in the early discovery of EEGs in sleep and wakefulness (Steriade et al., 1993). Since then, the frequency change with arousal has been shown on a finer gradient and a broader spectrum. Beyond wakefulness, high-frequency, low-amplitude EEG or LFP and cortical desynchronization are present in active behavior, such as walking and exploring, and in alert or attentive animals; and low-frequency, high-amplitude fluctuations in EEG or LFP are also present in quiescent and immobile animals, even when they are awake (Castro-Alamancos, 2004; Crochet and Petersen, 2006; Poulet and Petersen, 2008).

Particularly in rodents, active whisking has been shown to place the cortex into a de-synchronized state, and has been hypothesized to be a mode of active sensing that enhances tactile discrimination (Moore, 2004). During active whisking, the EEG or LFP displays high frequency fluctuations and the cortical response to an external stimulus is suppressed (Crochet and Petersen, 2006; Fanselow and Nicolelis, 1999; Poulet and Petersen, 2008; Poulet et al., 2012). Although whisking and sensory adaptation share commonalities, particularly cortical suppression and enhancement in tactile discrimination, whisking has exclusively top-down and internal mechanisms because the effect of whisking on brain state persists after the severing of afferent nerves (Fee et al., 1997; Hentschke et al., 2006; Poulet et al., 2012). Furthermore, stimulation of primary motor cortex area related to whiskers (vM1) can also induce de-synchronized state in S1 (Zagha et al., 2013). The mechanisms generating active whisking are still highly debated and clearly bear differences from passive rhythmic whisker movements such as those

during sensory adaptation. It is nonetheless possible that the downstream neurophysiological effects of active and passive whisker movements could converge, producing the same cortical representation of the stimulus, although the differences in the perception of the stimulus and possible awareness of the brain state modulated by different mechanisms remain to be investigated.

1.5 Experimental approach

To explore the effect of sensory adaptation on the detectability and the spatial discriminability of the stimulus, I employ voltage-sensitive dye (VSD) imaging in the anesthetized rat vibrissa pathway and rely on information theory to quantify the detectability and discriminability of a stimulus.

1.5.1 The rat vibrissa pathway

Akin to humans sensing the physical environment using our fingers, rodents use their whiskers, or facial vibrissae, to survey their surroundings. In the laboratory environment, rats have demonstrated the ability to perform a wide variety of tactile tasks, such as object location, texture discrimination, and aperture assessment (Arabzadeh et al., 2004; Carvell and Simons, 1990; von Heimendahl et al., 2007; Krupa et al., 2001; Petersen et al., 2001; Ritt et al., 2008; Wolfe et al., 2008). Accompanying this rich repertoire of behavioral tasks is the discrete nature the vibrissa pathway, making the rat an extraordinary model for somatosensory processing. There are columns of neurons (barrels) in the primary somatosensory cortex (S1) whose topography matches that of the whiskers on the face such that each whisker deflection evokes the strongest response in its corresponding barrel, termed the primary barrel (Woolsey and Van der Loos, 1970). Figure 1.2A illustrates this sensory system.

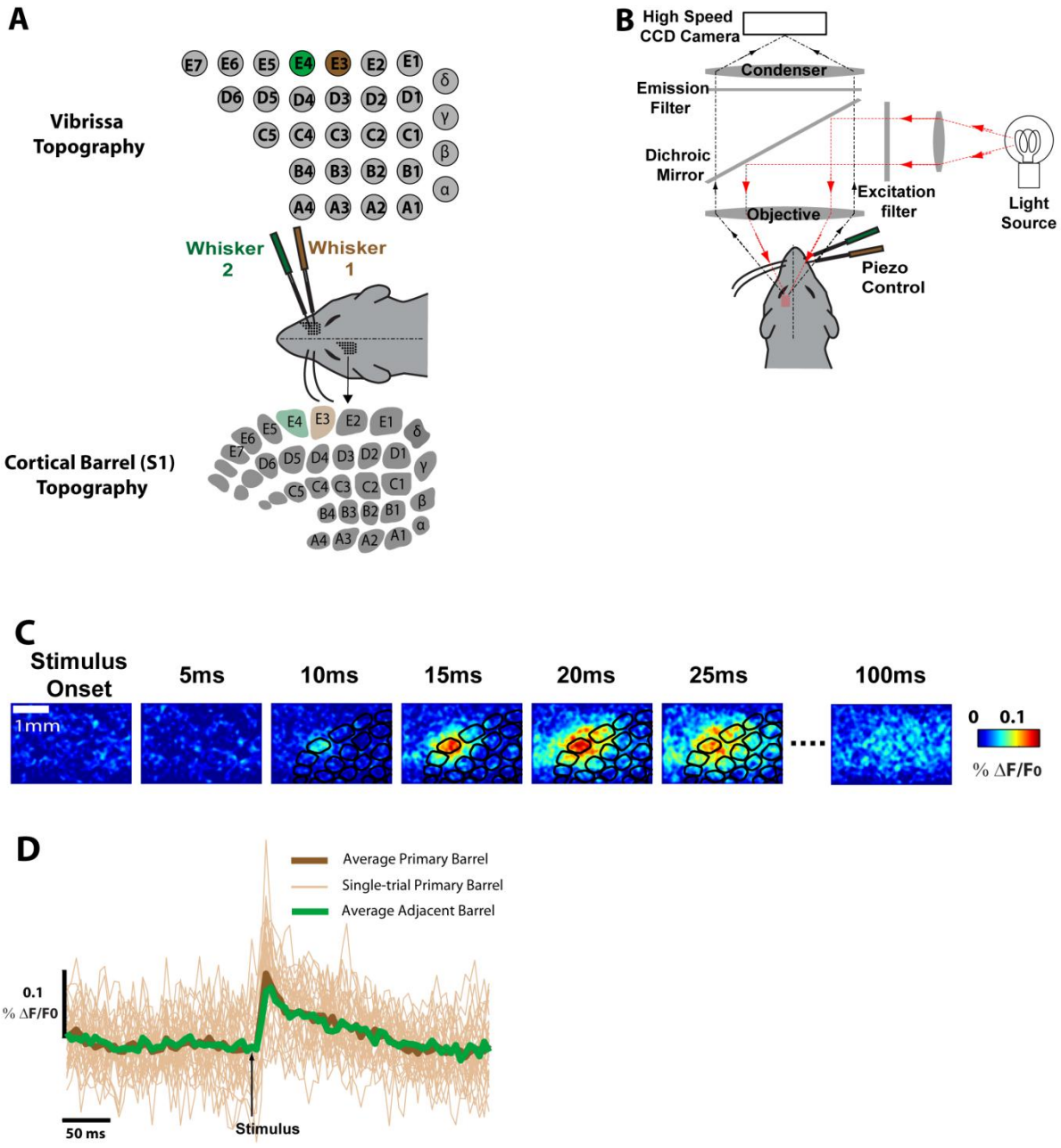

Figure 1.2 Voltage-sensitive dye imaging of the rat barrel cortex *in vivo*.
A. The rat vibrissa pathway is a well-suited model for somatosensory processing, as the primary cortical columns (barrels) are topographically mapped to the whiskers on the snout. Each whisker deflection evokes the strongest response in its corresponding barrel (primary barrel).
B. In the anesthetized rat, computer-controlled piezoelectric actuators stimulated the whiskers while the VSD camera system simultaneously collected the fluorescence signal from layer 2/3 of the primary somatosensory cortex.

C. An example response to a single punctate whisker deflection of 1200 °/s on whisker E3, averaged over 30 trials. Top of image corresponds to the medial side of the animal or row E; right side of the image corresponds to the posterior of the animal or arc 1. Upon the onset of the response at approximately 10 ms post-stimulus, the VSD (RH1691 dye) signal was constrained in the primary barrel-related column, but quickly spread to adjacent columns, and peaked at approximately 20 - 25 ms. An outline of the barrel map functionally registered using the responses to different whisker deflections was overlaid on the VSD images.
D. The corresponding time course for the response (average fluorescence in the cortical columns) shown in C. The adjacent barrel-related column was the E4 column.

1.5.2 Voltage-sensitive imaging

Electrophysiology as one of the oldest techniques of recording neural activity has provided us with a great deal of knowledge about the brain. However, an electrode can only sample a single cell, or the aggregate activity of local ensembles of cells at best. Even the modern multi-electrode arrays such as the Utah array have limitations on spatial resolution (Warren et al., 2001).

Voltage-sensitive imaging brings us closer to the goal of high-resolution population recording. Voltage-sensitive dye (VSD) is a molecule that binds to the membrane of the neuron, and changes its fluorescence proportionally to the change in membrane potential (Grinvald and Hildesheim, 2004). With wide-field imaging, VSD reports subthreshold population activity at both high spatial and temporal resolution. The voltage-sensitive dye used in this thesis, RH1691 dye molecule reports subthreshold activity at a temporal resolution of 5 ms and a spatial resolution of 19 um. RH1691 has been specifically engineered to have its excitation wavelength removed from the peak absorption of hemoglobin, making it much less susceptible to hemodynamics artifacts for *in vivo* studies (Shoham et al., 1999). Figure 1.2B illustrates the experimental set up.

Figure 1.2C shows an example of VSD imaging in barrel cortex. The signal first emerges at approximately 10 ms after stimulus onset, consistent with the latency in the pathway (Diamond and Arabzadeh, 2012; Petersen, 2007), then quickly spreads into adjacent columns. The approximate map of cortical columns was functionally registered onto the image as previously described (Wang et al., 2012) (see Methods, Chapter 2). The stimulus in this example was a punctate deflection of 1200 °/s in the rostral-caudal plane (exponential rise and decay). Figure 1.2D shows the corresponding time courses of the single trials and the averaged trial of the response in Figure 1.2C. The fluorescence was averaged within the primary and adjacent barrels.

1.5.3 Detectability and discriminability as a model for information processing

As the animal forms perception from a moment-to-moment basis, it is imperative to quantify the information carried about the stimulus on a trial-to-trial basis. As a model for behaviorally relevant information carried about the stimulus, detectability and the discriminability of the stimulus were quantified using detection theory (Macmillan and Creelman, 2004). Detectability is essentially the separability of the response distribution from the noise distribution. Discriminability is the separability of two response distributions to their respective stimulus. In general, the distance between the two distributions is determined by the distance between their means, their overall variance, and, in multi-dimension cases, their covariance. It can be equivalently quantified using multiple techniques, most commonly used are the discriminability index d', likelihood ratio test (LRT), and receiver operating characteristic (ROC) curve. Figure 1.3 illustrates the effect of mean and variance on the separability of two distributions in a simple one-dimensional response distribution case.

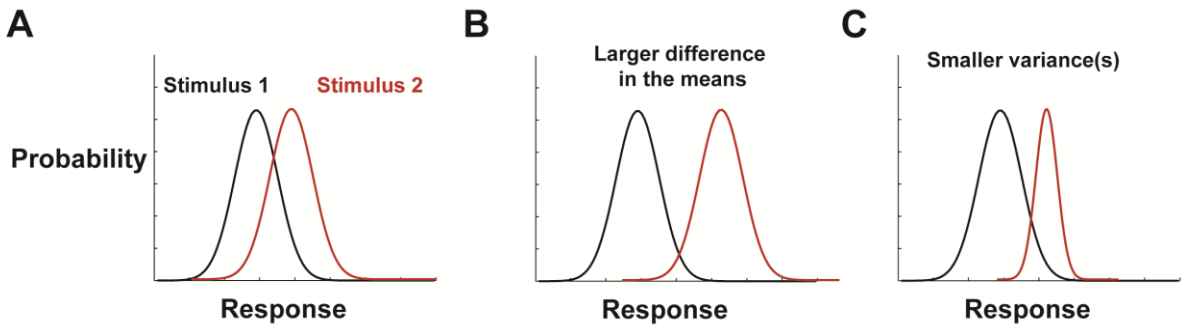

Figure 1.3 A cartoon illustration of the effect of mean and variance on separability of two response distributions.
A. Cartoon illustration of the probability density function of the response to two different stimuli.
B. An increase in the difference in the means of the distributions further separates the distributions.
C. A decrease in the variance of the distribution can also decrease the overlap between the two distributions.

1.6 Organization of the thesis

This thesis examines, under different dynamic states of the primary sensory cortex, how a stimulus is differentially encoded. Chapter 2 examines how sensory adaptation improves spatial discriminability at the expense of detectability on single trial basis. Chapter 3 explores the continuum of brain states modulated through the parameters of adaptation. Chapter 4 examines the information about internal brain state carried by the spontaneous activity and its relationship with sensory-evoked activity. Chapter 5 discusses the findings in relation to the brain state literature and future directions.

CHAPTER 2 Sensory adaptation, a bottom-up modulation of brain state

A modified version of this chapter was published as a research article:

Ollerenshaw, D. R., **Zheng, H. J. (co-first author),** Millard, D. C., Wang, Q., & Stanley, G. B. (2014). The Adaptive Trade-Off between Detection and Discrimination in Cortical Representations and Behavior. *Neuron*, *81*(5), 1152-1164.

Portions of this work were presented in poster form at the following:

Zheng, H. J. V., Wang, Q., Ollerenshaw, D. R., Millard, D. C., & Stanley, G. B. Adaptation Improves Spatial Localization of Stimuli in Rat Primary Somatosensory Cortex.

COSYNE meeting, Salt Lake City, UT, 2012.

SfN meeting, Washington D.C., 2011.

The work presented in this chapter was completed jointly with Douglas R. Ollerenshaw. Figures and text that represent behavior work completed by DRO are attributed below.

2.1 Introduction

A key process that modulates the state of the brain through bottom-up input is sensory adaptation. When facing repetitive and persistent stimuli, neurons, particularly cortical neurons decrease their firing rate on the time scale of hundreds of milliseconds. This cross-modal and ubiquitous property, known as rapid sensory adaptation, has long been known to shape the nature of information flow in sensory pathways, leading to changes in the perception of the stimulus (Ahissar et al., 2000; Chung et al., 2002; Fairhall et al., 2001; Higley and Contreras, 2006; Khatri et al., 2009; Maravall et al., 2007; Goble and

Hollins, 1993; Tannan et al., 2006; Vierck and Jones, 1970). Importantly, sensory adaptation has been shown to share common effects with the active brain states signified by high-frequency, small-amplitude spontaneous cortical fluctuation, such as active whisking and alertness. Both adapted state and active state are linked to thalamocortical (TC) synaptic depression and suppressed cortical representation of an external stimulus (Castro-Alamancos, 2004; Castro-Alamancos and Oldford, 2002; Chung et al., 2002; Poulet and Petersen, 2008; Poulet et al., 2012). Separately, in studies without the measurement of cortical fluctuation frequency, whisking or task-engaged animals also exhibit cortical suppression (Fanselow et al., 2001; Otazu et al., 2009). While active whisking is thought to improve tactile sensation (Kleinfeld et al., 2006; Moore, 2004), a number of studies suggest complex and important changes in coding properties in response to sensory adaptation that serve to improve information transmission in the face of complex inputs (Barlow, 1961; Clifford et al., 2007; Fairhall et al., 2001; Maravall et al., 2007; Moore, 2004; Moore et al., 1999; Sclar et al., 1989). This chapter examines the change in brain state following sensory adaptation, in terms of the cortical representation of an external stimulus, the modulation of thalamic activity, the information conveyed about the stimulus from the perspective of an ideal observer of the anesthetized cortex, and perceptual consequences in awake and behaving animals.

Thalamic activity has been shown to play a major role in modulating the cortical state. High-frequency fluctuations and desynchronization in the cortex, often associated with active behavior such as whisking, are linked to the depolarization and tonic firing of the thalamus (Castro-Alamancos, 2002; Harris and Thiele, 2011; Hirata and Castro-Alamancos, 2010; Poulet et al., 2012). In the visual pathway, it has been hypothesized that the thalamus serves to gate information flow, switching between bursting and tonic firing dynamics that would facilitate detection of transient visual inputs at the level of cortex and those that would enable transmission of details of the visual input required for

discrimination (Crick, 1984; Sherman, 2001a). In the specific context of the rodent vibrissa system, Moore (2004) hypothesized a trade-off between detection and discrimination mediated by the frequency content of tactile input. Relatedly, adaptation has been shown to be accompanied by thalamic desynchronization (Temereanca et al., 2008; Wang et al., 2010), and thalamic tonic firing (Whitmire et al., submitted).

In the context of spatial discriminability, perceptual studies in humans have demonstrated that sensory adaptation can lead to improved discriminability of tactile stimuli applied to the skin (Goble and Hollins, 1993; Tannan et al., 2006; Vierck and Jones, 1970). Separately, a number of studies have investigated the spatial sharpening of cortical representations in somatosensory cortex in response to repetitive, ongoing sensory stimulation (Kleinfeld and Delaney, 1996; Lee and Whitsel, 1992; Moore et al., 1999; Sheth et al., 1998; Simons et al., 2005; Tommerdahl et al., 2002), posited as a potential mechanism for enhanced spatial acuity (Lee and Whitsel, 1992; Moore et al., 1999; Vierck and Jones, 1970). The reductions in overall cortical activation, coupled with spatial sharpening of the cortical response, suggest a similar sensory trade-off: detectability, or maximum sensitivity to unexpected tactile inputs, can theoretically be sacrificed after adaptation to a stimulus in return for improved ability to discriminate the spatial location of the stimulus (Moore, 2004; Moore et al., 1999). To what extent these trade-offs exist behaviorally or electrophysiologically, however, is not clear, and the precise relationship between psychophysical findings and the underlying mechanisms responsible for these observations is unknown.

Here, we utilized the rodent vibrissa pathway to directly test the adaptive trade-off between detection and discrimination in behavior to quantify the relevant information content in cortical representations that may underlie the behavior and to evaluate the adaptive effects on the thalamic inputs as a potential mechanism. Using voltage-sensitive

dye (VSD) imaging of the cortex in anesthetized rats, we found that the reduction in the magnitude and sharpening of the cortical response resulted in enhanced spatial discriminability at the expense of detectability for an ideal observer of cortical activation. In a parallel set of behavioral experiments, rats were trained in vibrissa-based detection and spatial discrimination tasks, in which adaptation led to enhanced discrimination performance at the expense of stimulus detectability. Recordings in the ventroposterior medial (VPm) nucleus of the thalamus of awake animals further revealed a reduction in spike count and timing precision with adaptation. Together, these results provide direct evidence for the change in cortical dynamics and perception modulated through bottom-up sensory adaptation, and that the underlying adaptive regulation of thalamic input may play an important mechanistic role.

2.2 Methods

2.2.1 Surgery

All procedures were approved by Institutional Animal Care & Use Committee at Georgia Institute of Technology and in agreement with the National Institutes of Health guidelines. Nine female albino rats (Sprague-Dawley; 250-330g) were sedated with 4% vaporized isoflurane, then anesthetized with pentobarbital sodium (50 mg/kg i.p., initial dose). Supplemental doses were administered as needed to maintain a surgical level of anesthesia, confirmed by monitoring heart rate, respiration and eyelid/pedal reflexes to adverse stimuli (toe or tail pinch). Following the initial sodium pentobarbital dose, the animal was mounted on a stereotaxic device (Kopf Instruments, Tujunga, CA) on a vibration isolation table. Atropine (0.09 mg/kg, s.c.) was administered subcutaneously to keep the lungs clear of fluid. Lidocaine was injected subcutaneously into the scalp before the initial incision on the head. In all experiments, saline was administered (2 mL/kg/hour) to prevent dehydration. Body temperature was maintained at 37°C by a

servo-controlled heating blanket (FHC, Bowdoinham, ME). After the midline incision on the head, skin and tissue were resected and connective tissue was removed. A craniotomy (approximately 3 mm x 4 mm) was drilled on the left hemisphere over the primary sensory cortex (stereotaxic coordinates: 0-4 mm caudal to the bregma, and 4-7 mm lateral to the midline; Paxinos and Watson, 2007). The dura was left intact. A dental acrylic dam was constructed around the craniotomy. At the end of the surgical procedures, a light level of anesthesia was maintained with pentobarbital sodium. The animal was euthanized with an overdose of pentobarbital sodium solution after VSD imaging.

2.2.2 Staining

The dura was cleaned using a gentle flow of saline (0.9%), then dried with a gentle air blow for about 10-15 minutes or until it appeared "glassy" (Lippert et al., 2007). Voltage sensitive dye (VSD RH1691, Optical Imaging) was diluted in saline to approximately 1.5 mg/mL. The dye solution (~200 µL) was carefully placed into the dam using a micro-pipette. The craniotomy was covered to prevent the dye from photo-bleaching. The dye solution in the dam was circulated and replenished with fresh dye solution every 5-10 minutes (Lippert et al., 2007). After approximately 2 hours of staining, the unbound dye was washed out with saline. Saline was applied to the brain surface after washing. Imaging was performed through saline on the brain surface. Saline was replenished throughout the experiment.

2.2.3 Optical imaging

The excitation light source was a 150W halogen lamp filtered at 621-643nm. The fluorescence signals were collected with a MiCam02 camera system (BrainVision, Japan). The camera was focused onto layer 2/3, at approximately 300 µm below the pia surface (Petersen et al., 2003a). The frame was 184x123 pixels, at 200 Hz. Prior to each

trial, a background image of the craniotomy (F_0) was recorded. The objective lens was 1x and the condenser lens was 0.63x. The magnification was 1.6x. The field of view was 3.5 mm x 2.3 mm and the pixel size was 18.9 µm x 18.9 µm. All individual frames of 25-50 single trials were recorded.

2.2.4 Vibrissa stimulation

A multi-layered piezoelectric bending actuator (range of motion: 1 mm, bandwidth: 200 Hz; Polytec PI, Auburn, MA) generated vibrissa deflections. Each vibrissa was individually deflected in the rostral-caudal plane in a saw-tooth waveform of 17 ms in duration (τ = 2 ms). Each trial had 200 ms of pre-stimulus recording. In non-adapted trials, a single, strong deflection (800-1500 °/s) was delivered to either one of two adjacent vibrissae. In adapted trials, the same probe was preceded by a 1 second, 10 Hz pulsatile adapting stimulus. Stimulation protocols were presented in a random order and repeated 50 times with a minimum of 3.8 s of rest between trials.

2.2.5 Barrel mapping

A barrel map was obtained from cytochrome c oxidase staining of one animal. The barrels were outlined in Neurolucida software (MBF Bioscience,Williston, VT). This barrel map serves as a generic template for all other animals. In previous studies, the barrel map was found to be relatively well conserved across animals. For each animal, the initial VSD responses to several individual whisker deflections were superimposed to form a response map, as the initial responses are relatively constrained within the primary barrel (Petersen et al., 2003a). The template barrel map was then linearly scaled, translated, and/or rotated, so that the centroids of the responses to several individual whisker deflections and the geometric centers of the barrels produce minimal squared errors.

2.2.6 Data analysis

All analyses of VSD data were conducted in Matlab, and based on the change in the fluorescence relative to the background, or $\Delta F/F_0$. Specifically, the VSD frames were divided by the background image F_0 in a pixel-wise fashion. Additionally, to account for non-stationarities in the imaging data, a baseline frame was subtracted from all frames to ultimately form ΔF. For non-adapted trials and pre-stimulus frames, the baseline was the average of the first 50 ms of pre-stimulus frames. For adapted trials, the baseline was the first 50 ms immediately preceding the probe. The resulting frames were divided by the background F_0, to produce our primary measure $\Delta F/F_0$. The response frames were time-averaged from the typical onset to peak frame of cortical response (10-25 ms post-stimulus) for all stimulus conditions. Numerous studies have asserted that sensory detection can be modeled as temporal integration of the ongoing neural response (Carpenter 2004; Chen et al. 2008; Cook and Maunsell 2002; Fridman et al. 2010; Gold and Shadlen 2007; 2001; Huk and Shadlen 2005; Mazurek et al. 2003; Roitman and Shadlen 2002; Schall and Thompson 1999; Smith and Ratcliff 2004; Stüttgen and Schwarz 2010). Therefore, I integrated from a typical VSD signal onset time of 10 ms (consistent with the cortical response latency in this pathway), to a typical VSD signal peak time of 25 ms. The pre-stimulus frames (excluding those used as the baseline) within each trial were also time-averaged every 4 frames.

2.2.7 Ideal observer analysis

Response variables: For each animal, two regions of cortex were defined so that each highlighted the center of the response to the corresponding whisker stimulation. The region corresponding to whisker 1 stimulation was referred to as Region 1 and so on. For trials from whisker 1 stimulation, Region 1 was the center of the cortical response to its

primary whisker stimulation (hereon referred to as the Primary Region), Region 2 was that to the adjacent whisker stimulation (hereon referred to as the Adjacent Region). For whisker 2 stimulation trials, Region 2 was the Primary Region, and Region 1 was the Adjacent Region. To obtain the region for each whisker stimulation, the trial-averaged non-adapted response was spatially filtered with a 5x5 pixel (approximately 0.1 mm x 0.1 mm) median filter and a 5x5 pixel average filter, then fitted with a two-dimensional Gaussian function. The corresponding activation region was defined as the 98% height contour of the Gaussian fit. The two regions were non-overlapping and approximately the size of a cortical column (~300-500 μm in diameter), (Bruno et al., 2003). Once defined, the two regions were applied to the unfiltered, single-trial frames. The average fluorescence within each region was defined as a response variable.

Detection: The primary region response variable was defined as the decision variable (DV) for this analysis. For each of the three cases, pre-stimulus noise, non-adapted response, and adapted response, the DVs from all single trials were binned and fit with a Gaussian function to represent the probability mass function. The noise distribution was formed by the decision variables extracted from all pre-stimulus frames. Detectability was measured using a standard detection theory variable d', which quantifies the separability between two distributions, for both the adapted and non-adapted cases relative to the noise distribution.

Discrimination: For all single trials given whisker 1 stimulation, both response variables from Region 1 ($R_1|W_1$) and Region 2 ($R_2|W_1$) were extracted and plotted as a cluster, and the response variables from whisker 2 stimulation were plotted as another cluster. Linear Discriminant Analysis (LDA) was used to optimally separate the two clusters (Fisher linear discriminant, MATLAB). The response variables were then projected onto the axis orthogonal to the LDA line and formed two histograms and each was fitted a Gaussian

probability distribution. The projected response variable is defined as the decision variable. The separation of the decision variable distributions, measured as d', was used as the discriminability measure.

2.3 Results

2.3.1 Adaptation spatially constrains the cortical response

Voltage sensitive dye (VSD) imaging was employed in the cortex of anesthetized rats to capture sub-threshold activity of a large population of neurons in cortical layer 2/3 (Kleinfeld and Delaney, 1996; Petersen et al., 2003a), as computer-controlled piezoelectric actuators deflected the vibrissae (Figure 1.2). An anatomical barrel map was functionally registered to the images for illustration purposes (Wang et al., 2012). The cortical activation is reported as the percent change in fluorescence relative to the background level ($\%\Delta F/F_0$). The VSD signal initially appeared localized in the principal barrel at 10 ms after stimulus onset, quickly spread to neighboring barrels, peaked at approximately 20-25 ms, then gradually decayed back to baseline at approximately 100 ms, consistent with previous findings (Petersen et al., 2003a; Wang et al., 2012). Subsequent analyses were based on the time-averaged response from the typical onset to peak time (10-25ms).

Given the spatial spread of activation for a single whisker deflection, one immediate question is to what extent a single whisker stimulus activates adjacent barrels. An example of typical responses to separate deflections of two adjacent whiskers is shown in Figure 2.1A. Shown is the trial-averaged VSD response to Whisker 1 (top) or Whisker 2 (bottom) stimulation. Each of these responses was fit with a 2D Gaussian function, the half-height contour of which was superimposed on the VSD image, and combined on the right. In the absence of any prior deflection of the vibrissae, the cortical response was

recorded in what was referred to as the 'non-adapted' state (Figure 2.1A). Following an ongoing, adapting stimulus, the cortical activation was recorded in response to the same test probe stimulus in the 'adapted state' (Figure 2.1B). Note that the adapting stimulus in this case was a sequence of pulsatile (sawtooth) whisker deflections at a repetition rate of 10Hz. Qualitatively, the non-adapted responses were strong in both magnitude and spatial spread (Figure 2.1A), with significant spatial overlap, while the adapted responses were smaller in magnitude and spatial spread, and showed much less spatial overlap (Figure 2.1B). This suggests that from the perspective of an ideal observer of the cortex, the detectability of the test probe stimulus may degrade due to the decrease in magnitude but the spatial discriminability of the stimulus may improve due to the spatial constraint. However, the relationship between average response and quantitative information conveyed trial-to-trial is not trivial (Averbeck et al., 2006; Pouget et al., 1999).

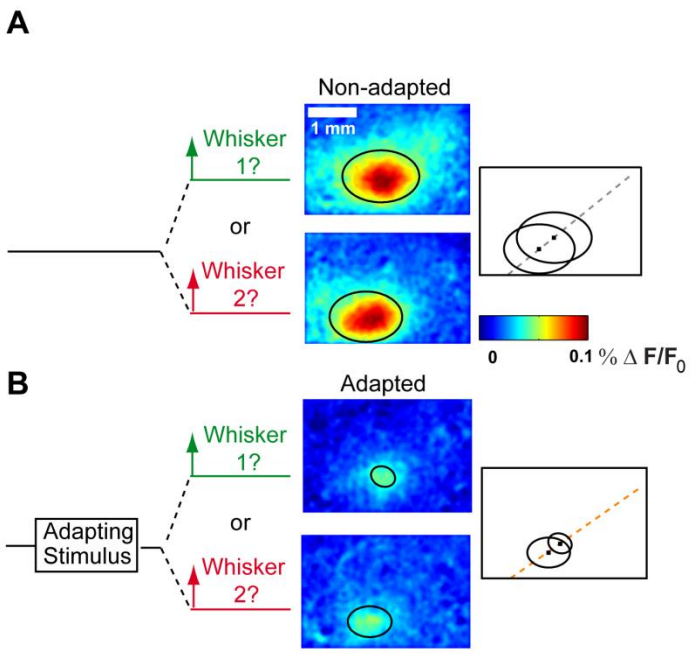

Figure 2.1 Adaptation spatially constrains the cortical response.
A. The cortical responses to a single-whisker stimulation in the absence of a preceding 10 Hz adapting stimulus. Whisker 1 (W1) and whisker 2 (W2) were adjacent to each other on the snout and stimulated separately. Images were averaged over 50 trials. The black

ellipses on the images were half-height contours of the two-dimensional Gaussian fits to the images. On the right is the superposition of the Gaussian contours.
B. In contrast, the same stimulus following a 10 Hz adapting stimulus evoked a cortical response that was significantly reduced in magnitude and in area.

2.3.2 Adaptation degrades stimulus detectability for an ideal observer

The detectability of a stimulus was measured against pre-stimulus noise on a single trial basis in the non-adapted and adapted states using optimal detection theory (Duda et al., 2001; Macmillan and Creelman, 2004). Each single-trial cortical response was represented as a decision variable (DV), used by the ideal observer to classify each trial as signal or noise. This was done by averaging the measured neural activity within an approximately barrel-sized region of interest (ROI) 10-25 ms after stimulus onset. Note that the results were not dependent on absolute ROI size, as long as it remained within the range of an individual cortical column (~300-500 μm in diameter). For each case, the DVs over all 50 trials were binned, and a Gaussian probability function was fit. Figure 2.2A shows a typical example of the noise (shown in black) and signal distributions in the non-adapted (grey) and adapted (orange) states (same ROI for all). Corresponding examples of trial-averaged VSD responses are shown for each of the three cases with the decision region overlaid in black. The adapted distribution lies closer to the noise than does the non-adapted, implying a reduction in detectability with adaptation. Detectability was measured using a standard detection theory variable d', which quantifies the separability between two distributions. There was a significant decrease in detection performance (d' between signal and noise) after adaptation (Figure 2.2B, non-adapted d': 1.24 +/- 0.076; adapted d': 1.05 +/- 0.078; $p < 0.005$, $n = 18$, paired t-test). Results were very similar using a related measure derived from the receiver-operating characteristic (ROC) curve (Figure 2.2C & D).

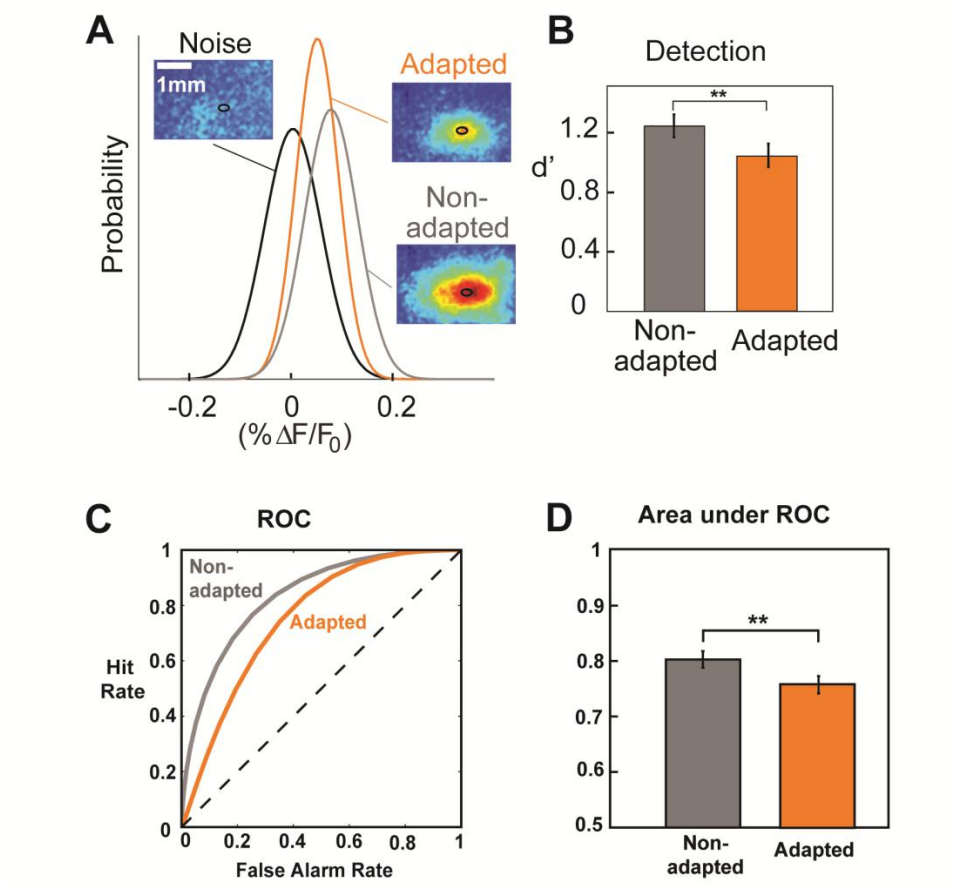

Figure 2.2 Ideal observer analysis - adaptation degrades detection.

A. A region of interest (ROI) approximately the size of a cortical column (300-500 μm in diameter) was defined as the 98% height contour of the 2D Gaussian fit to the trial-averaged non-adapted response. The insets show the corresponding trial-averaged images for each case (noise, non-adapted, and adapted), with the ROI outlined in black (same in all cases). The average fluorescence within the ROI was extracted from each single trial as a decision variable (DV).

B. The d' value, a measure of the separation of the signal and noise distributions, decreased following adaptation ($p < 0.005$, $n = 18$, paired t-test).

C. The performance of the observer relies on the use of a threshold around which to classify the response as belonging to signal or to noise. The separation of the signal distributions in panel A from the noise was quantified using a receiver-operating characteristic (ROC) curve, which evaluates the performance over all threshold choices.

D. The summary of the area under the ROC (AUROC) across all datasets, demonstrating that the overall detection performance decreased after adaptation (non-adapted AUROC: 0.80 +/- 0.015; adapted AUROC: 0.76 +/- 0.016; $p < 0.005$, $n = 18$, paired t-test). Note that this measurement takes into account all possible choices of threshold, but that for

intermediate ranges of threshold choice, there was as much as a 30% reduction in the hit rate for a given false alarm rate.

2.3.3 Adaptation enhances stimulus discriminability for an ideal observer

The ideal observer analysis was extended to measure changes in spatial discriminability resulting from deflections of adjacent vibrissae in the non-adapted and adapted states. Based on the cortical response to a single whisker deflection, the observer was tasked with identifying which of two possible whiskers caused it. The ROIs for the two whiskers were defined as described above and were applied to all single trials. After a deflection of whisker 1, the response in the corresponding ROI ($R_1|W_1$) was measured, as well as the response in the adjacent ROI ($R_2|W_1$). Figure 2.3A shows the response to each whisker deflection, with the two ROIs outlined in black. For a given whisker deflection, the corresponding ROI is shown in bold.

Figure 2.3B shows an example of all single-trial variables for a single dataset. Each point represents a single trial, with responses from deflections of whisker 1 shown in green (closed circles) and those from deflections of whisker 2 shown in red (open circles). Trials were excluded from analysis when the response fell below the 'detection threshold', which corresponded to a detection false alarm rate of 10%, based on the false alarm rate from related behavioral studies (Ollerenshaw et al., 2012; Stüttgen and Schwarz, 2008). The extent to which these two clusters can be discriminated determines how well an observer could correctly identify which whisker led to a particular cortical response. Linear Discriminant Analysis (LDA) was used to determine the line that maximally separated the two clusters, shown as the solid black line in Figure 2.3B. The raw variables were projected onto the line orthogonal to the LDA line and the separability of the two probability distributions, measured using the standard detection theory variable d', was used as the discrimination metric.

Figure 2.3C shows the adapted case, where the two variable clusters became more separated, resulting in a larger separation of the probability distributions. Due to the simultaneous reduction in signal amplitude, a higher percentage of trials fell below the detection threshold and were subsequently eliminated from the analysis. Discriminability was significantly improved following adaptation (Figure 2.3D, non-adapted d': 1.9 +/- 0.24; adapted d': 2.6 +/- 0.26; $p < 0.05$, n = 9 animals, paired t-test). Similar results emerged from a likelihood ratio test and results were relatively insensitive to chosen parameters.

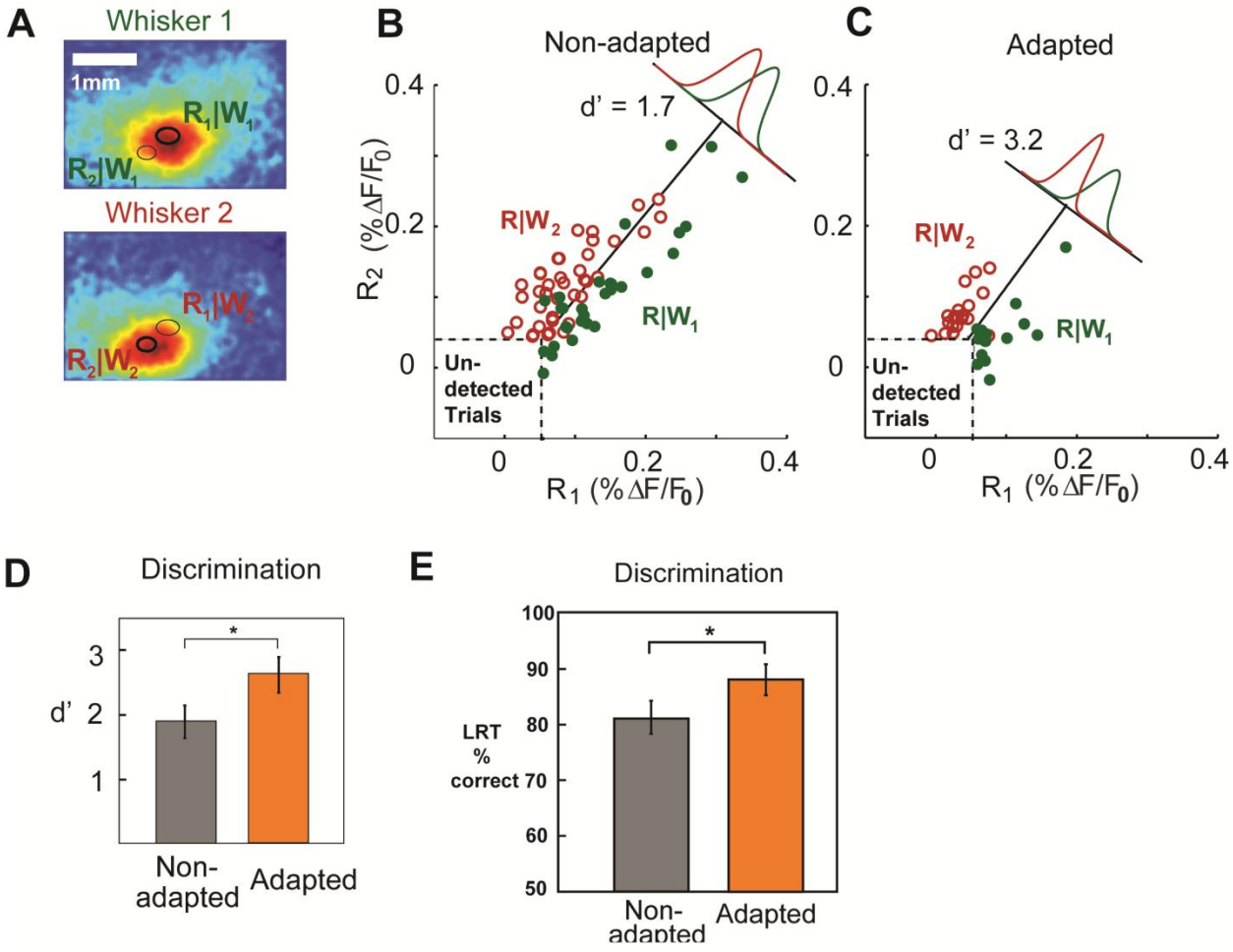

Figure 2.3 Ideal observer analysis - adaptation improves spatial discriminability.
A. The same method described in the detection analysis was used to derive the ROI for each of the two whisker stimulations (shown in bold ellipse). Both ROIs were applied to

all single trials. Two responses were calculated for each single trial: the average fluorescence within the principal barrel area (bold ellipse), and that within the adjacent barrel area (thin ellipse).
B. Responses above the detection threshold in the non-adapted case were grouped by whisker stimulation and separated using Linear Discriminant Analysis (LDA). The decision variable was defined as the projection of the response onto the axis orthogonal to the LDA line. The d' separation measure was then calculated for the two probability distributions of the decision variables. The d' in this example was 1.7.
C. Same analysis as in B for the adapted case. The d' in this example was 3.2.
D. Discrimination performance (d' of DV probability distributions) of the ideal observer significantly improved following adaptation ($p < 0.05$, $n = 9$, paired t-test). All error bars represent +/- 1 standard error of the mean.
E. Discrimination performance using the likelihood ratio test also significantly improved following adaptation. The performance in the non-adapted case was 80.6% +/- 3.1%. In the adapted case, the observer correctly classified 88.6 +/- 2.6%, again showing that discriminability was significantly improved for the ideal observer following adaptation ($p < 0.05$, $n = 9$, paired t-test). Error bars represent +/- 1 standard error of the mean.

2.3.4 Adaptation degrades stimulus detectability for awake, behaving animals

To directly test the perceptual effects of sensory adaptation, both a detection and spatial discrimination task were carried out using a separate set of head-fixed rats. The detection task was modeled closely off of detection tasks published previously by our lab and others (Ollerenshaw et al., 2012; Stüttgen and Schwarz, 2008), with the exception that the stimulus to which animals were trained to respond was preceded by a 12 Hz sinusoidal adapting stimulus on a subset of trials (Figure 2.4A). Each trial in the task was initiated by a 3 s tone, during which an adapting stimulus was presented randomly on half of the trials. A variable velocity stimulus was presented on a uniformly varying time interval between 0.5 and 2.5 s after the end of the tone, and animals had a 1 s window following the stimulus in which to emit a lick to receive a water reward.

Figure 2.4B shows the psychometric curves that resulted from the behavioral detection experiments for all animals. The black dashed line labeled as "chance" indicates the

response probability on catch trials, in which a deflection of a second piezoelectric actuator was substituted for the actuator attached to a whisker. The response probability on catch trials was 8.7% on nonadapted trials and 8.6% on adapted trials, which is consistent with the behavioral false alarm rate from similar studies (Ollerenshaw et al., 2012; Stüttgen and Schwarz, 2008) and also demonstrates that adaptation did not lead to a change in response criterion for the animals.

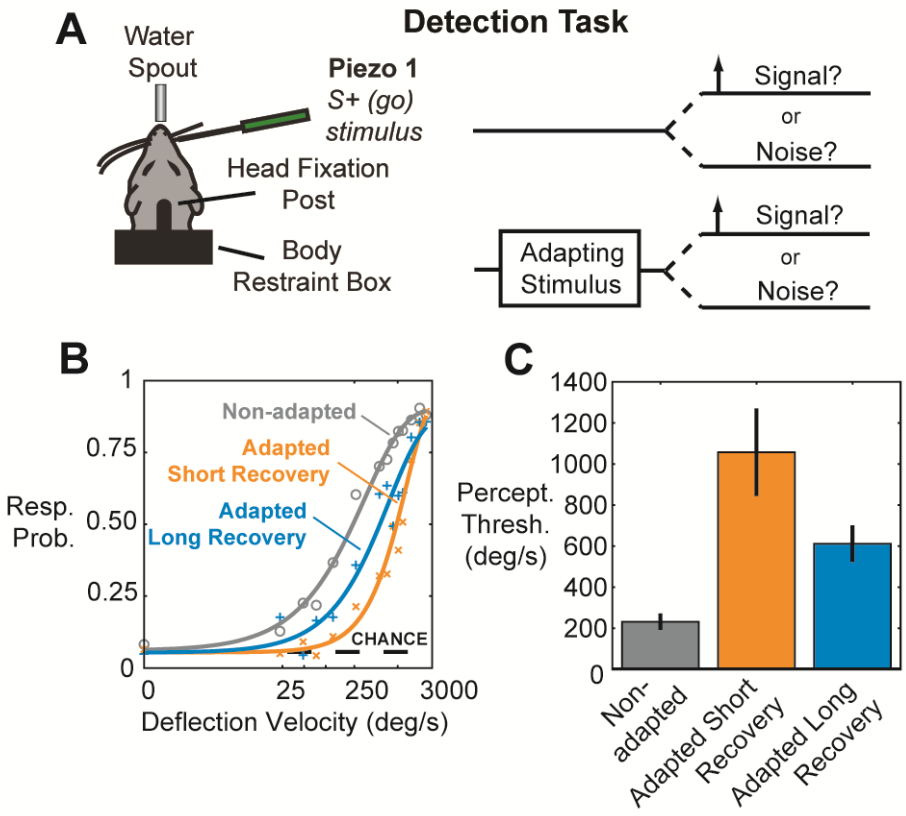

Figure 2.4 Behavioral detection thresholds are increased with adaptation (*courtesy of DRO*).

A. Detection task. A piezoelectric actuator was placed on a single whisker, and a variable velocity probe stimulus was presented at a randomized time. The probe was preceded by an adapting stimulus on 50% of trials.
B. Combined psychometric curve for all animals for the nonadapted (gray) and the adapted short recovery (orange) and long recovery (blue) cases. Error bars are omitted for clarity. The black dashed line indicates the chance performance level.
C. Quantification of perceptual thresholds. Each bar represents the perceptual threshold, measured as the 50% point of the sigmoidal fit (nonadapted to adapted short recovery:

$p < 0.05$; nonadapted to adapted long recovery: $p < 0.05$; paired t test, $n = 4$ animals). Error bars represent ±1 SEM.

The orange curve in Figure 2.4B shows the combined psychometric curve in response to stimuli falling in the short recovery period (0.5–1.5 s following adaptation). The curve is shifted to the right relative to the nonadapted (grey) curve, indicating that a much stronger stimulus must be delivered to achieve the same response probability. Importantly, the response probability for the strongest stimulus approached that seen in the nonadapted case, indicating that the change in performance is not due simply to changes in motivational level, or confusion on the part of the animals. The blue curve shows the psychometric function for stimuli occurring in the long recovery period (1.5–2.5 s following adaptation), indicating a return to baseline detection performance.

The observed decrease in detectability was quantified by measuring the change in the perceptual threshold, defined as the 50% point on the psychometric curve. Figure 2.4C shows the average threshold (232 ± 35°/s, nonadapted), which is very similar to that seen in a similar single-whisker detection task (Stüttgen and Schwarz, 2008). The average threshold increased to 1,057 ± 204°/s in the adapted short recovery state and then decreased to 611 ± 81°/s in the adapted long recovery state. Thus, detectability was reduced following adaptation to a sensory stimulus, with a 4-fold increase in stimulus velocity required to achieve the same threshold performance level ($p < 0.05$, $n = 4$, paired t test). Performance began to recover with timescales on the order of a few seconds, though detection thresholds remained significantly above those in the nonadapted state ($p < 0.05$, $n = 4$, paired t test). Reaction times were also observed to increase following adaption.

2.3.5 Adaptation improves spatial discriminability in awake, behaving animals

The same animals were then trained on a two-whisker go/no-go spatial discrimination task (Figure 2.5A). The S+ or "go" whisker remained the same as in the detection task. However, a second piezoelectric actuator was attached to a second neighboring whisker, which was deemed the S− or "no-go" whisker. The task proceeded as it had during the detection task, with the exception that on a given trial, the stimulus was randomly chosen as either the S+ or S− whisker with equal probability. To avoid cueing the animal as to which whisker would be stimulated, both whiskers were deflected together during the adaptation phase of the trial. The velocity of the probe stimulus remained fixed at 1,500°/s. Animals were rewarded for responding to the S+ stimulus as before but were penalized with a 5–10 s timeout paired with the house lights when they responded to the S− stimulus.

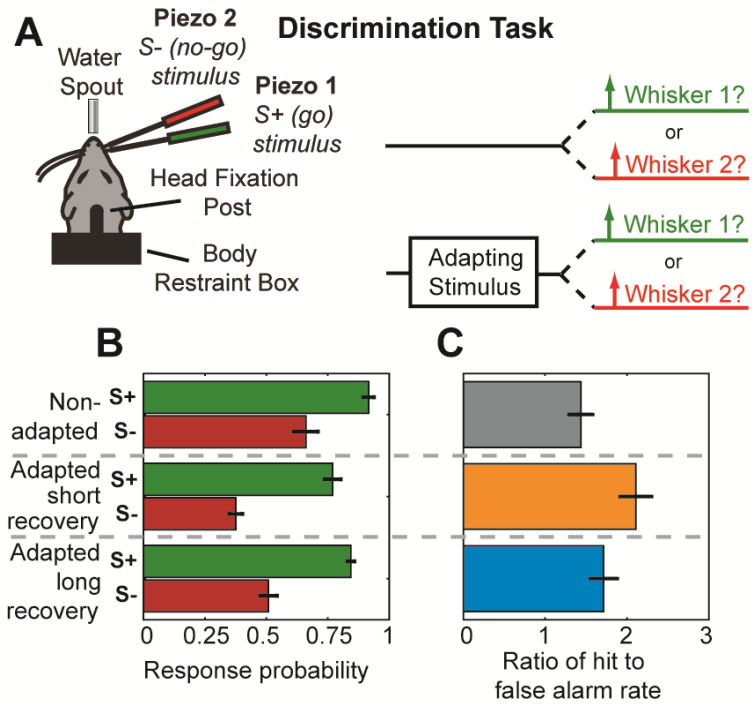

Figure 2.5 The spatial discrimination performance of the animals is improved with adaptation (*courtesy of DRO*).
A. Discrimination task. A second piezoelectric actuator was introduced on a nearby whisker. The task proceeded as in the detection task, with the exception that on a given trial either the S+ (go whisker) or the S− (no-go) whisker was deflected with equal probability using a fixed suprathreshold velocity. Animals were rewarded as before for responses to the S+ stimulus but were penalized with a timeout for responses to deflections of the S− whisker.
B. Raw response probabilities. Response probabilities to S+ and S− stimuli are shown in green and red. From top to bottom, each pair of bars represents the nonadapted state, the adapted short recovery state, and the adapted long recovery state.
C. Discriminability quantified as the ratio of the hit rate to the false alarm rate. Discriminability is measured using the data in **B** for the nonadapted (grey), adapted short recovery (orange), and adapted long recovery (blue) states (nonadapted to adapted short recovery: $p < 0.005$; nonadapted to adapted long recovery: $p < 0.05$; paired t test, $n = 5$). All error bars represent ±1 SEM.

Figure 2.5B shows the summary of response probabilities for all trials averaged across all animals. Hit and false alarm rates are shown in green and red, respectively. The three possible states of adaptation are presented from top to bottom. As expected based on the detection results, the overall hit and false alarm rates decreased from the nonadapted to adapted short recovery state and then increased somewhat with a longer period of recovery. However, it is difficult to determine from these values alone whether any change in discrimination performance exists across the states. Figure 2.5C shows that when the ratio of hit rate to false alarm rate was calculated, there was a significant increase in discrimination performance from the nonadapted state to the adapted short recovery state, with the ratio increasing from 1.44 ± 0.14 to 2.11 ± 0.19 ($p < 0.005$, $n = 5$, paired t test). With a longer recovery period, the discrimination performance decreased (hit to false alarm ratio of 1.72 ± 0.17), though it remained significantly above the nonadapted value ($p < 0.05$, $n = 5$, paired t test), indicating that recovery was not complete by 2.5 s after the end of adaptation.

2.3.6 Adaptation of the thalamocortical circuit of awake, behaving animals

Thalamic activity has been shown to play a key role in modulating the cortical state. We have previously demonstrated that adaptive shifts in cortical feature selectivity are strongly correlated with changes in thalamic firing and synchronization with adaptation (Wang et al., 2010). To uncover potential mechanisms underlying our observations here and to provide a link between the cortical activation and behavior, neural recordings were obtained from the ventroposterior medial (VPm) nucleus of the thalamus in three awake rats. Two of those animals were also trained to perform the detection with adaptation task described above.

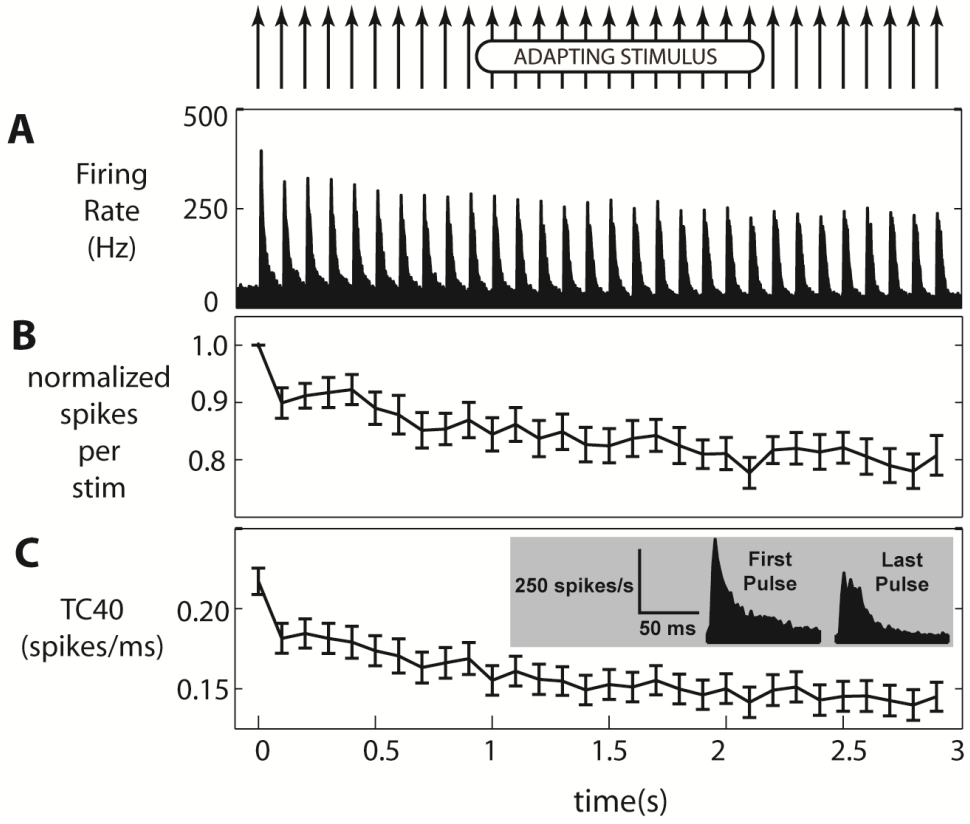

Figure 2.6 Adaptation of thalamic VPm cells in the awake animal (*courtesy of DRO*).
A. The combined PSTH for all animals and recording sessions.
B. The number of spikes per stimulus for each pulse in the 3 s, 10 Hz train of adapting stimuli, normalized to the spike count in response to the first pulse. After adaptation, the firing rate was 79.2% of its nonadapted value.

C. Timing precision, as measured using TC40, decreased from 0.217 ± 0.008 spikes/ms in the nonadapted state to 0.145 ± 0.008 spikes/ms after adaptation. The inset shows the first and last PSTH combined across all animals and recording sessions. All error bars represent ±1 SEM (all values $p < 0.005$, $n = 56$, two sided t test comparing response to first pulse with response to the final three pulses combined).

The effect of adaptation to a pulsatile (sawtooth) stimulus at a base rate of 10 Hz can clearly be seen in Figure 2.6A, showing the average peristimulus time histogram (PSTH) of multiunit activity across all sessions of all three animals. Figure 2.6B shows the mean normalized spike count across all sessions, which displayed a sharp decrease in firing rate from the first to the second pulse in the adapting train, recovered slightly, then approached a steady-state level of adaptation of 79.2% of the nonadapted firing rate.

Here, we used timing precision of the multiunit recording as a proxy for population synchrony across multiple single units within a barreloid (Butts et al., 2007; Desbordes et al., 2008). A quantitative measure of timing precision is the "temporal contrast," or TC40 metric (Pinto et al., 2000). TC40 is defined as the number of spikes representing 40% of the total response magnitude in a 30 ms poststimulus window, divided by the time required to generate the first 40% of the total response magnitude. Figure 2.6C shows that timing precision decreased by approximately 33%, from 0.217 spikes/ms (nonadapted) to 0.145 spikes/ms (adapted), with the qualitative effects shown in the inset, very similar to the percentage reduction in synchrony measured in the anesthetized animal (Wang et al., 2010).

Taken together, the results here demonstrate that bottom-up sensory adaptation induces a brain state where the cortical representation of an external stimulus is suppressed, resulting in a trade-off of detectability and discriminability of the stimulus both in the ideal observer of the anesthetized cortex and in awake, behaving animals, and that the

thalamic activity driven by the adapting stimuli likely contributes to modulating the cortical state in the awake animal.

2.4 Discussion

In the presence of persistent stimulation, sensory systems have long been shown to exhibit various forms of rapid and reversible adaptation (Ahissar et al., 2000; Barlow, 1961; Chung et al., 2002; Fairhall et al., 2001; Higley and Contreras, 2006). It has been posited that these forms of adaptation do not just represent deleterious reductions in firing, but instead represent fundamental changes in coding properties that likely possess ethological relevance. Specifically demonstrated here is the switch of cortical processing modes from conveying information favoring the detection of the stimulus to conveying information favoring the spatial discrimination of the stimulus.

A wide range of studies characterizing cortical representations in the face of persistent or adapting stimuli (Lee and Whitsel, 1992; Sheth et al., 1998; Simons et al., 2005) have made qualitative inferences regarding the relationship between the observed spatial sharpening and the improved acuity in psychophysical studies (Tannan et al., 2006; Vierck and Jones, 1970). It is important to note, however, that a sharpened cortical response alone is not sufficient to improve discriminability, and that in many cases sharpened representations can lead to a reduction in information transmission (Pouget et al., 1999). Here, considered were both the mean, trial-averaged cortical responses, which provide the qualitative "sharpening" of the cortical response observed with adaptation, as well as the trial-by-trial cortical activation that the animal would have access to in a behavioral context. From the classical signal-detection perspective, the key measure of being able to discriminate between sensory inputs lies in the separability of the probability distributions of the assumed response variable. A major contribution here,

which goes above and beyond the previous studies where sharpened cortical responses have been demonstrated, is that the quantitative trial-by-trial analysis demonstrated a measureable enhancement in discriminability, a result which was not preordained by the sharpened cortical representations alone. This is even more the case given the fact that the adaptation unambiguously reduces neural activity in cortex even at the center of cortical activation, which could produce a wide range of perceptual effects.

This result in the cortex is bolstered by a parallel set of behavioral experiments performed in our laboratory. A separate group of rats were trained in vibrissa-based detection and spatial discrimination tasks, in which adaptation led to enhanced discrimination performance at the expense of stimulus detectability. In the vibrissa system, the animal's own whisking motion has been proposed to lead to a state similar to that achieved through adaptation to passively applied stimuli, switching the system from a state in which it is more sensitive to inputs to one in which it is more selective (Moore, 2004; Moore et al., 1999). Under this scenario, inputs arriving when the pathway is in the non-adapted state are more likely to generate a large cortical response, alerting an otherwise quiescent or inattentive animal to the presence of an unexpected stimulus (Chung et al., 2002; Diamond and Arabzadeh, 2012; Fanselow and Nicolelis, 1999; Khatri et al., 2009; Sherman, 2001b), presumably at the expense of specificity. However, with active exploration of an object, the system is placed into an adapted state, subsequently reducing the magnitude of the cortical response, but improving the ability of the system to discern the finer features of sensory stimuli (Fanselow et al., 2001; Kohn and Whitsel, 2002; Maravall et al., 2007; Moore, 2004). Studies with freely behaving animals have demonstrated that the cortical response to peripheral inputs is reduced when the animal is whisking (Castro-Alamancos, 2004; Crochet and Petersen, 2006; Fanselow and Nicolelis, 1999; Ferezou et al., 2006, 2007; Hentschke et al., 2006; Poulet et al., 2012), and exploratory whisking in air drives activity along the pathway (Curtis and Kleinfeld, 2009;

Leiser and Moxon, 2007), potentially implying that the animal's own self-motion serves to place it into an adapted state similar to that described here. Indeed, detectability is significantly improved in the absence of whisking (Ollerenshaw et al., 2012), potentially part of an active strategy by the animal to facilitate information flow in this very specific context. While the frequencies of the adapting stimuli used in the present study were chosen to fall within the natural 5-15 Hz whisking range (Berg and Kleinfeld, 2003; Bermejo et al., 2002; Brecht et al., 1997; Carvell and Simons, 1990), a more complete characterization of the effects of adaptation across a broader range of frequencies would be important in understanding how natural behaviors modulate the observed detectability/discriminability trade-off.

Despite the fairly widely observed phenomenon of spatial sharpening of cortical representations, the underlying mechanism has not been explored extensively. One possibility long postulated involves the dynamic engagement of inhibitory mechanisms at the level of cortex or more peripherally, shifting the E/I balance (von Békésy, 1967; Kyriazi et al., 1993; Mountcastle, 1968; Simons and Carvell, 1989; Simons et al., 1992). Using micro-electrode recordings of single-units in S1, Brumberg et al. (1996) demonstrated that when a whisker was continuously stimulated with white noise, the deflection of an adjacent whisker led to a more constrained cortical response than when the whisker was deflected alone, a result that could be attributed to thalamic decorrelation. The cortical results here, supported by the behavior results in awake animals would seem to indicate that the improved discriminability with adaptation cannot be fully explained by top-down mechanisms (Gilbert and Li, 2013), which are of course absent in the anesthetized animal. Sensory adaptation has been shown to lead to a decrease in firing synchrony of thalamic neurons (Temereanca et al., 2008), a phenomenon that has been shown to lead to decreased stimulus detectability and improved velocity discriminability at the cortex (Wang et al., 2010) due to the extreme

sensitivity of layer 4 cortical neurons to the timing of thalamic inputs (Alonso et al., 1996; Bruno, 2011; Roy and Alloway, 2001; Stanley et al., 2012; Usrey et al., 2000) and its importance in determining cortical feature selectivity (Stanley, 2013; Stanley et al., 2012).

In the separate set of behavior experiments performed in our laboratory, recordings in the ventroposterior medial (VPm) nucleus of the thalamus of awake animals further revealed a reduction in spike count and timing precision with adaptation. Recovery of spike count and timing precision was found to be on a timescale that matched recovery in behavioral performance (data not shown), and reductions in both quantities were predictive of a reduction in behavioral detection performance. The measured thalamic firing statistics were used to drive a model of the thalamocortical circuit, which demonstrated a less synchronous drive from the thalamus could produce a sharpening effect with adaptation similar to that measured with VSD in the anesthetized cortex. Together, these results provide direct behavioral and cortical evidence for the trade-off between detectability and discriminability, that this trade-off is modulated through bottom-up sensory adaptation, and that the underlying adaptive regulation of convergent thalamic input may play an important mechanistic role.

Although as with linking any behavioral percept to the underlying neural activity, it cannot be directly asserted that the percepts utilized by the animal to perform the detection and discrimination tasks in this study exist in S1, the ideal observer analysis shows us that the necessary information is present at this level of processing and that the adaptive modulation of the detectability/discriminability trade-off is also reflected at this stage. The neural activity in the primary sensory cortex has long been considered the fundamental neural basis for downstream sensory percepts and behavior. However, there are some contradictory experimental studies on this point, with some demonstrating a

complete abolishment of abilities to perform whisker related tasks with the inactivation of S1 (O'Connor et al., 2010), others demonstrating only a severe degradation of detection abilities (Hutson and Masterton, 1986; LaMotte and Mountcastle, 1979), and some studies showing that micro-stimulation of S1 directly influences an animal's stimulus detection and discrimination performance (Houweling and Brecht, 2008; Huber et al., 2008; Romo et al., 1998, 2000). Taken together, it can be, at minimum, concluded that S1 is a major role player in simple behaviors such as detection. Nonetheless, in order to investigate the cortical mechanism underlying stimulus perception, it is ideal to record the cortical activity simultaneously in awake, behaving animals. Although the stimuli provided here can effectively influence stimulus coding and perception, they are passive deflections of the whisker, which can bear subtle mechanistic differences when compared to active whisking. In the imaging of awake, behaving animals, the neurophysiological and perceptual differences should be tested for the bottom-up and top-down regulations of processing states.

CHAPTER 3 Sensory adaptation encompasses a continuum of brain states

A modified version of this chapter was published as a research article:

Zheng, H. J., Wang, Q., & Stanley, G. B. (2015). Adaptive Shaping of Cortical Response Selectivity in the Vibrissa Pathway. *J Neurophysiol., 113(10):3850-65.*

Portions of this work were presented in talk form at the following:

Zheng, H. J. V., Ollerenshaw, D.R., Millard, D.C., Wang, Q., & Stanley, G.B. Adaptive Shaping of Feature Selectivity in the Rodent Vibrissa System: Coding and Behavior. Southeast Neuroscience Meeting, Augusta, GA, 2014.

Portions of this work were presented in poster form at the following:

Zheng, H. J. V., Ollerenshaw, D.R., Millard, D.C., Wang, Q., & Stanley, G.B. Adaptive Shaping of Feature Selectivity in the Rodent Vibrissa System: Coding and Behavior. COSYNE meeting, Salt Lake City, UT, 2014.

Zheng, H. J. V., Ollerenshaw, D. R., Millard, D. C., & Stanley, G. B. The Continuum of Adaptation Shapes the Trade-off between Detection and Discrimination. COSYNE meeting, Salt Lake City, UT, 2013.

Zheng, H. J. V., Wang, Q., Ollerenshaw, D. R., Millard, D. C., & Stanley, G. B. Properties of Adapting Stimuli Differentially Shape Spatial Decoding in Rat Barrel Cortex. SfN meeting. New Orleans, L.A., 2012.

3.1 Introduction

We live in a complex sensory environment, where different sensory cues are important for perception and decision-making in different contexts. Not only is there evidence for different information being parsed into different pathways (Goodale and Milner, 1992), sensory information processing within a pathway may also be context-dependent, where competing coding schemes coexist (Crick, 1984; Sherman, 2001a). Specifically, sensory pathways may switch from conveying information for detecting novel features in the environment, to conveying information for discerning fine details (Moore, 2004; Adibi et al., 2013; Lesica and Stanley, 2004; Lesica et al., 2006; Sherman, 2001b; Wang et al., 2010), setting the stage for a complex and dynamic coding scheme that may be particularly important for interacting with the natural environment (Stanley, 2013). One process that modulates state-dependent sensory information processing is sensory adaptation, during which neurons decrease firing rate in response to repeated stimuli in hundreds of milliseconds and recover on a similar time scale (Webber and Stanley, 2006). Adaptation is a ubiquitous and cross-modal phenomenon where the pathway shifts its dynamic range in response to persistent external stimuli, resulting in both perceptual and electrophysiological manifestations.

In somatosensation, psychophysical studies have shown that adaptation heightens spatial acuity in tactile discrimination tasks (Vierck and Jones, 1970; Goble and Hollins, 1993; Tannan et al., 2006), while electrophysiological studies qualitatively show a spatially constrained cortical representation of repetitive stimuli, proposed as a potential mechanism for enhanced acuity (von Bekesy, 1967; Lee and Whitsel, 1992; Sheth et al., 1998; Moore 2004). Despite the potentially profound implications for sensory coding, however, this phenomenon has not been extensively quantified. Analogous to the spatial acuity enhancement observed in humans, Chapter 2 demonstrates that adaptation induces a brain state where cortical representation of a stimulus is suppressed, and both awake

rats and the ideal observer of the cortex can better discriminate the spatial location of a whisker stimulus (i.e. which one of two adjacent whiskers was deflected). However, the detectability (i.e. the probability that the animal reports the sensation of a whisker deflection or the probability that the ideal observer classifies the trial as a detected signal as opposed to noise) is degraded at the same time, suggesting a fundamental change in spatial acuity that has implications for texture processing (Ollerenshaw, Zheng et al., 2014). Although a range of electrophysiological studies have demonstrated the effects of adaptation on cortical activation in the rodent vibrissa pathway (Sheth et al., 1998; Chung et al, 2002; Khatri et al., 2004; Moore, 2004; Webber and Stanley, 2004; Boloori and Stanley, 2006; Higley and Contreras, 2007; Khatri et al., 2009; Ganmor et al., 2010; Adibi et al., 2013), the extent to which the nature of the adapting stimulus shapes the spatial activation in the cortex is unknown, as is the ultimate effect on detectability and discriminability.

I used voltage-sensitive dye (VSD) imaging to measure cortical activation in the anesthetized rat, to explicitly test spatially distributed S1 vibrissa representations for a range of adapting stimuli. I specifically modulated the energy in the adapting stimulus through co-variation of the frequency and velocity, two primary parameters comprising the kinetic signature (Arabzadeh et al., 2005) of whisker motion in whisking behavior and texture contact (Wolfe et al., 2008). Increasing amounts of adaptation resulted in cortical representations that were increasingly degraded in the overall activation and constrained spatially. Single-trial based ideal observer analysis revealed a decrease in detectability of the whisker input with increasing adaptation and an increase in spatial discriminability for moderate levels of adaptation but degraded discriminability for more extreme levels of adaptation. Taken together, the results suggest that adaptation operates on a continuum and modulates the tradeoff between detectability and discriminability in

an ethologically relevant way that emphasizes the competing demands that different tasks place on the system.

3.2 Methods

3.2.1 Surgery

All procedures were approved by the Institutional Animal Care & Use Committee at Georgia Institute of Technology and in agreement with the National Institutes of Health guidelines. Seven female albino rats (Sprague-Dawley; 250-330g) were sedated with 4% vaporized isoflurane, then anesthetized with sodium pentobarbital (50 mg/kg i.p., initial dose). Supplemental doses were administered as needed to maintain a surgical level of anesthesia, confirmed by monitoring heart rate, respiration and eyelid/pedal reflexes to adverse stimuli (toe or tail pinch). Following the initial sodium pentobarbital dose, the animal was mounted on a stereotaxic device (Kopf Instruments, Tujunga, CA) on a vibration isolation table. Atropine (0.09 mg/kg, s.c.) was administered subcutaneously to keep the lungs clear of fluid. Lidocaine was injected subcutaneously into the scalp before the initial incision on the head. In all experiments, saline was administered (2 mL/kg/hour) to prevent dehydration. Body temperature was maintained at 37°C by a servo-controlled heating blanket (FHC, Bowdoinham, ME). After the midline incision on the head, skin and tissue were resected and connective tissue was removed. A craniotomy (approximately 3 mm x 4 mm) was drilled on the left hemisphere over the primary sensory cortex (stereotaxic coordinates: 1.0-4.0 mm caudal to the bregma, and 3.0-7.0 mm lateral to the midline; Paxinos and Watson, 2007). The dura was left intact. A dental acrylic dam was constructed around the craniotomy. At the end of the surgical procedures, a light level of anesthesia was maintained with sodium pentobarbital. The animal was euthanized with an overdose of sodium pentobarbital solution after VSD imaging, which lasted approximately 2 hours.

3.2.2 Staining

The dura was cleaned using a gentle flow of saline (0.9%), then dried with a gentle air blow for about 10-15 minutes or until it appeared "glassy" (Lippert et al., 2007). Voltage sensitive dye (VSD RH1691, Optical Imaging) was diluted in saline to approximately 1.5 mg/mL. The dye solution (~200 µL) was carefully placed into the dam using a micro-pipette. The craniotomy was covered to prevent the dye from photo-bleaching. The dye solution in the dam was circulated and replenished with fresh dye solution every 5-10 minutes (Lippert et al., 2007). After approximately 2 hours of staining, the unbound dye was washed out with saline. Saline was applied to the brain surface after washing. Imaging was performed through saline on the brain surface. Saline was replenished throughout the experiment.

3.2.3 Optical imaging

The excitation light source was a 150W halogen lamp filtered at 621-643nm. The fluorescence signals were collected with a MiCam02 camera system (BrainVision, Japan). The camera was focused onto layer 2/3, at approximately 300 µm below the pia surface (Petersen et al., 2003a). The frame was 184x123 pixels, at 200 Hz (5 ms per frame). Prior to each trial, a background image of the craniotomy (F0) was recorded. The objective lens was 1x and the condenser lens was 0.63x. The magnification was 1.6x. The field of view was 3.5 mm x 2.3 mm and the pixel size was 18.9 µm x 18.9 µm. All individual frames of 25-50 single trials were recorded.

3.2.4 Vibrissa stimulation

Vibrissae were deflected with an exponentially rising (τ = 2 ms) and decaying saw-tooth waveform of 17 ms in duration in the rostral-caudal plane. Each trial had 200 ms of pre-stimulus recording. Under the non-adapted condition, a single deflection, referred to as the test probe, was delivered to a single vibrissa. In adapted trials, the same probe was preceded immediately by an adapting stimulus train of 1000 ms on the same vibrissa,

with no additional time between the adapting train and the test probe. The same protocol described above was presented to an adjacent vibrissa in the next trial.

I varied the stimulus protocol in imaging experiments such that for some animals, the adapting stimulus was delivered onto both whiskers at the same time, and for others onto a single whisker. There were no qualitative differences. Because of the physiological variations, the adjacent pair of vibrissae stimulated was not always the same pair across animals. Typically, the surgery technique allowed a craniotomy centered around D2; barrels with good VSD staining and devoid of bleeding were chosen (for animal #1: E3 and E4; #2: D2 and D3; #3: E1 and E2; #4: C2 and C3; #5, #6: C1 and C2; #7: D1 and D2).

Each trial was 5000 ms, and there was at least 3800 ms of rest between the last deflection and the next trial. Stimulation protocols were presented in random order and repeated 25-50 times. Therefore, a test probe under the same adapting condition was separated from its next presentation by at least 120 seconds. The design to interleave adapting stimulus conditions controls for physiological state changes over time, such as those related to anesthesia and spontaneous cortical activity.

The frequency of the adapting stimulus train was 4, 10, 20, or 40 Hz, and the deflection velocity was 100, 500, 1200, 2500, or 3500 °/s. The total energy in the adapting stimulus was the square of whisker displacement integrated over time. In order to evoke a robust non-adapted response in each animal, the test probe ranged from 1200 °/s to 3500 °/s among 7 animals.

3.2.5 Data analysis

Raw VSD images were processed in MATLAB as previously described in the Methods of Chapter 2. To normalize each dataset, the non-adapted response was trial-averaged and spatially-filtered (a 5x5-pixel or approximately 0.1 mm x 0.1 mm median, then a 5x5-pixel average spatial filter). The filtered image was then fitted with a 2-dimensional Gaussian function by the least squared error algorithm. All $\Delta F/F_0$ pixel values were normalized to the amplitude of this Gaussian function for each vibrissa. The magnitude and area of the response for each adapting stimulus condition were quantified. The response for each stimulus condition was trial-averaged and spatially filtered as described above. To produce more accurate Gaussian fits, the elliptical parameters produced by the non-adapted Gaussian fit (center pixel and major/minor axes ratio) were imposed on the filtered image. The filtered image was then rotationally averaged. A pixel value threshold (see *Adaptation Intensity* below) was applied to the image, then the least square algorithm was used to derive a 2-dimensional Gaussian fit. The magnitude of the response was the amplitude of the Gaussian fit, and the area was represented by the pixels within +1 standard deviation of the Gaussian center.

3.2.6 Adaptation intensity

To quantify the extent of cortical adaptation for each stimulus condition, an adaptation intensity was defined as follows. First, the response ratio for a given stimulus condition was calculated, which is the total fluorescence in the trial-averaged adapted response divided by that in the trial-averaged non-adapted response. For each stimulus condition, the trial-averaged image was filtered with a 5x5-pixel (approximately 0.1 mm x 0.1 mm) median then a 5x5-pixel average spatial filter. Total fluorescence was the sum of all pixels above the pre-stimulus noise threshold, defined as the mean + 1 standard deviation of all pixel values from the trial-averaged pre-stimulus frames. Adaptation intensity

equals 1 minus the response ratio, so that intuitively, the most intense adaptation condition corresponds to an adaptation intensity of 1, while an adaptation intensity of 0 signifies non-adapted condition.

3.2.7 Ideal observer analysis

Detection: The response variables were extracted as described in Chapter 2. The primary region response variable was defined as the decision variable (DV) for this analysis. For each stimulus condition, the DVs from all single trials were binned and fit with a Gaussian probability function, referred to as the signal distribution. A pre-stimulus noise distribution was formed by the decision variables extracted from pre-stimulus frames (150 ms preceding the first stimulus) in all non-adapted trials, referred to as the noise distribution. From the perspective of an ideal observer of cortical activation, each single trial in the signal distribution and noise distribution was classified as either signal or noise using the Likelihood Ratio Test (LRT). Given a single trial response variable *R*, the log ratio of the probability that the response was a signal, *P(S|R)*, to the probability that the response was noise, *P(N|R)*, was used to classify the trial. A non-negative log likelihood ratio classifies the trial as signal, and otherwise noise. With an equal probability of signal and noise, Bayes' rule expresses the log likelihood ratio as follows:

$$\ln\left(\frac{P(S|R)}{P(N|R)}\right) = \ln\big(P(R|S)\big) - \ln\big(P(R|N)\big) \qquad Eq(1)$$

For normal distributions, this expression becomes:

$$-\frac{1}{2}\,(R-\mu_s)'{\Sigma_s}^{-1}\,(R-\mu_s) - \frac{1}{2}\ln|\Sigma_s| - \left(-\frac{1}{2}\,(R-\mu_n)'{\Sigma_n}^{-1}\,(R-\mu_n) - \frac{1}{2}\ln|\Sigma_n|\right)$$

Eq (2)

where μ_s is the mean of the signal response variables, $\sum_s$ is the covariance (variance in this one-dimensional variable case), and μ_n , $\sum_n$ the mean and covariance of the noise response variables (Duda et al., 2001). The likelihood ratio test is validated with the "leave-one-out" method, where a detection decision for a single trial is made based on the model (average and variance) calculated using the rest of the trials. The fraction of correctly classified trials was the final measure for detectability. The same noise distribution was used in all adapting conditions. To ensure the results were not sensitive to the choice of pre-stimulus time frames, the analysis was repeated using noise distributions derived from the time frame following the adapting stimulus. Briefly, for each adapting condition, the set of frames in the 25 ms period preceding the test probe (after the adapting stimulus) was used to form its own "adapted noise distribution". Using adapted noise distributions for each corresponding adapted signal, the detection performance still showed a monotonic decrease with adaptation (see Figure 3.3F).

Discrimination: As the animal likely further distinguishes the stimulus features only after it is detected, only detectable trials were considered for discrimination analysis. The primary response variable of a single trial must be above the detection threshold, which was calculated from the noise distribution of each whisker stimulation data where the threshold value yielded the 10% false-alarm rate observed in previous behavioral studies (Stüttgen et al., 2006; Stüttgen and Schwarz 2008; Ollerenshaw et al., 2012). The noise distribution was formed as described in the detection analysis. The detection threshold is a value such that the probability of obtaining a pre-stimulus noise value above the threshold, thus resulting in a misclassification of noise as a signal (false alarm rate) is 10%. To ensure that the discrimination result does not solely depend on a particular level of detection threshold, the analysis was repeated for a range of assumed thresholds. Specifically, the discrimination analysis was performed with the threshold set to 0, 25, 50, 75, and 100% of the detection threshold. Regardless of the detection threshold value,

including the 0% level which essentially constituted no threshold, the discrimination result was qualitatively the same (see Figure 3.5E). The analysis was repeated using noise distributions after the adapting stimulus. Detection thresholds were derived specific to each adapting condition, using the adapted noise distributions described above (see *Detection*). Again, the discrimination performance was qualitatively similar (see Figure 3.5F).

As with all electrophysiological studies, the data are impaired by limited trials. The duration of data collection in an average VSD experiment is limited to approximately 2 hours, mainly due to photo-bleaching. Thus, the number of trials for each stimulus condition is low. To rectify this, all response variables from 7 animals were normalized (see Data Analysis), merged, and grouped according to their adaptation intensity. The majority of data sets were normally distributed. Gaussian probability functions were then fitted to the merged data to obtain estimates of the parameters (mean, variance, and covariance). As the raw data are limited and noisy samples, unlimited samples from the fitted parametric model were used.

In detail, for each stimulus condition, the adaptation intensity was calculated from its trial-averaged image. For each detected trial within that stimulus condition, the response variables in the two adjacent barrels, $\boldsymbol{R}$ (R_1, R_2), were extracted and normalized (see *Data Analysis*, Chapter 3). Because the responses from two adjacent whisker deflections were approximately symmetric, for each adaptation intensity, all primary and adjacent variables were designated as trials from whisker 1 stimulation, duplicated with reversed primary and adjacent values, and designated as trials from whisker 2 stimulation. All response variables across 7 animals (14 whisker deflections) with the same adaptation intensity were merged, and the mean μ (μ_1, μ_2), standard deviation σ (σ_1, σ_2), and covariance σ_{12} were calculated. The centers of the cluster, marked with black crosses,

represent the trial-average responses μ (μ_1, μ_2). The ellipses outline 2 standard deviations. The eccentricity of the ellipse represents the noise correlation (Pearson correlation coefficient) between R_1 and R_2.

Regression analysis was used to determine the relationship between these parameters and adaptation intensity, and to determine the simplest and most appropriate perspective for the subsequent analyses. The difference between the primary and adjacent means, which determines the distance between the cluster centers, did not show any correlation with adaptation intensity (r = -0.17, p = 0.61, data not shown) or with the mean of the cluster (r = 0.46, p = 0.16, data not shown). Because the standard deviation of primary barrel variables is correlated with that of the adjacent barrel variables (r = 0.87, p = 0.0005, see Figure 3.5B), they are presented as a combined standard deviation, $\sqrt{\frac{(\sigma_1^2+\sigma_2^2)}{2}}$. The combined standard deviation is highly correlated with primary (r = 0.97, p <0.0005) and adjacent (r = 0.97, p <0.0005) standard deviation and the covariance (r = 0.99, p <0.0005). The noise correlation was defined as the ratio of the covariance to the product of the primary and adjacent standard deviations, which is the Pearson correlation coefficient between R_1 and R_2.

Trials (n=1000) were drawn from a 2-dimensional Gaussian distribution with the parameter values indicated in Figure 3.5B and C. Because the distance between the cluster centers did not change with adaptation, the values shown here all used a typical value from the non-adapted state. Each single trial was then classified using the Likelihood Ratio Test. Similar to the detection analysis in Figure 3.3, the direction of stronger adaptation on the map was determined by the decreasing combined standard deviation with adaptation intensity (for adaptation intensity and μ_1, r = -0.73, p = 0.011, for μ_1 and the combined standard deviation, r = 0.62, p = 0.043, data not shown). For

the observed response $\boldsymbol{R}$ on a given trial, the log ratio of the probability that the response resulted from whisker 1 stimulation, $P(W_1|\boldsymbol{R})$, to the probability that the response resulted from whisker 2 stimulation, $P(W_2|\boldsymbol{R})$, was used to classify the trial. A non-negative log likelihood ratio classifies the trial as whisker 1 stimulation, and otherwise whisker 2 stimulation. The likelihood ratio is:

$$\ln\left(\frac{P(W_1|\boldsymbol{R})}{P(W_2|\boldsymbol{R})}\right) = \ln(P(\boldsymbol{R}|W_1)) - \ln(P(\boldsymbol{R}|W_2)) \qquad Eq(3)$$

For normal distributions, this expression becomes:

$$-\frac{1}{2}(\boldsymbol{R}-\mu_1)'\Sigma_1{}^{-1}(\boldsymbol{R}-\mu_1) - \frac{1}{2}\ln|\Sigma_1| - \left(-\frac{1}{2}(\boldsymbol{R}-\mu_2)'\Sigma_2{}^{-1}(\boldsymbol{R}-\mu_1) - \frac{1}{2}\ln|\Sigma_2|\right.$$

Eq (4)

where μ_1 is the mean of the whisker 1 stimulation response vectors, $\sum_1$ the covariance matrix, and μ_2, $\sum_2$ the mean and covariance matrix of the whisker 2 stimulation response vectors (Duda et al., 2001). The likelihood ratio test is validated with the "leave-one-out" method, and the fraction of correctly classified trials was the final measure for discriminability. Because the data satisfy the condition that, $\mu_1\sigma_2^2 > \mu_2\sigma_1^2$, the outcome of the LRT was directly determined by the unity line. That is, for whisker 1 deflection data points, any trial that is below the unity line would be correctly classified as whisker 1 deflection, and any trial that is above the unity line (meaning the adjacent barrel fluorescence is greater than the primary barrel value) would be misclassified as whisker 2 deflection.

3.3 Results

To investigate how the dynamics of sensory adaptation mediate the spatiotemporal activation of the cortex and the possible implications for the cortical code, I employed voltage-sensitive dye (VSD) imaging of the cortex in response to a range of tactile inputs in the rat vibrissa system. I then performed ideal observer analysis to analyze the potential effects of sensory adaptation on cortical information coding. For a detection task, each trial was classified as detected signal or noise based on the average fluorescence in the primary barrel; for a discrimination task, each trial was classified as whisker 1 or whisker 2 deflection, based on the average fluorescence in both primary and adjacent barrels.

3.3.1 Frequency and velocity of adapting stimuli differentially shape cortical response

It is well established that the barrel cortex is highly sensitive to the frequency and velocity of whisker deflections, which are primary parameters comprising the kinetic signature of whisker motion (Arabzadeh et al., 2004, 2005; Chung et al., 2002; Khatri et al., 2004; Moore, 2004; Ritt et al., 2008; Temereanca et al., 2008; Wolfe et al., 2008). Therefore, I investigated to what extent these properties of the adapting stimulus shape the cortical response, particularly the spatial activation, through VSD imaging. An example of this characterization is shown in Figure 3.1. I compared the cortical responses to a 1200°/s punctate deflection, referred to here as the test probe, recorded under different conditions. First, in the absence of any prior adapting deflections of the vibrissae, the recorded cortical response to the test probe was referred to as the non-adapted response, a typical example of which is shown on the top panel of Figure 3.1. For the adapted responses, the cortical activation was recorded in response to the test probe stimulus following an adapting stimulus of varying frequency and velocity (see

Methods). In this example, 9 different adapting trains were derived from the combination of 3 frequencies (4, 10, and 20 Hz) and 3 deflection velocities (100, 500, and 1200 °/s), while the test probe remained a single deflection of 1200 °/s on either one of two adjacent whiskers before and following adaptation. Each image in the grid shows the response to the test probe following an adapting stimulus of a certain frequency and velocity. The responses shown are time-averaged from signal onset to peak (10-25 ms post-stimulus).

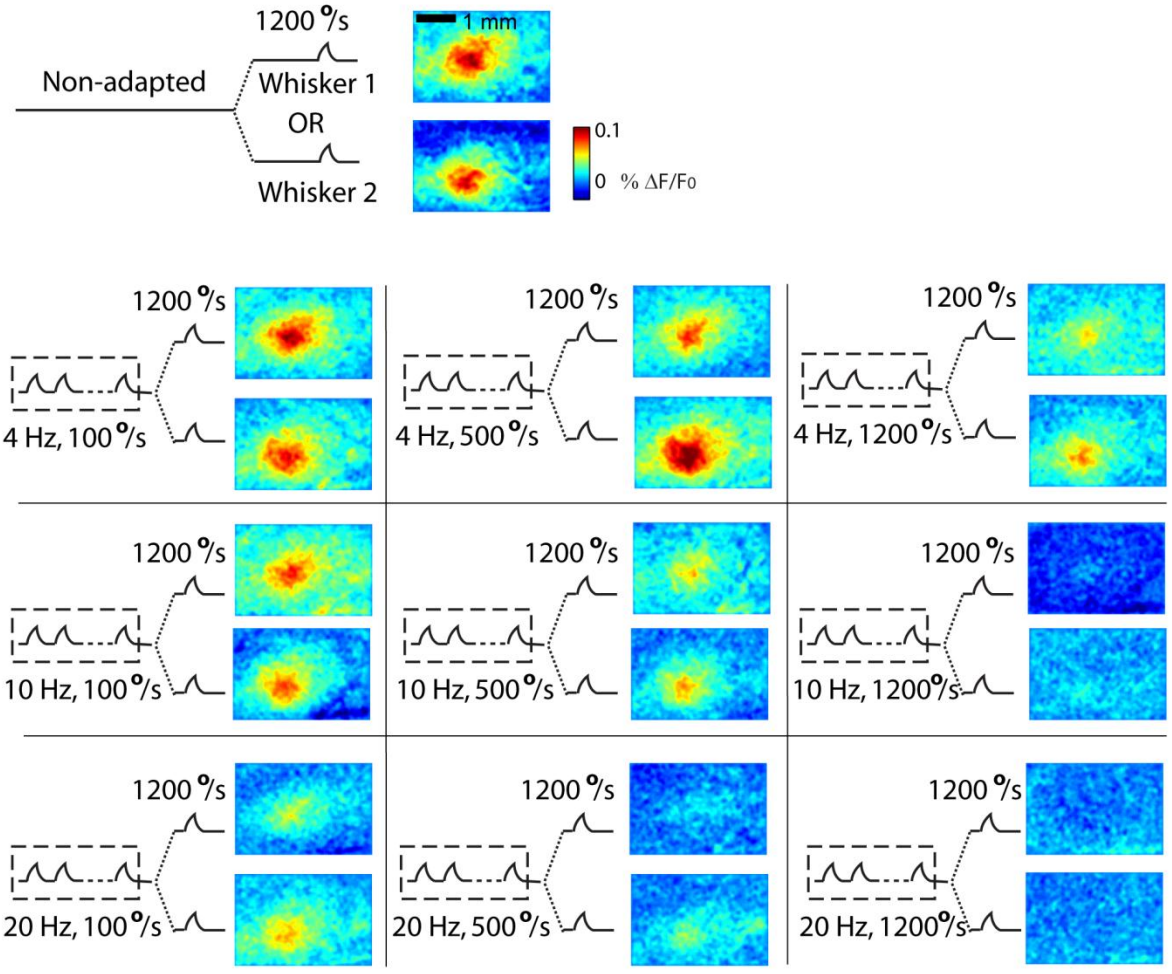

Figure 3.1 Cortical responses to separate deflections on two adjacent whiskers. Whiskers deflected were E3 and E4 separately, responses were averaged over 30 trials. **Top:** Non-adapted response, stimulus protocol consisted of two separate single deflections on the two adjacent whiskers (top image shows the response to a deflection on E3 only, bottom image shows the response to a deflection on E4 only).

Bottom: Adapted responses. For a given trial, an adapting stimulus train was applied on a single whisker for 1000 ms at 4, 10, or 20 Hz and each deflection within the adapting stimulus was 100, 500, or 1200 °/s, resulting in 9 combinations of adapting stimuli. A single deflection followed on the same whisker as a probe, at a fixed velocity across all adapting stimulus conditions. Images were trial-averaged and time averaged from signal onset to peak (10 – 25 ms after stimulus onset). The cortical response became increasingly suppressed with increasing frequency and/or velocity.

The non-adapted state showed significant qualitative overlap of the cortical responses to adjacent whisker stimuli. Adaptation tended to attenuate the magnitude of the cortical responses, while also spatially localizing the response, consistent with previous studies describing the spatial "sharpening" of the cortical response following adaptation (von Békésy, 1967; Kleinfeld and Delaney, 1996; Lee and Whitsel, 1992; Moore, 2004; Moore et al., 1999; Ollerenshaw et al., 2014; Sheth et al., 1998; Simons et al., 2005). This effect, however, was very dependent upon the nature of the adapting stimulus. At any given velocity of the adapting stimulus, as the frequency of the adapting stimulus increased (top to bottom), the cortical response to the test probe decreased in magnitude and in area. Similarly, at any given frequency, as the velocity increased (left to right), the cortex was also increasingly suppressed. Most importantly, different adapting stimulus trains led to similar cortical responses. For example, an adapting stimulus with low frequency but high velocity (such as 4 Hz and 1200 °/s) and one with higher frequency but lower velocity (such as 10 Hz and 500 °/s) had qualitatively similar effects on the response to the same probe stimulus. Note that in this experiment, I additionally tested the entire range of velocities coupled with a frequency of 40 Hz, but the resulting cortical response was largely suppressed, even more so than for the 20 Hz case (not shown). These same qualitative effects were noted across all experiments (n = 7 animals, 14 whiskers), although the exact combinations of the velocities and frequencies of the adapting stimuli were slightly different across different animals (see Methods).

This qualitative observation, coupled with previous findings (Arabzadeh et al., 2004), suggested that the total energy in the adapting stimulus might be the relevant determinant of the degree of adaptation. Here, I define the total energy in the stimulus as the square of the whisker deflection angle, integrated over the duration of the adapting stimulus, as in the top of Figure 3.2A. Although this would be analytic for purely sinusoidal inputs, for the pattern of exponentially rising and decaying deflections presented, the energy was computed numerically (see Methods). Figure 3.2A shows that the adapting stimulus energy increased with higher frequency and/or velocity. An adapting stimulus with higher frequency but lower velocity had a similar energy as one with lower frequency but higher velocity. In terms of the cortical response, the adaptation intensity was derived as a metric for the degree of adaptation, similar to those commonly used in studies characterizing adaptation in spiking activity (Chung et al., 2002; Higley and Contreras, 2007; Khatri et al., 2004). It was defined as 1 minus the ratio of the total fluorescence in the trial-averaged image of the adapted response to that of the corresponding non-adapted response (see Methods). Figure 3.2B shows that the adaptation intensity increased with increasing adapting stimulus energy ($r = 0.96$, $p < 0.0005$), demonstrating that a continuum of adapted responses exists, and that the degree of adaptation is shaped by the temporal feature of the adapting stimulus. Note that each data point is the average of all adaptation intensities within a range of adapting stimulus energy. Thus, different frequency and velocity combinations can result in similar adaptation intensities.

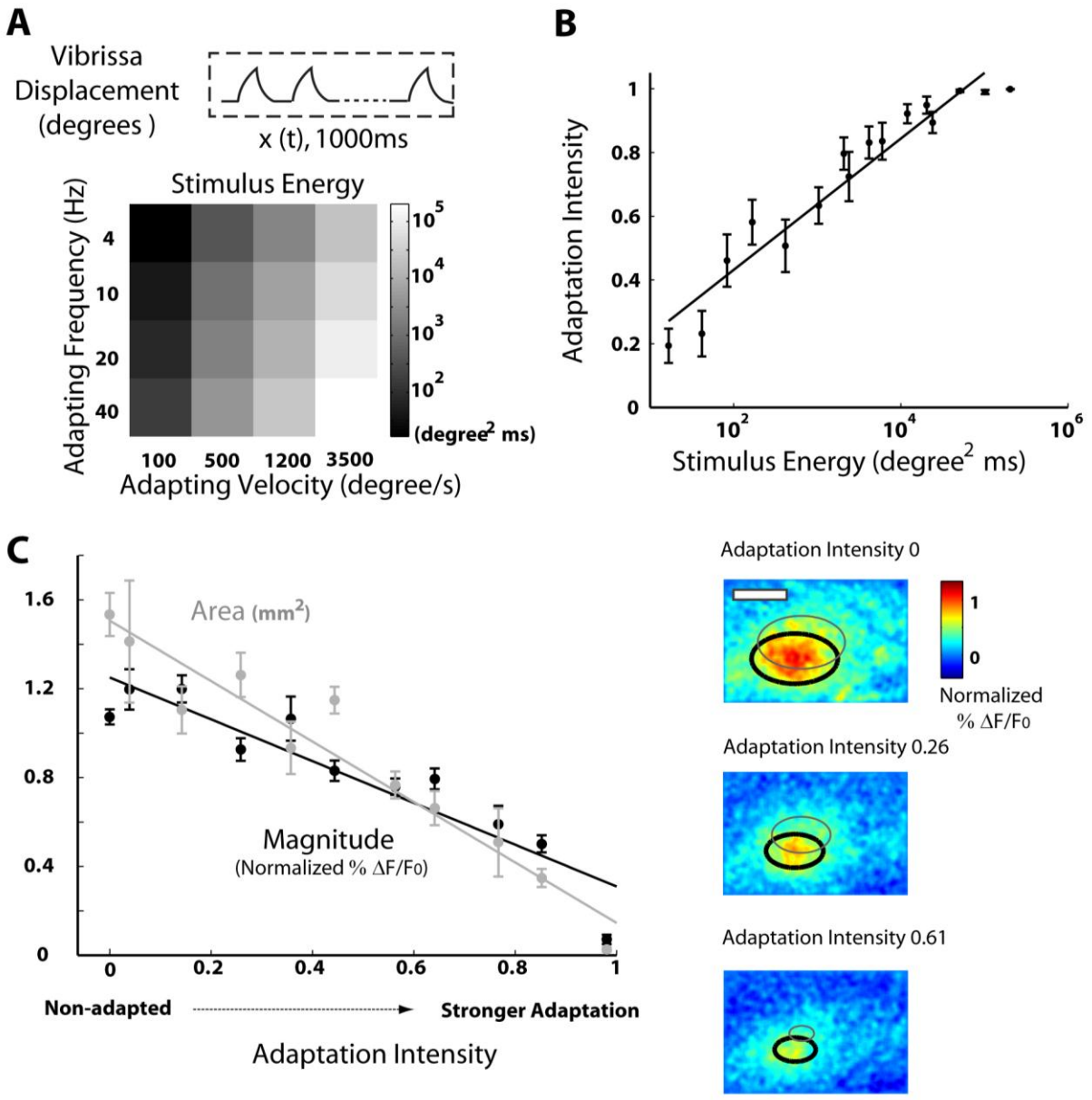

Figure 3.2 Cortical response decreased in both magnitude and area with stronger adapting stimulus energy.

A. The total energy in the adapting stimulus increased with frequency and/or velocity such that a high frequency / low velocity adapting stimulus contained similar energy as a low frequency / high velocity stimulus, as shown in the grid on log scale.

B. Adapting stimulus energy determined the extent of cortical suppression. Adaptation intensity, defined as 1 minus the ratio of total fluorescence in the trial-averaged adapted response to that of the corresponding non-adapted response (see Methods), was used to quantify the extent of cortical response suppression. A higher adaptation intensity

indicated stronger adaptation. Average adaptation intensity was correlated with the total energy in the adapting stimuli. Error bars represent +/-1 standard error of the mean.
C. Both magnitude and area of the response decreased with adaptation. With stronger adaptation, or higher adaptation intensity, both the magnitude and the area of the response decreased. An example of this phenomenon is shown on the right. In the non-adapted state (adaptation intensity of 0), the trial-averaged image (over 30 trials) had a strong magnitude and a large area spread. The contour of a two-dimensional Gaussian fit was superimposed (black) to show the quantification of area. With stronger adaptation, there was a gradual decrease in magnitude and area spread. The Gaussian contour of the response to the corresponding adjacent whisker deflection was superimposed (grey outline), demonstrating that stronger adaptation reduced area overlap between the responses from the adjacent barrels.

As shown qualitatively in Figure 3.1, as the cortex adapts, both the magnitude and the area of the response tend to decrease together. To quantify the above observations in detail, a two-dimensional Gaussian model was fit to the trial-averaged image (see Methods). The magnitude of the response was defined as the amplitude of the Gaussian fit, and the response area was defined as the area of the Gaussian contour at 1 standard deviation (examples of which are shown in Figure 3.2C, right column of VSD images). Figure 3.2C shows the trial-averaged magnitude (black curve) and the area (grey curve) spanning the adapting stimulus energy range. The trial-averaged magnitude and area for each stimulus condition were binned according to their adaptation intensity, thus each data point represents the mean and standard error of multiple trial-averaged responses in the same range of adaptation intensity. As an example, the right column shows the trial-averaged responses at three different adaptation intensities. As adaptation intensified, the response magnitude decreased (correlation between average magnitude and adaptation intensity $r = -0.93$, $p < 0.0005$), as demonstrated in the example images. At the same time, the area of the response also decreased ($r = -0.97$, $p < 0.0005$), as shown by the bold black outlines in the example images. When the contour of the response to the corresponding adjacent whisker deflection was superimposed (grey outlines), it was evident that the responses to the two adjacent whisker deflections became less overlapped

as adaptation intensified. Qualitatively, this seems to suggest that as the magnitude decreased, the response may become harder to detect; however, as the area also decreased, it may become easier to discriminate between the responses to adjacent whisker deflections. Although many studies have posited that a spatially sharpened response at the level of cortex may be a potential mechanism for enhanced spatial acuity observed in psychophysical studies (von Békésy, 1967; Lee and Whitsel, 1992; Moore, 2004; Moore et al., 1999; Sheth et al., 1998; Simons et al., 2005), the relationship between average response and quantitative information conveyed trial-to-trial is not trivial (Averbeck et al., 2006; Pouget et al., 1999). Only recently has the cortical response been analyzed on a single-trial basis in terms of what information is available for detection and discrimination tasks (Ollerenshaw et al., 2014; Wang et al., 2010). However, these studies investigated the cortical information and detection-discrimination tradeoff in a binary manner, either in the presence or absence of an adapting stimulus. How the properties of adapting stimulus and the continuum of cortical responses may shape the detectability and spatial discriminability of the whisker inputs, therefore, is unknown. Furthermore, it is also the case that accurately determining the cortical area of activation involves several arbitrary assumptions and is itself non-trivial. I therefore turn to ideal observer analysis as a simpler and more powerful description of the information conveyed by the cortical signals.

3.3.2 Adaptation degrades detectability of the stimulus

To assess the potential significance of the changes in the cortical activation following adaptation, I evaluated the ability of an ideal observer to discern between the spatially disparate whisker stimuli. Because the adaptation affects not only the area of cortical activation, but also the magnitude of cortical activation above the intrinsic noise level, I considered both the discriminability of spatially disparate stimuli as well as their detectability, as the coupling between these two aspects of cortical activation suggested a

tradeoff between detectability and discriminability. In the detection task, the ideal observer of the cortical recordings was required to report whether a whisker had been deflected; in the discrimination task, the ideal observer reported which of the two adjacent whiskers was deflected.

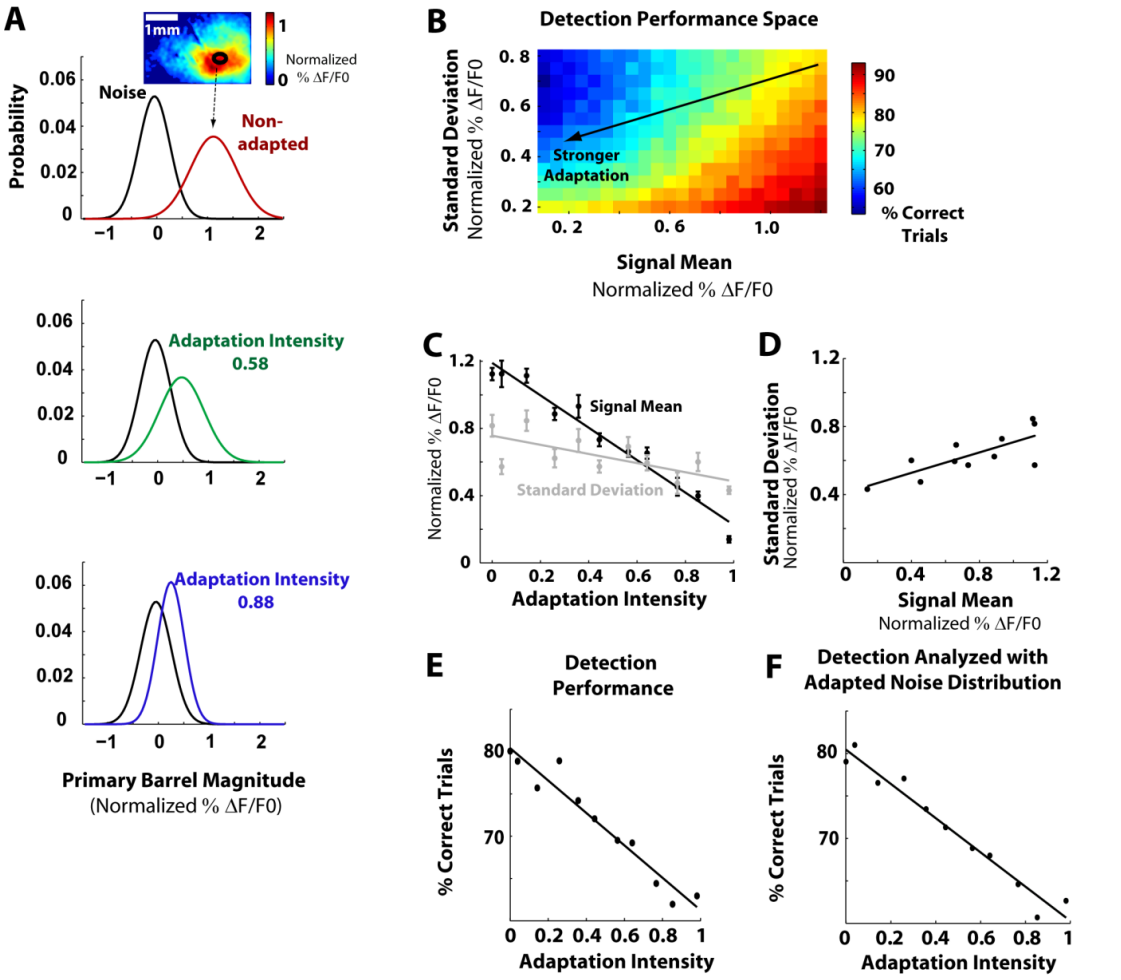

Figure 3.3 Detectability of the stimulus was degraded with adaptation.
A. Detection performance of an ideal observer measures the separation of the signal distribution from the noise distribution. This was defined as the percentage of trials correctly classified as signal or noise using the Likelihood Ratio Test (LRT, see Methods). As the three examples demonstrated, the mean and standard deviation of the signal distribution both decreased with adaptation, which would have opposite effects on the separation of signal from noise.
B. The optimal detection performance increased with larger signal mean but smaller standard deviation. The change in standard deviation and mean induced by adaptation is indicated by the black line. The arrow indicates the direction of stronger adaptation.

C. The mean ($r = -0.98$, $p < 0.0005$) and standard deviation ($r = -0.7$, $p = 0.017$) of the signal distribution decreased with adaptation intensity.
D. The standard deviation of the signal distribution is correlated with its mean ($r = 0.76$, $p = 0.0068$).
E. As signal mean and standard deviation both decreased with stronger adaptation, the detection performance on the line shown in B also decreased with stronger adaptation.
F. Detection performance is qualitatively the same when analyzed using the noise distribution following the adapting stimulus.

Figure 3.3 shows the detection performance on a single-trial basis from the ideal observer's perspective. Figure 3.3A shows examples of signal and noise probability distributions from one animal at 0 (non-adapted), medium, and high adaptation intensities. The signal distribution consisted of all single-trial responses, where each trial was represented by the average fluorescence in the primary barrel (Figure 3.3A inset, see Methods). Both the noise and signal distributions were characterized as Gaussian distributions (see Methods). In the framework of conventional signal detection theory, the detectability of a signal is a function of the separation between the signal distribution and the noise distribution – a correct classification of an observation as signal depends on attributing the observation to the signal distribution and not to the noise distribution, and vice-versa (Macmillan and Creelman, 2004). The separation between the signal distribution and the noise distribution is determined by two factors: the distance between their means and their standard deviations. Qualitatively, a smaller distance between the means obscures the distinction between two distributions, and a smaller standard deviation has the opposite effect (Macmillan and Creelman, 2004).

To fully quantify the effects of the mean and standard deviation on detectability in this framework, the optimal classification performance for a range of these parameters was calculated (Figure 3.3B). For each mean and standard deviation (corresponding to a single square in the color map in Figure 3.3B), 1000 single trials were drawn from a normal distribution with the given signal mean and standard deviation designated as

"signal" trials, and 1000 single trials from a normal distribution with the constant pre-stimulus noise mean and standard deviation designated as "noise" trials. Any given single-trial response $\boldsymbol{R}$ was optimally classified by the Likelihood Ratio Test (LRT), where the probability that $\boldsymbol{R}$ was a signal trial, $P(S|\boldsymbol{R})$, was compared to the probability that it was a noise trial, $P(N|\boldsymbol{R})$. A single trial was correctly identified as a signal if $P(S|\boldsymbol{R}) > P(N|\boldsymbol{R})$, but misclassified as noise if $P(S|\boldsymbol{R}) < P(N|\boldsymbol{R})$. Any given single noise trial was similarly classified. The percentage of trials correctly classified was defined as detectability. Therefore, each square on the color map represents the theoretical optimal classification performance given a noise distribution and a signal distribution, where chance is 50%. I show that, for a given noise distribution, detectability decreased with smaller mean of the signal distribution, but increased with smaller standard deviation.

However, as shown in Figure 3.3A, both the mean and the standard deviation of the signal distribution decreased with more intense adaptation, making the possible effects of adaptation on detection ambiguous. Thus, I quantified the relationship between the mean and the standard deviation of the signal distribution as the system adapts. As shown in Figure 3.3C and D, with increasing adaptation intensity, both the mean and standard deviation of the signal distribution decreased (for mean $r = -0.98$, $p < 0.0005$, for standard deviation, $r = -0.7$, $p = 0.017$), and the standard deviation decreased with smaller mean (Figure 3.3D, $r = 0.76$, $p = 0.0068$). Mean and standard deviation were averaged across animals (n = 14 barrels, 7 animals). The linear relationship between the mean and the standard deviation in Figure 3.3D was traced by the black line on the LRT color map in Figure 3.3B, with the arrow indicating the direction of stronger adaptation (same as the direction of decreasing mean with stronger adaptation, as quantified in Figure 3.3C). Extracting the LRT results along the line, detection performance decreased nearly 20% monotonically with stronger adaptation (Figure 3.3E).

For simplicity in the analysis, the same noise distribution was used in all adapting conditions. To ensure the result was not sensitive to the choice of pre-stimulus time frames, analyses were repeated using noise distributions derived from the time period following the adapting stimulus (see Methods). The detection performance still showed a monotonic decrease with adaptation from approximately 80% to 60%, as shown in Figure 3.3F.

3.3.3 Moderate extent of adaptation enhances discriminability of the stimulus

Figures 3.4 and 3.5 show the discrimination performance on a single-trial basis from the ideal observer's perspective. Each single trial was represented with a two-dimensional variable, consisting of the average fluorescence in the cortical barrel-related columns corresponding to the two adjacent whiskers (denoted R_1 for barrel 1 and R_2 for barrel 2, Figure 3.4A, see Methods). The response of barrel 1 to deflection of whisker 1 is denoted $R_1|W_1$, while the response of barrel 2 to deflection of whisker 1 is denoted $R_2|W_1$, and so on. For each stimulus condition, all trials form a scatter plot (Figure 3.4B).

As it is unlikely that either the animal or the ideal observer could distinguish the stimulus features without detecting the stimulus first, only detectable trials were considered for discrimination analysis. Because behaving animals are observed to respond to approximately 10% of stimulus-absent trials in a detection task (Stüttgen et al., 2006; Stüttgen and Schwarz 2008; Ollerenshaw et al., 2012), I utilized a detection threshold value that yielded 10% false-alarm rate (see Methods).

Due to experimental constraints in the VSD imaging, the trials available for discrimination were limited. Thus, all detectable trials across all animals were normalized to the maximum value in the non-adapted response (see Methods), merged, and grouped

according to their corresponding adaptation intensity (n=7 animals). The responses to either whisker deflection were approximately symmetric, in that the response in the primary and adjacent barrels to a single whisker stimulus mirrored the analogous responses when the adjacent whisker was stimulated. Under this assumption, the responses were further combined, reducing the responses to the primary ($R_1|W_1$), ($R_2|W_2$), and adjacent barrel ($R_2|W_1$), ($R_1|W_2$) responses. Adjacent whisker stimulation responses were mirrored from the combined result.

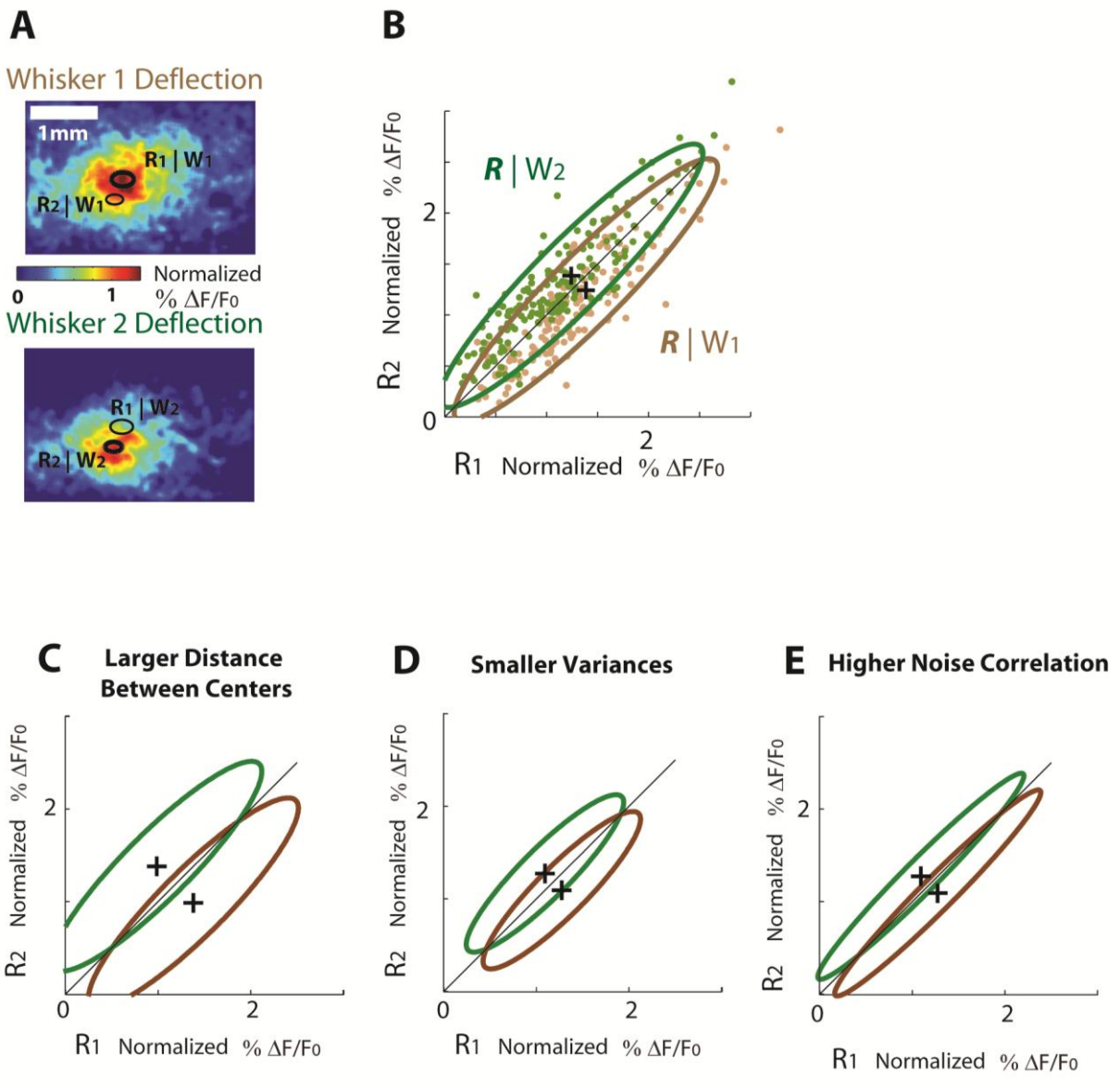

Figure 3.4 Ideal observer analysis of spatial discrimination.
A. The average fluorescence signals in the two stimulated barrels (highlighted with black ellipses) were collected to represent each single trial. The average fluorescence in the barrel corresponding to whisker 1 was designated as R_1 and so on. For whisker 1 stimulation, R_1 was the primary barrel variable, and R_2 the adjacent variable.
B. For each adaptation intensity, the response variables above the detection threshold were collected from all single trials across animals (see Data Analysis in Methods). The response variables R_1 and R_2 were the average fluorescence in the two adjacent barrels (with R_1 corresponding to the primary barrel of whisker 1 and R_2 to that of whisker 2), normalized to amplitude of trial-averaged non-adapted response (see Methods). The brown ellipse outlines the trials from whisker 1 stimulation, and the green ellipse whisker 2. A single trial was classified as a response to either whisker 1 or whisker 2 stimulation using the Likelihood Ratio Test (see Methods). The discrimination performance was defined as the percentage of trials correctly classified. The outcome of the LRT was directly related to the separability of the two clusters, which was determined by the distance between the centers of the clusters (indicated by the crosses), standard deviation (in both horizontal and vertical directions), and correlation of the clusters.
C. A cartoon illustration of improved discriminability by the increased distance between the centers of the clusters.
D. A cartoon illustration of improved discriminability by decreased standard deviations.
E. A cartoon illustration of improved discriminability by increased noise correlation.

An example of the response clusters is shown in Figure 3.4B. The trials from whisker 1 deflection are outlined by the brown ellipse, and the trials from whisker 2 deflection (mirrored from whisker 1 deflection) are outlined in green. The overlap of the two response clusters directly determines the level of performance to expect in discriminating between the deflections of either of the two whiskers. Qualitatively, the overlap of the two-dimensional clusters is determined by the distance between the cluster means (black crosses), their overall standard deviations, and the noise correlation between R_1 and R_2. Noise correlation is computed as the Pearson correlation between R_1 and R_2, as the correlation across trials is not dependent on the average responses to the stimulus, but on the trial-to-trial variability (Averbeck et al., 2006). Figure 3.4C-E provides illustrations of how these key parameters influence the degree of overlap, and thus the level of discriminability. As shown in Figure 3.4C, if the centers of the clusters are farther apart

(compare to the original cluster outlines in Figure 3.4B) while variability and noise correlation were held constant, then the ellipses are farther away from each other. Similarly, if the variability of the individual column response is smaller while the centers and noise correlation remained unchanged (Figure 3.4D), the area overlap between the ellipses also decreases. Finally, if the noise correlation of the responses across columns is higher with the same centers and variability (Figure 3.4E), the ellipses become more elongated and the ellipses are thus less overlapped.

The theoretical optimal classification performance in relation to its determinants is quantified in the color map in Figure 3.5A. The distance between the cluster means was not strongly influenced by adaptation, and was thus not included (see Methods, data not shown). Furthermore, because the variability along the horizontal axis (σ_1, standard deviation of primary barrel variable) and that along the vertical axis (σ_2, standard deviation of adjacent barrel variable) were correlated ($r = 0.87$, $p = 0.0005$, Figure 3.5B), they were jointly presented as a combined standard deviation (see Methods) for a clearer visualization. Thus, assuming a fixed distance between the cluster means, for each given standard deviation and noise correlation combination, the optimal discrimination performance was quantified by classifying 1000 single trials drawn from a normal distribution with the given parameters, which essentially approximates the area overlap between the ellipses. The discrimination performance was evaluated with the Likelihood Ratio Test. Given a particular single-trial response $\boldsymbol{R} = (R_1, R_2)$, the probability that it resulted from whisker 1 stimulation, $P(W_1|\boldsymbol{R})$, was compared to the probability that it resulted from whisker 2 stimulation, $P(W_2|\boldsymbol{R})$. A single trial that was truly drawn from whisker 1 deflection was correctly classified if $P(W_1|\boldsymbol{R}) > P(W_2|\boldsymbol{R})$, but otherwise misclassified as whisker 2 stimulation. Discrimination performance increased with higher noise correlation at a given standard deviation, and with smaller standard deviation at any given noise correlation.

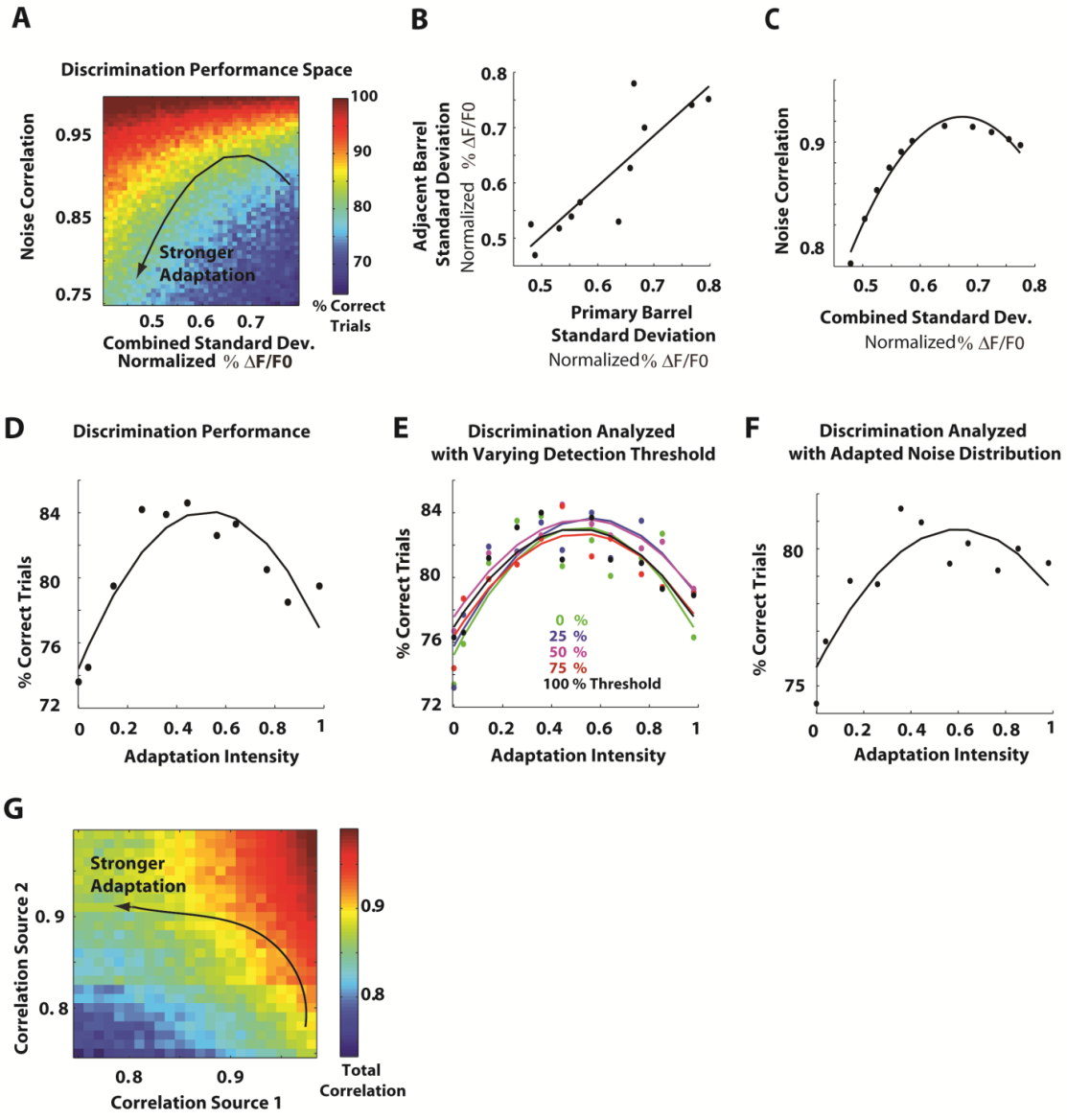

Figure 3.5 Discrimination performance peaked at intermediate adaptation intensity. **A.** Discrimination performance was strongly influenced by variability within column and noise correlation across columns. Discrimination performance increased with higher noise correlation but lower standard deviation of the variable clusters. The change in standard deviation and noise correlation induced by adaptation is indicated by the black curve. The arrow indicates the direction of stronger adaptation. For simplicity, the combined primary and adjacent barrel variable standard deviation is shown on the map because they were well correlated ($r = 0.87$, $p = 0.0005$). The distance between the cluster centers was not included as a factor because it did not demonstrate correlation

with adaptation intensity ($r = -0.17$, $p = 0.61$) or the cluster mean ($r = 0.46$, $p = 0.16$, data not shown).
B. The standard deviation of the primary barrel variables and that of the adjacent barrel variables were correlated ($r = 0.87$, $p = 0.0005$).
C. Correlation across columns was maximal at intermediate within-column variability (combined primary and adjacent barrel standard deviation).
D. The values on the performance map along the black curve in A were extracted and plotted against adaptation intensity. Similar to Figure 3.3C and 8D, the combined standard deviation decreased with stronger adaptation (data not shown). The discrimination performance peaked at an intermediate adaptation intensity.
E. The discrimination performance is relatively insensitive to the detection threshold. Each discrimination performance was evaluated using a fraction of the detection threshold value that yielded 10% false alarm rate (see Methods).
F. Discrimination performance was qualitatively the same when analyzed using the noise distribution following the adapting stimulus.
G. A possible computational mechanism for the overall nonlinear noise correlation. Each axis represents a component of correlated neural activity and each square is the overall noise correlation that is the sum of the two components. The black curve represents a possible scenario where one component increases its noise correlation with adaptation, while the other decreases its noise correlation, thus creating an overarching effect for the overall noise correlation. The arrow indicates the direction of stronger adaptation.

Next, I located where the experimental observations reside in the theoretical optimal performance map in Figure 3.5A. The standard deviation was expected to decrease with adaptation, as shown in Figure 3.3. However, it was not immediately clear how the noise correlation co-varied with standard deviation, and how this would affect discriminability. I found that, similar to data presented in Figure 3.3C and D, the combined standard deviation decreased with stronger adaptation, and that noise correlation was maximal at an intermediate standard deviation (Figure 3.5C, see Methods). This nonlinear relationship between the combined standard deviation and the noise correlation is indicated by the black curve on the color map in Figure 3.5A. The arrow indicating the direction of stronger adaptation in Figure 3.5A is in the direction of decreasing standard deviation. Extracting the LRT results along the curve, I show that discrimination performance followed a similar trend as the noise correlation and reached a maximum at

an intermediate adaptation intensity (Figure 3.5D). This nonlinearity could arise from multiple mechanisms that have opposing effects on correlated activity (see Discussion and Figure 3.5G). Note that relatively modest changes in the noise correlation resulted in a nearly 10% increase in discrimination performance.

Although the choice of detection threshold was based on animal task performance from previous studies (Ollerenshaw et al., 2012; Stüttgen and Schwarz, 2008; Stüttgen et al., 2006), to ensure that the discrimination result does not solely depend on a particular level of detection threshold, the analysis was repeated for a range of assumed thresholds in Figure 3.5E. Specifically, the discrimination analysis was performed with the threshold set to 0, 25, 50, 75, and 100% of the detection threshold. Regardless of the detection threshold value, including the 0% level which essentially constituted no threshold, the discrimination result was qualitatively the same, where the discriminability was the highest at a moderate adaptation intensity of approximately 0.5, but lower at either end of the adaptation spectrum.

In these analyses, the noise distributions were derived from the non-adapted cases for simplicity. It is however possible that the adaptation influences the noise distributions against which signals would be compared. To directly test whether this produced a significant effect, detection thresholds were derived specific to each adapting condition, using the adapted noise distributions described above (see Detection). The discrimination performance was qualitatively the same (Figure 3.5F).

Taken together, the results thus far suggest that varying degrees of adaptation shape detectability and discriminability in distinctly different ways. The detection and discrimination performances as a function of adaptation intensity are summarized in Figure 3.3E and 3.5D. The fact that the detectability decreased monotonically with

increasing amounts of adaptation implies that a stimulus is most detectable in the non-adapted state (adaptation intensity = 0). In contrast, the probability of correctly discriminating a stimulus given that it was detected was the highest at an intermediate adaptation intensity. As described in Figure 3.2B, the adaptation intensity is a function of the overall energy in the adapting stimulus. As a result, the intermediate adaptation intensity corresponds non-uniquely to a range of velocities and frequencies that lead to a stimulus energy of approximately 500 deg^2 ms. For the experimental conditions here, this corresponds to a low velocity adapting stimulus that is in the 10-20 Hz range, or one that has a lower frequency of 4 Hz but a higher velocity. These different modes of vibrissa motion with complementary frequency and velocity could be related to natural whisking behavior that is thought to adapt the sensory pathway in behaving rats and speculated to improve tactile discrimination (Semba and Komisaruk, 1984; Fanselow and Nicolelis, 1999; Moore, 2004).

3.4 Discussion

Rats can reliably discriminate between stimulation of adjacent whiskers, further enhanced by adaptation (Ollerenshaw et al., 2014). Although as in most behavioral studies, this was an artificial task, the performance reflects spatial acuity, much like two-point tactile discrimination in humans. As the rodents palpate objects with their whiskers, the spatial resolution at which the sensors are represented centrally affects information transmitted. If adjacent whiskers cannot be distinguished, they likely convey redundant information, even though they contact different parts of the object. Further, the form of adaptation here carries ethological relevance. Moderate adaptation resulted from either a low-velocity adapting stimulus at a high frequency (10-20 Hz), or one of high velocity but low frequency (4 Hz). In behavioral studies, different frequencies of natural whisking have been observed (Semba and Komisaruk, 1984; Fanselow and Nicolelis, 1999). Importantly, similar to what was demonstrated with passive adaptation here, the higher

frequency range whisking exhibited smaller amplitude and vice versa. I speculate that the frequency-amplitude switch in whisking behavior likely conserves energy in whisking movements, producing similar effects on spatial acuity. With high-energy adaptation, both detectability and spatial discriminability degrade, resulting from high-frequency, high-velocity adapting stimuli not observed in natural whisking. These observations are thus consistent with a continuous modulation of information processing to facilitate the tradeoff between detectability and spatial acuity in the natural environment.

Although adaptation has been widely studied, there is no consensus as to a single hallmark effect or biophysical mechanism, likely pointing to a range of mechanisms and manifestations. Particularly, although a range of studies have shown consistent decreases in firing with adaptation, recent studies have suggested more nuanced effects, with diverse functional consequences across cortical laminae and cell types (Heiss et al., 2008; Higley and Contreras, 2006; Khatri et al., 2004). Demonstrated here with VSD, which captures the aggregate subthreshold activity across cell types within layer 2/3, is a net suppressive effect of adaptation, but the relative contributions of different cell types and mechanisms cannot be determined with this approach. However, the most prominent feature of adaptation, the reduction in cortical activity, is linked to thalamocortical synaptic depression (Chung et al., 2002) and thalamic de-synchronization (Temereanca et al., 2008; Wang et al., 2010), as demonstrated in awake animals (Ollerenshaw et al., 2014). The response modulation by adaptation likely reflects a complex combination of these mechanisms and others. The fact that the cortical response is continuously modulated suggests that at least one mechanism may also operate on a continuum. Finally, it is likely that the adaptive effects observed here are affected by anesthesia. However, it is clear from Chapter 2 (Ollerenshaw et al., 2014) that in the awake state, adaptation results in similar trends in the tradeoff between detectability and discriminability. It further demonstrated in the awake animal clear adaptation effects on

the thalamic inputs that drive the cortical activation, strikingly similar to those observed under anesthesia (Chung et al., 2002; Ganmor et al., 2010; Khatri et al., 2004; Temereanca et al., 2008; Wang et al., 2010). Thus, the fundamental findings here likely reflect how similarly adapting stimuli would shape activation in the awake animal.

Adaptation-induced spatial sharpening has long been speculated as a mechanism for enhanced spatial acuity in psychophysical studies (von Békésy, 1967; Lee and Whitsel, 1992; Moore et al., 1999; Sheth et al., 1998; Simons et al., 2005; Tommerdahl et al., 2002). However, average responses do not dictate the information conveyed (Averbeck et al., 2006; Pouget et al., 1999). In fact, I found that the main factor shaping the discriminability was the noise correlation of activation across cortical columns. Although many studies point out the peril of noise correlation in coding efficiency (Zohary et al., 1994; Abbott and Dayan, 1999; Middleton et al, 2012; Adibi et al 2013), it should be noted that noise correlation can have different effects on coding efficiency, depending on the relationship between the average responses (Averbeck et al., 2006). For neurons sharing functional feature selectivity, such as those in the same column, a stimulus evokes similar average responses in the units recorded. That is, the average responses to two separate stimuli would both be located along the unity line (see Averbeck et al., 2006, Figure 1). In contrast, in the context of the spatial discriminability here, the functional units recorded are two adjacent columns, where a stimulus evokes dissimilar average responses, with the primary barrel having the stronger average response. Thus, increased noise correlation results in an increase in the separability of the responses (see Figure 3.4E).

To explore population correlation and its impact on neural coding, I measured the correlation between the averaged population activity in the primary and adjacent barrels. As briefly discussed in Methods, the neural signal that supports the detection of a sensory

input can be temporally integrated. In particular, decision making often requires integration of information over time (Gold and Shadlen 2007; Huk and Shadlen 2005). In addition, it is unlikely that an animal makes multiple decisions every few milliseconds on a simple stimulus over a very short period of time, as the VSD signal decays after 100 ms. After the peak frame, the VSD signal decays in the primary barrel and spatially spreads throughout the cortex. It can be inferred that these later time frames are not used by the animal in this context since the spatially homogeneous cortical activation in later frames would preclude spatial discrimination, inconsistent with our previous behavioral observations (Ollerenshaw et al., 2014). Therefore, the response in each barrel was further time-averaged from the typical onset time (10 ms post-stimulus, consistent with the cortical response latency in this pathway) to peak of cortical response (25 ms). Although VSD measures population activity, the local VSD signal corresponds well with single unit subthreshold whole-cell recording, indicating an overall high level of synchrony in subthreshold population activity in the cortex (Petersen et al., 2003b). This is consistent with our result of relatively high noise correlation and with findings in cat and monkey visual cortex (Lampl et al, 1999; Chen et al, 2006). However, action potentials in the whole-cell recordings are not detected in the VSD signals. Possibly due to the diverse receptive field properties of layer 2/3 neurons (Simons, 1978), the low firing rate correlation measured in single neuron pairs (Gawne and Richmond, 1993; Zohary et al., 1994; Lee et al., 1998; Romo et al., 2003, Middleton et al 2012) is likely a nonlinear transformation of the population subthreshold correlation measured with VSD. Nevertheless, consistent with part of our findings, Adibi and colleagues (2013) also demonstrated that adaptation increased noise correlation, albeit of firing rates in both single unit pairs and populations.

Further, I found that adaptation non-monotonically influenced the noise correlation. It has been shown that, regardless of stimulus condition, noise correlation in single unit firing

rates is inversely proportional to the mean (Adibi et al., 2013). Here, adaptation monotonically decreased the magnitude of the response to the subsequent whisker deflection. The little-to-moderate range of adaptation was thus consistent with observations from Adibi et al. The more extreme range of adaptation deviates from this prediction, however, likely due to exceedingly strong suppression of activity in this regime. This nonlinearity could arise from several mechanisms having opposing effects on correlated activity. The pre-stimulus noise correlation indicates stimulus-independent correlated activity, likely mediated by internal brain state (Arieli et al., 1996; Kohn et al, 2009; Middleton et al., 2012). The stimulus likely induces another stimulus-dependent noise correlation, which could be mediated by multiple and opposing mechanisms such as background synaptic field and feed-forward inhibition (Middleton et al, 2012). Similar to whisking, adaptation likely places the cortex into a de-synchronized state, thus decreasing the noise correlation (Poulet and Petersen, 2008). On the other hand, adaptation decreases the firing rate in response to the probe stimulus, increasing the noise correlation. Additionally, adaptation has been shown to shift the excitation-inhibition balance (Heiss et al., 2008), which is implicated in high-frequency gamma, thus possibly increasing the noise correlation in the spontaneous state. The nonlinearity in noise correlation likely arises from these diverse mechanisms. Figure 3.5G illustrates the simplest case where the overall cortical activity is the linear sum of stimulus-independent and stimulus-dependent components. Adaptation could potentially increase the noise correlation of one component while decreasing that of the other (traced by the black curve, arrow indicates more profound adaptation), making the overall noise correlation initially increase but decrease with more profound adaptation. However, further investigation is needed to fully elucidate this issue.

Although the results here relate to the effects of passive, bottom-up adaptation on sensory processing, there are potential ties to top-down, internally-regulated processing. The

adapted state has been shown to display similar effects with those brain states signified with high-frequency cortical fluctuation, typically associated with active behavior, such as active whisking. In both adapted state and high-frequency active state, the thalamus displays tonic firing, TC synapse is depressed, and the cortical representation of a stimulus is suppressed. Tonic firing is hypothesized to lead to cortical activities more selective of fine features, as opposed to burst firing that leads to a large sensory-evoked cortical response, favoring detection (Crick, 1984; Lesica and Stanley, 2004; Lesica et al., 2006; Sherman, 2001b). Behaviorally, we demonstrated the improvement of tactile discrimination by adaptation in Chapter 2. Relatedly, rodents move their whiskers rhythmically when exploring the environment, speculated to enhance tactile discrimination (Carvell and Simons 1995; Fanselow and Nicolelis, 1999; Harvey et al., 2001; Moore 2004). Active whisking suppresses S1 response to a single stimulus (Crochet and Petersen, 2006; Fanselow and Nicolelis, 1999; Ferezou et al., 2007), similar to what has been demonstrated through passive adaptation (Ollerenshaw et al., 2014), in alert or task-engaged animals, and in high-frequency active states (Castro-Alamancos, 2004; Otazu et al., 2009). Although the direct effects of centrally-regulated, active whisking and the indirect effects of the associated brain states on cortical representations are not the same as the effects of passive adaptation, the functional similarities of the modulation in activity suggest that these aspects may synergistically reinforce the continuous control of information transmission described here. Furthermore, the continuous effect of adapted states provides further evidence that the brain state is a continuum, rather than discrete states (Harris and Thiele, 2011).

CHAPTER 4 The intrinsic brain states

Portions of this chapter have been presented in poster form in the following:

Zheng, H. J. V., Whitmire, C.J., He, B. J. , & Stanley, G. B., Context-dependent Information Decoding of Sensory-evoked Responses.

Society for Neuroscience (SfN) meeting. Washington D.C., 2014.

Computational and Systems Neuroscience (COSYNE) meeting, Salt Lake City, UT, 2015.

Society for Neuroscience (SfN) meeting. Chicago, IL., 2015.

4.1 Introduction

A fundamental pursuit in neuroscience has been to understand how sensory stimuli are represented in the brain and how this representation translates to perception. The primary somatosensory cortex (S1) is considered one of the most fundamental stages where tactile information is processed and has been shown to play an important role in an animal's perception of a stimulus (O'Connor et al., 2010; Hutson and Masterton, 1986; LaMotte and Mountcastle, 1979; Houweling and Brecht, 2008; Huber et al., 2008; Romo et al., 2000). An important property of the S1 is the high variability of response to the same stimulus under well controlled experimental conditions relative to the lower response variability in earlier stages of the pathway, which implies increasingly more complex and nonlinear processing along the pathway (Lottem & Azouz, 2011, Arabzadeh et al., 2005, Scholvinck et al., 2015).

The cortical response variability arises at least partially from the internal state of the brain. Brain state encompasses a variety of cortical and sub-cortical dynamics, including short-term synaptic plasticity such as thalamocortical (TC) synaptic depression, network

dynamics such as the excitation-inhibition balance, spontaneous spiking and membrane potential fluctuations in individual cells, and the correlated activity among a subset of cells (Buonomano and Maass, 2009; Harris and Thiele, 2011). Brain state is at least partially reflected in the spontaneous activity in the cortex and can be influenced by neuromodulators, bottom-up mechanisms such as adaptation and top-down mechanisms like arousal (Harris and Thiele, 2011; McCormick et al., 2015).

An important distinction of brain states can be made in sleep and wakeful EEG patterns. During sleep, the EEG activity exhibits a characteristic low frequency, large amplitude fluctuation, termed "synchronized state", and switches to a high frequency but small amplitude fluctuation, termed "de-synchronized state", in wakefulness (Moruzzi and Magoun, 1949; Steriade et al., 1993). A variety of top-down behavior changes such as arousal or active whisking in rodents have also been shown to de-synchronize the cortical activity, reflected in the EEG or LFP recordings in the primary sensory cortex, and typically associated with thalamic tonic firing and TC synaptic depression (Castro-Alamancos, 2004; Crochet and Petersen, 2006; Fanselow et al., 2001; Nicolelis and Fanselow, 2002; Poulet et al., 2012). Not only does the spontaneous cortical activity reflect behavior, it has been shown to shape the cortical dynamics and representation of a stimulus. In the synchronized state, the cortex exhibits synchronized low frequency fluctuation, and a sensory stimulus evokes a relatively large response in the cortex, whereas in the de-synchronized state, the cortical response is suppressed (Castro-Alamancos, 2004; Crochet and Petersen, 2006; Curto et al., 2009; Ecker et al., 2014; Poulet and Petersen, 2008; Poulet et al., 2012). These studies suggest that the cortical spontaneous activity provides the context under which the stimulus is encoded and serves to identify the characteristics of responses under behavior-relevant states that may support different tasks of the sensory system.

It has been shown that the state of cortex can spontaneously change, even under anesthesia (Clement et al., 2008; Curto et al., 2009), providing an experimental paradigm to investigate the cortical variability of sensory-evoked response under well-controlled anesthesia without the influence of behavior. Moreover, it has been proposed that the synchronized low-frequency fluctuation is generated by the alternation of UP state (when cells are depolarized) and DOWN state (where cells are silent or hyperpolarized) (McCormick et al., 2015). UP and DOWN states can also occur spontaneously, even under anesthesia (Anderson et al., 2000; Petersen et al., 2003b; Sachdev et al., 2004). During DOWN state, the cortical response to a stimulus is larger than the response in UP state (Li et al., 2009; Petersen et al., 2003b). Hence, within the synchronized state, the phase during which the stimulus occurs could also shape the sensory-evoked response.

Here, under controlled anesthesia and without behavioral influences, I examined the intrinsic cortical states and the sensory evoked response under these states in the rat primary somatosensory cortex. I recorded the local field potential (LFP) in the rat S1 under controlled anesthesia and showed that a whisker stimulus evokes a larger cortical response in the synchronized state than in the de-synchronized state. Within the synchronized state, the same stimulus evokes a larger response in the DOWN state than in the UP state. From the perspective of an ideal observer, the detectability of the stimulus is the highest in the DOWN state, and the spatial discriminability of the stimulus is the highest in the de-synchronized state.

4.2 Methods

4.2.1 Surgery

All procedures were approved by the Institutional Animal Care & Use Committee at Georgia Institute of Technology and in agreement with the National Institutes of Health

guidelines. Seven female albino rats (Sprague-Dawley; 250-330g) were sedated with 4% vaporized isoflurane, then anesthetized intravenously through the tail vein with a Fentanyl cocktail (Fentanyl / Dexmedotodomine / Midazolam 5ug / 150ug / 2mg per mL of cocktail, dosed at 0.5ug / 15ug / 0.2mg per mL of cocktail, 1mL/kg). Following the initial Fentanyl dose, the animal was mounted on a stereotaxic device (Kopf Instruments, Tujunga, CA) on a vibration isolation table. Atropine (0.09 mg/kg, s.c.) was administered subcutaneously to keep the lungs clear of fluid. Lidocaine was injected subcutaneously into the scalp before the initial incision on the head. In all experiments, saline was administered (2 mL/kg/hour) to prevent dehydration. Body temperature was maintained at 37°C by a servo-controlled heating blanket (FHC, Bowdoinham, ME). After the midline incision on the head, skin and tissue were resected and connective tissue was removed. A craniotomy (approximately 3 mm x 4 mm) was drilled on the left hemisphere over the primary sensory cortex (stereotaxic coordinates: 0-4 mm caudal to the bregma, and 4-7 mm lateral to the midline; Paxinos and Watson, 2007). The dura was left intact. A dental acrylic dam was constructed around the craniotomy. At the end of the surgical procedures, a light level of anesthesia was maintained with the Fentanyl cocktail. The animal was euthanized with an overdose of pentobarbital sodium solution after data collection.

4.2.2 Electrophysiology

A low-impedance tungsten electrode (< 1M Ω) was lowered into a barrel typically at a depth of approximately 300-600 μm below pia using a hydraulic micropositioner (Kopf Instruments, Tujunga, CA). A stainless steel skull screw (~1.4 mm in diameter) was installed approximately 2-3 mm posterior and medial to the craniotomy and was driven approximately 1 mm into the skull to make contact with the cerebral spinal fluid (CSF) and the surface of the brain. The skull screw was used as both the electrical ground for the animal and the reference for the recording electrode. The recording electrodes were

manufactured by FHC (impedance: 300-500K Ω, shank diameter: 75 µm, tip taper angle: 15-20º, Bowdoin, ME.) or A-M Systems (impedance: 500K Ω, shank diameter: 127 µm, tip taper angle: 12º, Sequim, WA). The principle whisker was identified by manually deflecting all whiskers that elicited responses at the location of recording and selecting the whisker that evoked the strongest response. The process was repeated until the strength of response to the principle whisker candidate was unambiguously stronger than the responses to all neighboring whiskers. Local field potential was collected at 1K Hz with a Cerebus system (Black Rock Microsystems, Salt Lake City, UT) or a TDT system (Tucker-Davis Technologies, Alachua, FL). The data collected on Cerebus was high-pass (1^{st} order) filtered at 0.3 Hz and low-pass (3^{rd} order) filtered at 7.5K Hz. Because an anti-aliasing filter was not imposed in the Cerebus system, simultaneous data sampled at 30K Hz was analyzed for the frequency content to ensure there was no significant aliasing effect. The frequency content (see 4.2.4 Data analysis, Frequency ratio section) calculated from 1K Hz data and the 30K Hz data were highly correlated ($r > 0.98$, $p < 0.001$). The data collected on TDT systems was high-pass filtered at 0.4 Hz and low-pass filtered at 500 Hz.

4.2.3 Vibrissa stimulation

A multi-layered piezoelectric bending actuator (range of motion: 1 mm, bandwidth: 200 Hz; Polytec PI, Auburn, MA) or a Galvo motor (Cambridge Technology, Bedford, MA) generated vibrissa deflections. The vibrissa was inserted into a 4-cm section of a 20-µl glass pipette (inner diameter ~0.65 mm) fixed to the end of a piezoelectric actuator, or inserted into a hole on the Galvo motor actuator (inner diameter ~0.65 mm). The end of the actuator was then situated 10 mm from the face. Actuator inputs were controlled by a programmable, real-time computer.

Each vibrissa was individually deflected in the rostral-caudal plane in an exponentially rising (τ = 2 ms) and decaying saw-tooth waveform of 17 ms in duration. Each trial had 5000 ms of pre-stimulus recording. A single deflection (average velocity of 200, 500, or 1000-1200 °/s) was delivered. Stimulation protocols were presented in a random order and repeated 50 - 100 times. Each trial was at least 7 seconds.

4.2.4 Data analysis

Normalization: Raw LFP recordings were imported from Cerebus into MATLAB using the software package provided by Black Rock. Aberrant trials with exceeding noise (where non-stimulus related LFP amplitude was outside of the -4mV to 1mV range) were removed. These trials are generally less than 10 per data set and comprise less than 8% of the total trials. To account for the response variability across animals, each dataset (recordings from 1 barrel, 50-100 trials) was normalized to the mean of that dataset, which is the minimum value between stimulus onset and 100 ms post-stimulus of all single trials averaged across trials of that data set. The stimulus-evoked response was defined as the peak value of each normalized single trial from stimulus onset to 100 ms post-stimulus, minus the baseline value at stimulus onset. To ensure that the result did not depend on normalization, the same analyses were performed on un-normalized data. The results were qualitatively similar (see Results). Baseline subtraction did not qualitatively change the results in the de-synchronized and synchronized state. However, the difference in the evoked response amplitude in UP and DOWN states was only relative to the baseline activity (see Discussion).

Frequency ratio: To quantify the frequency content, the spontaneous activity 1000 ms before the stimulus onset was normalized as described above, and the mean value of this epoch of spontaneous activity was subtracted. The frequency content was calculated using a fast Fourier transform (data length 1 second, sampling rate 1K Hz). A frequency

ratio was defined as the ratio of total amplitude in the 1-4 Hz band to that in the 1-50 Hz band, which has been shown to be a good indicator of cortical synchrony (Curto et al., 2009). The amplitude is the complex modulus of the FFT, $\sqrt{Re^2 + Im^2}$, where *Re* and *Im* are the real and imaginary part of the FFT at the given frequency. Figure 4.2A illustrates this definition. Within each dataset, the trials whose frequency ratios were below 33 percentile of the frequency ratio values within that dataset were classified as high-frequency trials; trials with frequency ratios above 67 percentile were low-frequency trials. The rest were medium-frequency trials (Figure 4.2C).

Phase calculation: The instantaneous phase of the LFP was calculated using a Hilbert transform, which convolves the original LFP signal x(t) with the function $1/\pi t$ to obtain the analytical signal y(t).

$$y(t) = \frac{1}{\pi} \int_{-\infty}^{\infty} \frac{x(t)}{t - \tau} d\tau$$

The instantaneous phase φ(t) is the inverse tangent of the ratio of the imaginary and real parts of the analytical signal y(t) (Le Van Quyen et al., 2001). This method has been used widely in MEG and EEG signals to study phase locking and synchrony in neural signals (Le Van Quyen et al., 2001; Pikovsky et al., 2001). The discrete-time analytical signal is implemented by MATLAB based on the algorithm introduced by Marple (1999). Figure 4.3A shows an example of spontaneous LFP activity and its corresponding phase. Because the stimulus onset almost always evokes an upward response in the normalized LFP activity, the pre-stimulus phases are biased towards $-\pi/2$ (see Figure 4.3C for example). Figure 4.3B shows the histogram of phase values of spontaneous activity (2000 ms before stimulus onset, bin size 0.05π, all normalized datasets were merged to obtain a smoother histogram), whereas Figure 4.3D shows the histogram of phase values at stimulus onset, with distinct clusters at $-\pi/2$. Therefore, before calculating the pre-

stimulus phase, the stimulus-evoked activity was truncated from each trial. To avoid the edge effect introduced by truncating, instantaneous phase at 50 ms before the stimulus onset was defined as the pre-stimulus phase. Figure 4.3E shows the distribution of the instantaneous phase 50 ms before stimulus onset, which is similar to the distribution of spontaneous activity phase shown in Figure 4.3B (two-sample Kolmogorov-Smirnov test, $p > 0.05$). The UP state was defined as the period where the normalized spontaneous LFP activity was positive, that is, $|\varphi| < \pi/2$. The DOWN state was defined as the period where the normalized spontaneous LFP activity was non-positive, or, $|\varphi| >= \pi/2$. Within each dataset, trials that were in the synchronized (low-frequency) state were further parsed into UP and DOWN states.

Detection and discrimination.

Detection performance of the ideal observer was defined as the d' between the noise distribution and the response distribution. The noise distribution was formed by the pre-stimulus activity from all trials, which was the normalized LFP averaged over 50 ms pre-stimulus period. The response distribution was formed by the stimulus-evoked response in the primary barrel from all single trials. The trials were first normalized as described above, the evoked response was the peak value of the normalized LFP in the 100 ms post-stimulus period minus the baseline value at stimulus onset. Discrimination performance of the ideal observer was defined as the d' between the primary barrel response distribution in the adjacent barrel response distribution. Figure 4.4A illustrates the tasks for the ideal observer. Because the number of trials in each dataset becomes small after being parsed into different states, all trials from all datasets were pooled together and a bootstrap method was used to test for statistical significance (Efron and Tibshirani, 1993). Half of the data was randomly chosen to calculate detection and discrimination performance, and the process was repeated 7 times, same as the number of datasets. The error bars represent 1 standard error of the 7 iterations.

4.3 Results

To investigate what information about the brain state may be extracted from the spontaneous activity and how the brain state affects the information encoded about the stimulus in the sensory-evoked activity, the cortical LFP was recorded in the rat barrel cortex in both the primary barrel and an adjacent barrel. The LFP has been shown to be a reliable measure of brain state in a range of studies (Curto et al., 2009; Harris and Thiele, 2011; Haslinger et al., 2006; Hirata and Castro-Alamancos, 2010; Okun et al., 2010; Poulet et al., 2012). Each trial of spontaneous activity recording was followed by a single whisker deflection on the primary whisker. A single low-impedance tungsten electrode was used to record the LFP in the primary barrel, using a skull screw as the ground and the reference (see Methods). In a subset of experiments, a second electrode recorded the LFP simultaneously in an adjacent barrel. Figure 4.1A illustrates the experiment setup and Figure 4.1B shows an example data set from a primary barrel recording of one animal. Single-trial raw LFP recordings are shown in grey, and the black trace represents the average of 50 single trials. Using the spontaneous activity, I classified the trials into the de-synchronized and the synchronized states and the UP/DOWN states within the synchronized state and quantified the effect of the brain state on the evoked response to a single stimulus and the information carried about the stimulus.

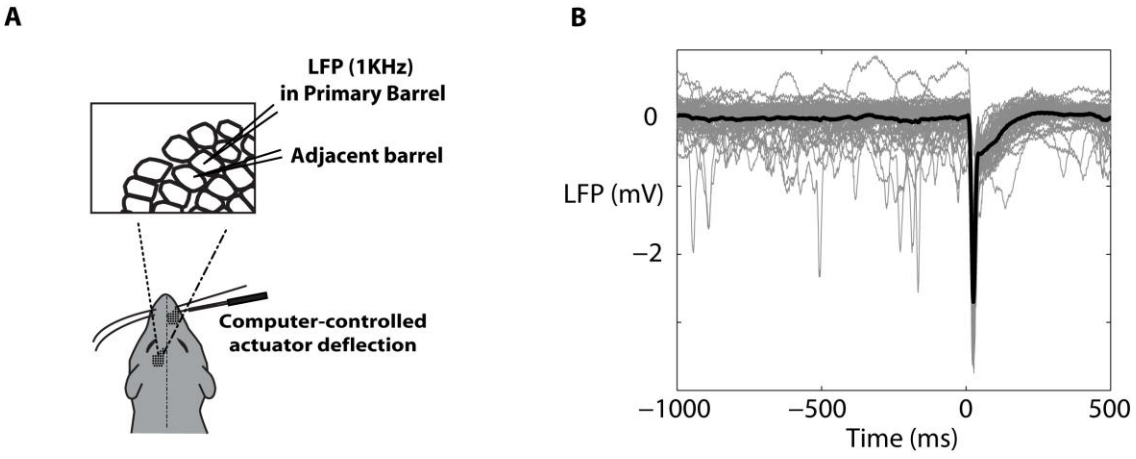

Figure 4.1 Experiment setup.
A. The experiment setup. A low-impedance electrode records the LFP activity in the primary barrel of an anesthetized rat. A second electrode records the LFP in an adjacent barrel in a subset of experiments.
B. An example raw LFP recording from one barrel of one animal. Grey lines are single trials and black line is the average across 50 trials.

4.3.1 Brain state modulates sensory-evoked activity

Although the brain states categorized by cortical fluctuation frequency were originally discovered in sleep and wakefulness, more recent studies have indicated that the difference in cortical frequency content also exists in smaller ranges of brain states such as quiet wakefulness and alertness, even spontaneously under anesthesia (Castro-Alamancos, 2004; Clement et al., 2008; Curto et al., 2009; Hasenstaub et al., 2007; Hirata and Castro-Alamancos, 2010; Luczak et al., 2013; Poulet et al., 2012). As previously described, frequency content is typically associated with cortical synchrony. More low-frequency content signifies higher cortical synchrony, and more high-frequency content signifies a relatively de-synchronized state (Curto et al., 2009; Poulet and Petersen, 2008). Here, I examine the brain states that occur spontaneously without behavioral influence or stimulation and how it influences the representation of an external stimulus.

First, the trials were classified into "de-synchronized" (relatively more high-frequency) and "synchronized" (relatively more low-frequency) state using the frequency content in the pre-stimulus spontaneous LFP activity. Figure 4.2A illustrates the analysis of the frequency content in the spontaneous activity in relation to the evoked response. Each single trial within each data set was normalized to the mean of that data set (see Methods). The evoked response is the peak value in the 100 ms window post-stimulus

relative to the baseline at stimulus onset. The frequency spectrum for the pre-stimulus spontaneous activity was calculated for each trial using a Fast Fourier Transform (FFT, data length 1 second). To quantify the frequency content in the spontaneous activity, a frequency ratio was defined as the ratio of total amplitude in the 1-4 Hz band to that in the 1-50 Hz band in 1000 ms of spontaneous activity immediately preceding the stimulus (Curto et al., 2009, see Methods). A larger frequency ratio indicates more low-frequency content and signifies more synchronized cortical activity. To ensure the frequency content below 2 Hz was adequately captured using a data length of 1 second, pure sinusoid signals with amplitude of 1 and a given frequency were generated and the errors estimating the amplitude of the sinusoid signal using various data lengths were calculated. For each given frequency and data length, the error is defined as 1 (known amplitude of the sinusoid) minus the amplitude of the FFT at the given frequency. Figure 4.2B shows the error for each given frequency and data length. The lowest frequency used in frequency ratio calculation was 1 Hz, and the error estimating the frequency at 1 Hz using FFT of a data length of 1 second was 0.01, which is 1% of the original amplitude of the sinusoid signal.

Within each data set, trials with frequency ratio below the 33 percentile value were classified as de-synchronized trials, those above the 67 percentile value were classified as synchronized trials, and the intermediate ones were classified as medium frequency trials. Figure 4.2C illustrates this classification. There were no distinct clusters of frequency ratio values at high or low ranges, suggesting that the degree of synchrony is likely a continuum. Figure 4.2D shows two example single trials of LFP recordings. Note that the synchronized trial (red, frequency ratio = 0.52) exhibited relatively large but slow oscillations in the pre-stimulus activity, and has a larger stimulus-evoked response, in comparison to the de-synchronized trial (blue, frequency ratio = 0.36). The inset shows their respective frequency spectrum of 1000 ms pre-stimulus activity (FFT amplitude, see

Methods). Figure 4.2E shows the frequency spectrum of synchronized trials vs. de-synchronized trials averaged over 16 data sets, and the thin lines represent 1 standard error. Note that when compared to the synchronized frequency spectrum (red), the de-synchronized spectrum (blue) showed not only a decrease in low-frequency range but also an increase in the high-frequency range. Therefore, the difference in the frequency content was not simply due to the fluctuation of physiological effects such as heart rate (approximately 4 Hz) and respiratory rate (approximately 1 Hz). The difference in frequency ratio was also not simply due to the difference in total amplitude of the frequency spectrum in different states, as the total amplitude from 1-50 Hz band was not different across states (Fig 4.2E inset, error bar = 1SE, paired t-test, n = 16, $p > 0.05$). Note that a relatively small increase in the high frequency content on the logarithm scale can be large, and even small changes in frequency content could have significant effects on perception and behavior (Cardin et al., 2009; Poulet et al., 2012; Sachidhanandam et al., 2013). Figure 4.2F shows an example data set of 100 ms of spontaneous activity and sensory-evoked response for synchronized and de-synchronized states. Thick lines represent the average across trials, thin lines represent +/-1 standard error. The inset summarizes the sensory-evoked response amplitude across the degree of synchrony, averaged over 16 datasets. Error bars are 1 standard deviation. The stimulus was a strong whisker deflection (1000-1200 º/s). The same stimulus evoked the largest LFP amplitude in the synchronized state, significantly larger than both de-synchronized and the medium-frequency states (de-synchronized mean: 0.97 +/- 0.014 SE, medium frequency mean: 0.99 +/- 0.016 SE, synchronized mean: 1.04 +/- 0.01 SE, paired t-test, n = 16, $p<0.05$). The un-normalized data show qualitatively similar results (de-synchronized mean: -929 µV +/- 254 SE, medium frequency mean: -944 µV +/- 266 SE, synchronized mean: -992 µV +/- 269 SE, paired t-test, n = 16, $p<0.05$).

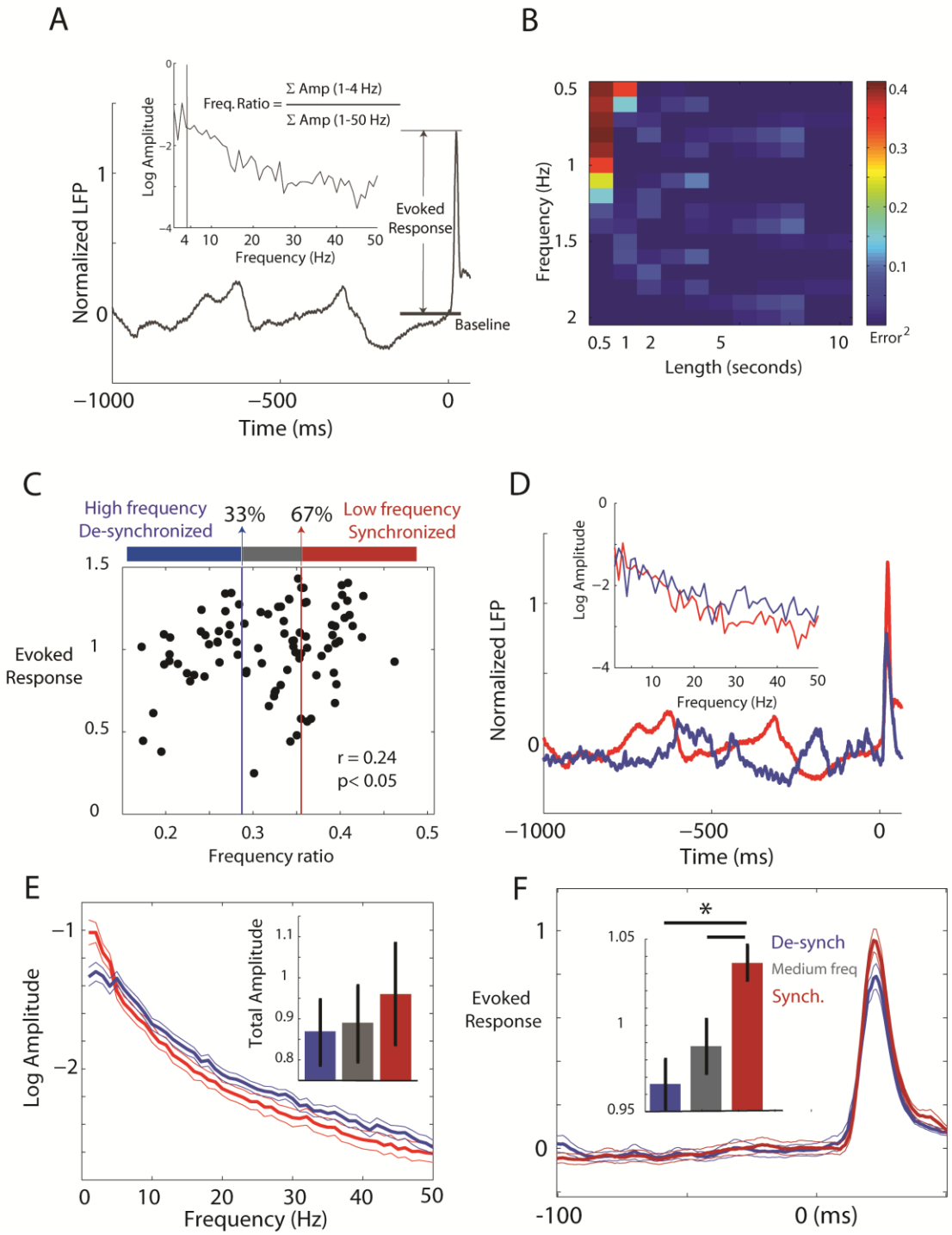

Figure 4.2 The degree of cortical synchrony modulates stimulus-evoked activity. **A.** Illustration of analysis. The frequency ratio was defined as the ratio of the total amplitude in 1-4 Hz to that in 1-50 Hz in the 1000 ms of spontaneous activity before stimulus onset. The sensory evoked response is the maximum value in 100 ms window after stimulus onset, minus the baseline at 1 ms before stimulus onset. **B.** Quantification

of error estimating frequency content using FFT of different time window sizes (horizontal axis). At each given frequency, error was defined as the difference between the known amplitude of generated sinusoid and the amplitude of the FFT at the given frequency. **C.** An example data set of frequency ratios and illustration of trial classification. Within each set, trials were classified by the percentile of frequency ratio values. **D.** An example synchronized trial where the spontaneous activity exhibits low frequency fluctuation (red, frequency ratio = 0.52), and an example de-synchronized trial (blue, frequency ratio = 0.36). The inset shows their respective frequency spectrum. **E.** The average frequency spectrum of synchronized trials (red) and de-synchronized trials (blue). The thin lines represent +/-1 standard error (n = 16). Note that the total amplitude in the 1-50 Hz band was not different across states (inset, paired t-test, $p > 0.05$). **F.** An example set of stimulus-evoked responses for synchronized trials (red), and de-synchronized trials (blue). The thick lines (middle) represent the mean across trials, the thin lines represent +/-1 standard error bands. Insets: the amplitude of evoked responses across states, averaged over 16 data sets, error bars represent 1 standard error.

Furthermore, it has been proposed that the low-frequency synchronized state is generated by the alternating UP (cortical cells are depolarized) and DOWN (cortical cells are silent) states (McCormick et al., 2015; Petersen et al., 2003b), and it has been shown that during the DOWN state, the cortical response to a stimulus is larger than the response in the UP state (Petersen et al., 2003b; Li et al., 2009; Sachdev et al., 2004). Without accounting for UP and DOWN states, the effect of the synchronized state on sensory-evoked response can be obscured. Therefore, I further parsed the synchronized state into UP and DOWN states.

Because the synchronous depolarization (UP) and hyperpolarization (DOWN) produce the low frequency, large amplitude fluctuation (McCormick et al., 2015), UP states should correspond to time periods where the normalized LFP activity is positive, and DOWN states correspond to negative periods, which can be informed by the instantaneous phase of the LFP activity. Therefore, a Hilbert transform was used to calculate the phase of pre-stimulus spontaneous activity in order to classify the synchronized trials into UP/ DOWN states (see Methods). The Hilbert transform has been

used widely in MEG and EEG signals to study phase locking and synchrony in neural signals (Le Van Quyen et al., 2001; Pikovsky et al., 2001). Figure 4.3A shows an example single-trial spontaneous LFP (black trace) and its phase φ (red trace). The phase values range from -π to π. The peak of spontaneous activity corresponds to a phase value of 0, and the trough has a phase of -π or π because the phase value wraps around every 2π. The transition from a positive period of spontaneous fluctuation (UP state) to the negative period of the fluctuation (DOWN state) has a phase of π/2 and the transition from DOWN to UP state has a phase of -π/2. The UP state can be identified when $|\varphi| < \pi/2$, and the DOWN state when $|\varphi| >= \pi/2$. Figure 4.3B shows the distribution of phase values for spontaneous activity (at 2 s before stimulus onset, bin size 0.05 π), pooled across all synchronized trials of 16 data sets. In order to classify trials where the stimulus was delivered during the UP or DOWN state, the phase at the stimulus onset was extracted. However, because the stimulus almost always evoked an upward response in the normalized LFP activity, the phase at stimulus-onset is biased towards $-\pi/2$. An example trial is shown in Figure 4.3C. Figure 4.3D shows the distribution of phase values at stimulus onset, with a distinct cluster at $-\pi/2$ (bin size 0.05 π, pooled across all synchronized trials of 16 data sets). Therefore, the stimulus-evoked activity was truncated from each trial. To avoid the edge effect introduced by truncating, instantaneous phase at 50 ms before the stimulus onset was defined as the pre-stimulus phase. Figure 4.3E shows the distribution of the instantaneous phase 50 ms before stimulus onset, which is similar to the distribution of spontaneous activity phase shown in Figure 4.3B (two-sample Kolmogorov-Smirnov test, $p > 0.05$). Figure 4.3F shows an example dataset of sensory-evoked response in the UP and DOWN states (mean +/- 1 SE). The inset summarizes the evoked response amplitude across all data sets ($n = 16$, paired t-test, $p < 0.05$). The evoked amplitude was larger in the DOWN state (UP mean: 0.93 +/- 0.02 SE, DOWN mean: 1.1 +/- 0.02 SE, paired t-test, $n = 16$, $p<0.05$), consistent with the findings

in the literature (Petersen et al., 2003b; Sachdev et al., 2004; Li et al., 2009). The un-normalized data show qualitatively similar results (UP mean: -907 µV +/- 245 SE, DOWN mean: -1041 µV +/- 283 SE, paired t-test, n = 16, $p < 0.05$).

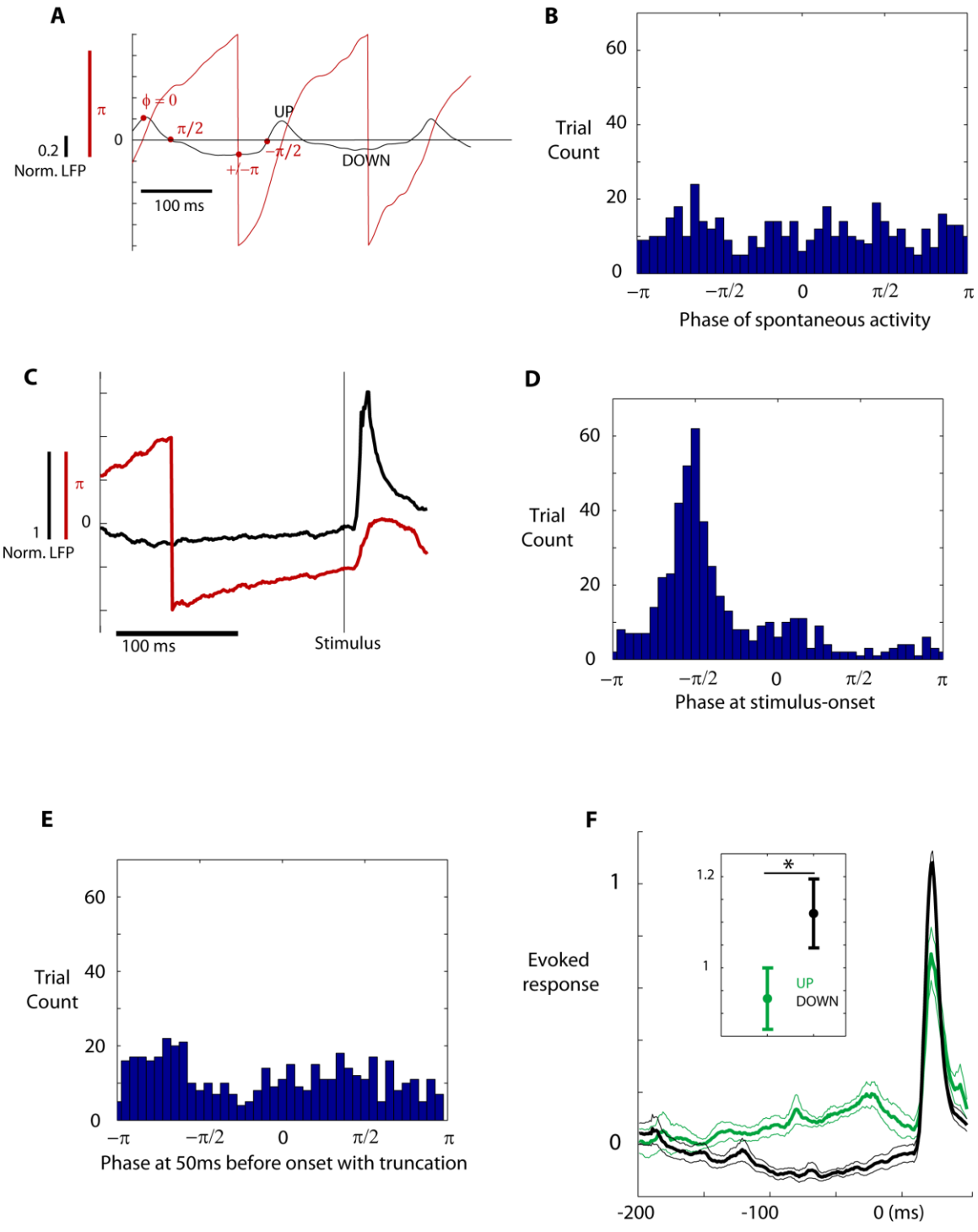

Figure 4.3 The UP/DOWN states modulate stimulus-evoked activity.
A. An example of the phase value of the spontaneous LFP oscillation. **B.** The distribution of phase values of spontaneous activity (2 s before stimulus onset) pooled across all data sets. **C.** An example of the stereotypical upward deflection of the stimulus-evoked activity biasing the phase near and post stimulus-onset. **D.** The distribution of phase values at stimulus onset pooled across all data sets. There is a distinct cluster centered around $-\pi/2$, due to the effect of the stimulus-evoked activity. **E.** The distribution of phase values at 50 ms before stimulus-onset, after the truncation of stimulus-evoked activity pooled across all data sets. The distribution was not different from the spontaneous activity phase distribution shown in B (two-sample Kolmogorov-Smirnov test, $p > 0.05$). **F.** An example set of sensory-evoked response in UP and DOWN states. The inset summarizes the amplitude of evoked response across all data sets ($n = 16$, paired t-test, $p < 0.05$).

4.3.2 Brain state modulates the information encoded about the stimulus

The results so far show that spontaneous activity carries information about the state of the cortex and these brain states modulate the sensory-evoked response. This prompts the hypothesis that the information encoded about the stimulus is also state-dependent. To test this, an ideal observer analysis was performed to quantify the detectability and discriminability of the stimulus (a 200 °/s deflection on a single whisker) across the cortical states identified above: de-synchronized and synchronized states, and within the synchronized state, the UP and DOWN states. Figure 4.4A illustrates the detection and discrimination tasks. An example set of pre-stimulus and evoked response in the primary barrel (black) and simultaneously recorded adjacent barrel (grey) is shown. The thick lines are the average across trials, and the thin lines are +/-1 standard deviation. The detection task is illustrated on the left. The task is to separate the response distribution in the primary barrel from the noise distribution, which was formed by the pre-stimulus activity across trials. The pre-stimulus activity was the average over 50 ms of LFP activity before stimulus onset. The detectability was defined as the d' value between the noise distribution and the response distribution in the primary barrel. The discrimination task is illustrated on the right. The task is to discriminate the spatial location of the

stimulus given the responses in two barrels, one primary to the whisker stimulus, the other adjacent. The d' between the primary response distribution and the adjacent response distribution quantifies how well the ideal observer can separate the primary barrel response from the adjacent barrel response, thus how well the primary whisker can be identified.

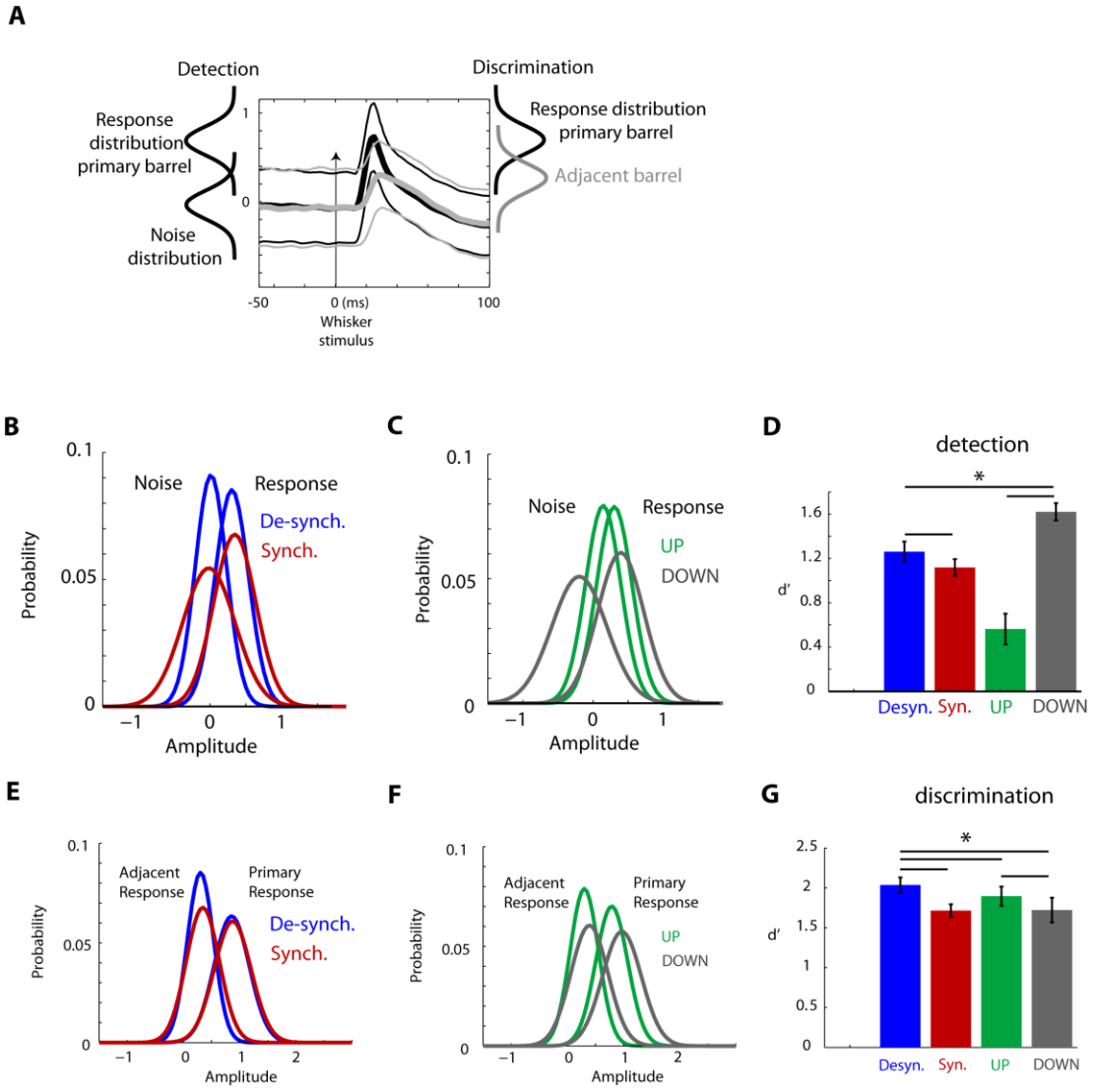

Figure 4.4 The detectability and discriminability of the stimulus are state-dependent.

A. An illustration of the detection and discrimination tasks for the ideal observer. The detection task is to separate the evoked response distribution from the noise distribution. The spatial discrimination task is to separate the distribution of evoked response in the

primary barrel from that in an adjacent barrel. **B.** The noise and response distribution in the synchronized and de-synchronized states. **C.** The noise and response distribution in the UP/ DOWN states within the synchronized state. **D.** The detectability of the stimulus across states as measured by d' between noise and response distributions. **E.** The response distributions in the primary and an adjacent barrel in the synchronized and de-synchronized states. **F.** The response distributions in the primary and an adjacent barrel in the UP/DOWN states within the synchronized state. **G.** The spatial discriminability of the stimulus across states as measured by d' between the primary barrel response distribution and the adjacent barrel response distribution.

Figure 4.4B-D summarizes the detection performance. Figure 4.4B shows the distributions of noise and primary barrel response to a 200 º/s deflection on a single whisker in the synchronized and de-synchronized states, and figure 4.4C shows the distributions in the UP and DOWN states. The distributions shown consist of trials pooled from all datasets (n = 7, see Methods). Given the larger evoked response in the synchronized state on average (see Figure 4.2F inset), one may speculate that the synchronized state should favor the detectability of the stimulus, possibly serving as a wake-up call to the animal that is typically in a less behaviorally alert state (Crick, 1984; Fanselow and Nicolelis, 1999; Sherman 2001a). However, when quantified against the noise distribution, the detectability is higher in the de-synchronized state (Figure 4.4D, paired t-test, n = 7, $p < 0.05$), largely due to the less variable noise distribution (see Figure 4.4B). Furthermore, when the synchronized state was parsed into UP and DOWN states, the detectability was the highest in the DOWN state, due to a hyperpolarized noise floor (see Figure 4.4C). Figure 4.4E-G summarizes the spatial discrimination performance. Figure 4.4E shows the distributions of the primary barrel response and an adjacent barrel response to a 200 º/s deflection on a single whisker in the synchronized and de-synchronized states, and figure 4.4F shows the distributions in the UP and DOWN states. The spatial discriminability of the stimulus is higher in the de-synchronized state than in the synchronized state, including UP and DOWN states (Figure 4.4G, paired t-test, n = 7, $p < 0.05$). These results suggest that, the spontaneous activity carries the

information about the state of the cortex, which modulates both the sensory evoked response and pre-stimulus activity, resulting in different detectability and spatial discriminability about the stimulus across brain states.

4.4 Discussion

The results in this chapter show that pre-stimulus spontaneous activity in S1 carries relevant information about the state of the context. Specifically, the synchronized and de-synchronized states can be identified by the frequency content of the spontaneous activity, and the UP/DOWN states within the synchronized state can be further extracted by the instantaneous phase of the spontaneous activity. These cortical states modulate the sensory-evoked response and the information conveyed about the stimulus.

The frequency of spontaneous cortical fluctuation, measured with EEG or LFP, has long been tied to the arousal level of the animal, with high frequency, small amplitude fluctuation signifying alert states and low frequency, large amplitude fluctuation signifying the other end of the arousal spectrum like sleep and anesthesia (Steriade et al., 1993). In the de-synchronized state, the cortical neurons are less correlated, and is typically associated with increased tonic firing of the thalamus (Castro-Alamancos, 2004; Crochet and Petersen, 2006; Curto et al., 2009; Poulet and Petersen, 2008; Poulet et al., 2012) that results in short-term thalamocortical synaptic depression (Castro-Alamancos, 2002; Chung et al., 2002). Thus, the response to an external stimulus in the de-synchronized state is likely to be more suppressed due to weaker thalamocortical synaptic efficacy (Harris and Thiele, 2011), consistent with the results shown here (Figure 4.2F).

It has been proposed that the slow cortical fluctuations in the synchronized state is generated by the alternation between UP (cells are depolarized) and DOWN (cells are

silent or hyperpolarized) states (McCormick et al, 2015). Although UP and DOWN states were originally discovered with whole cell recordings in single cells, the mechanisms of UP and DOWN states involve, respectively, the synchronous activation and refraction of local recurrent networks (see below), which can be reasonably captured by the LFP recordings here in a cortical column (Harris and Thiele, 2011; Crochet and Petersen, 2006; Okun et al., 2010; Poulet and Petersen, 2008). During the DOWN state, cortical neurons are largely silent. An excitatory input, whether spontaneous (could be triggered by single oscillating cell, Buszaki et al., 2004) or driven by inputs from subcortical or intracortical regions, ignites the recurrent excitation network and also engages the local recurrent inhibition, pushing the cortex into the UP state (McCormick et al., 2015). Over time, refractory mechanisms, such as synaptic depression and Ca^+ and Na^+ dependent K^+ conductance, build up until the network is unable to maintain activity and falls into the DOWN state again (McCormick et al., 2015). Consistent with the literature, our results here show that the sensory evoked responses during the DOWN state are relatively larger, likely because the cortex is initially silent and the inhibitory network is not yet engaged. In the UP state, a number of explanations have been offered in the literature for the relatively small response - the inhibitory cells are engaged, driving force for excitation is reduced in depolarized state, input resistance decreases in UP state, and the AP threshold is higher in the UP state (McCormick et al., 2015; Petersen et al., 2003b; Sachdev et al., 2004).

Given that the evoked response in the synchronized state is larger on average and that synchronized state is typically associated with lower level of arousal, one may speculate that the synchronized state should favor the detectability of the stimulus, possibly serving as a wake-up call to the animal that is typically in a less behaviorally alert state (Crick, 1984; Fanselow and Nicolelis, 1999; Sherman 2001a). However, we found that the detectability was higher in the de-synchronized state, consistent with the behavior report

from Sachidhanandam et. al. (2013), where mice trained on a detection task exhibit less low-frequency content in the cortical cell membrane voltage fluctuation. The noise distribution in the de-synchronized state was less variable due to small-amplitude spontaneous fluctuations, and the smaller noise variability out-compensates the smaller average evoked amplitude, resulting in a larger d' between the noise and response distributions. Furthermore, the synchronized state contains both UP and DOWN states, both known to modulate sensory evoked response, possibly obscuring the detectability in the synchronized state. Indeed, when the synchronized state was further parsed into UP and DOWN states, we found that the detectability was better in the DOWN state than in the de-synchronized state. The spatial discriminability of the stimulus (d' between primary and adjacent response distributions) was better in the de-synchronized state than in the synchronized state, including both UP and DOWN states, consistent with the idea that the de-synchronized state is typically associated with arousal and alertness. Furthermore, there is a trade-off of detectability and discriminability between UP and DOWN states – detectability is better in the DOWN state because of a lower noise floor and discriminability is better in the UP state because of smaller response variability. This suggests that the brain state has dynamic impacts on the information conveyed about the stimulus, and may help the animal cope with different demands of the sensory tasks.

The sensory-evoked response was defined as the peak amplitude of the LFP relative to the baseline activity at stimulus onset. Subtracting the baseline did not make a qualitative difference in evoked responses between the de-synchronized and synchronized states. However, the difference in evoked responses between UP and DOWN states was only relative to the baseline. This is consistent with the findings in the literature that the post-synaptic potential (PSP) in the UP state is smaller, but only relative to its higher baseline membrane potential that defines the UP state (Petersen et al., 2003b; Sachdev et al., 2004). Implicit in this analysis is the assumption that the neurons downstream from S1

are able to extract the difference of evoked response strength between UP and DOWN states. One possible scenario is that the elevated spontaneous activity in S1 neurons during UP state may cause short term synaptic depression on the downstream neurons, making them less excitable in response to a stimulus input delivered during UP state. In addition, despite being closer to the action potential threshold, S1 cells fire less actions potentials in the UP state in response to sensory input, thus sending less output to the downstream neurons (Petersen et al., 2003b; Sachdev et al., 2004). Nonetheless, the UP and DOWN states are cycles within the synchronized state, which has its behavior correlates. Whether the different evoked responses in UP and DOWN states make a difference in behavior needs further investigation.

The difference between the evoked responses in the de-synchronized and synchronized trials shown here was quantitatively small. This is likely due to both the fact that the brain states state investigated in this work are intrinsic under anesthesia without the influence of explicit stimulation or behavioral influences, and the fact that the synchronized state contains two distinct states, UP and DOWN states known to modulate sensory evoked responses. Although the EEG frequency signature was discovered in sleep and wakefulness, and brain state was originally thought to be a dichotomy between sleep and wakefulness, more modern studies have shown the slow oscillation also exists during drowsiness or inattentiveness in the awake state, suggesting brain state is likely a continuum as opposed to distinct states (Castro-Alamancos, 2004; Crochet and Petersen, 2006; Curto et al., 2009; Poulet and Petersen, 2008; Poulet et al., 2012; Zagha et al., 2013). The spontaneous cortical states under anesthesia could represent a relatively small range in the continuous spectrum. Although there are certainly differences between anesthesia and sleep, under the maintenance phase of general anesthesia, the cortex also displays low frequency EEG that closely resembles the EEG pattern in slow wave sleep, and shares some common mechanisms with sleep (Brown et al., 2010). Both Fentanyl

and non-REM sleep reduce acetylcholine and are typically associated with burst firing in the thalamus (Brown et al., 2010). The difference between the synchronized and de-synchronized trials shown here under Fentanyl could be similar to, and possibly smaller than, the difference between low frequency EEG in non-REM sleep and higher frequency EEG in REM sleep.

In conclusion, the results here suggest that, different modes of frequency oscillations can occur without explicit stimulation of relevant nuclei for neuromodulation or behavioral influence. The spontaneous activity carries the information about these brain states that have distinct impacts on the decoding of the stimulus. The state dependence of sensory responses may help support different demands of the sensory system under various behavioral states and tasks. Finally, the states demonstrated are possibly a small part of a dynamic and high-dimensional brain state space that would require simultaneous recording in awake, behaving animals to more fully elucidate the mechanisms and functions of cortical dynamics.

CHAPTER 5 CONCLUSION AND FUTURE WORK

This thesis examines the dynamics of sensory stimulus encoding under the context of brain state in the rat primary somatosensory cortex (S1). I show that sensory adaptation modulates brain state through bottom-up thalamic mechanisms that result in fundamental changes in the information conveyed about the stimulus. The intrinsic brain states are at least partially reflected in the spontaneous activity in S1, which modulate sensory evoked response and the information conveyed about the stimulus. The results suggest that brain state is a multi-dimensional continuum, where multiple mechanisms can coexist and interact. Interpreting sensory stimuli under the context of brains state improves the efficiency in extracting relevant information from the cortical representation of the stimulus. The regulation of brain state through behavior, cognitive functions, and thalamic mechanisms thus provides support for different demands on the sensory system depending on the type of task.

5.1 Sensory adaptation induces bottom-up modulation on brain state

The results in Chapter 2 demonstrate that sensory adaptation changes the cortex from a state where a stimulus evokes a relatively large response emphasizing the presence of the stimulus to a state where the same stimulus evokes a more suppressed response and spatial localization is enhanced. This tradeoff between the detection and discrimination of the stimulus is true in both the ideal observer of the cortex of the anesthetized rat and in behavioral responses from awake animals.

Although the adapted state and the de-synchronized state are two fundamentally different brain states, it is worth noting that adaptation shares common effects and mechanisms

with the de-synchronized state, especially the active whisking state, in their effects on behavior and evoked neural responses. In comparison to their respective opposing states (non-adapted state, or synchronized/quiescent non-whisking states), the cortical response to a stimulus is suppressed (Castro-Alamancos, 2004; Crochet and Petersen, 2006; Ferezou et al., 2007; Ollerenshaw et al., 2014; Poulet et al., 2012; Sheth et al., 1998; Chung et al, 2002; Khatri et al., 2004; Moore, 2004; Webber and Stanley, 2004; Boloori and Stanley, 2006; Higley and Contreras, 2007; Khatri et al., 2009; Ganmor et al., 2010). In behavior studies where the animal is engaged in a task, or actively whisking, the cortex also demonstrates suppression in sensory-evoked activity, albeit without the measurement of spontaneous frequency fluctuation (Fanselow and Nicolelis, 1999; Otazu et al., 2009). Following adaptation, the animal and the ideal observer can better perform a whisker spatial discrimination task (Ollerenshaw et al., 2014). There are many examples in the literature of enhanced stimulus feature discriminability following adaptation (Vierck and Jones, 1970; Goble and Hollins, 1993; Tannan et al., 2006; Adibi et al., 2013; Fairhall et al., 2001; Lesica et al., 2007; Maravall et al., 2007; Wang et al., 2010); and active whisking is widely thought to enhance tactile sensation (Carvell and Simons 1995; Fanselow and Nicolelis, 1999; Harvey et al., 2001; Moore 2004). In both adaptation and de-synchronized state, the cortical suppression is tightly linked to thalamocortical synaptic depression (Castro-Alamancos, 2002, 2004; Chung et al., 2002; Hirata and Castro-Alamancos, 2010). In the case of de-synchronized states, it has been shown that acetylcholine release can depolarize the thalamic cells (Steriade et al., 1990; Williams et al., 1994), which in turn facilitates tonic firing in the thalamus (McCormick, 1992). In the adapted state, it has been shown that the thalamic firing is desynchronized, likely a result of thalamic depolarization and tonic firing (Temereanca et al., 2008; Wang et al., 2010; Whitmire et al., submitted). These pieces of evidence strongly suggest that although active whisking has additional top-down control pathways, passive adaptation and active whisking share common thalamic mechanisms and result in similar changes in behavior.

What is the function of rapid cortical suppression, and why is it associated with better discriminability of the stimulus? In the context of detection and spatial discrimination task in this thesis, the initial conjecture was that the larger S1 response in non-adapted state produces more discernable signal for the ideal observer and possibly for the animal for a better detection, and the spatially constrained signal produces a bigger difference between the average activity in primary and adjacent column for a better spatial discrimination. While it is true that a larger cortical response would form a response distribution farther removed from the noise distribution, it may carry out other functions to facilitate detection. The spatially large response may facilitate communication with other cortical areas and projections to neuromodulatory nuclei to promote alertness. The results in Chapter 3 show that the difference between primary and adjacent column actually did not change significantly with adaptation, but it was rather the reduction in variability and change in the correlation between primary and adjacent column activity that determined the discriminability of the stimulus. The change in variability and neural correlation is often seen in brain state changes, such as in attention and adaptation (Adibi et al., 2013; Cohen and Maunsell, 2009; Ecker et al., 2014; Harris and Thiele, 2011; Kohn et al., 2009; Scholvinck et al., 2015). The suppressed cortical response may represent localized processing. Once the animal has already been alerted by the first stimulus in the non-adapted or drowsy state, the processing of known stimuli may not require other sensory information integration or a motor response and can thus be localized in the primary column.

5.2 Information theory and sensory stimulus decoding

As the animal forms perception from a moment-to-moment basis, it is imperative to quantify the information carried about the stimulus on a trial-to-trial basis. Parallel to

animal behavior, the ideal observer analysis of neural activity using information theory provides us with the knowledge of what information may be available in the brain to the animal and what calculation the brain may be performing to extract this information about the stimulus. As a model for behaviorally relevant information carried about the stimulus, this thesis focuses on the detectability and the spatial discriminability of the stimulus in the vibrissa pathway using detection theory (Macmillan and Creelman, 2004).

As hypothesized by many others (Sheth et al., 1998; Sherman, 2001a,b; Fanselow and Nicolelis 1999; Moore 2004; Castro-Alamancos, 2002), the initial conjecture about the detectability and discriminability modulated by sensory adaptation was that the larger S1 response in non-adapted state favors detection, and the spatially constrained signal favors spatial discrimination. However, the average response alone does not dictate the information conveyed (Averbeck et al., 2006; Pouget et al., 1999). Detectability depends on the distance between the mean of the noise distribution and the mean of the response distribution and their overall variance, not simply the mean of the response as initially speculated. In the de-synchronized state, the detectability is better, contrary to speculation in the literature (Sherman, 2001a,b; Fanselow and Nicolelis 1999; Moore 2004) because the lower variability of the noise distribution (due to the high-frequency, small-amplitude fluctuations in the de-synchronized state) out-compensates the smaller mean of the evoked response.

In the adapted state, the main factor shaping the discriminability was the noise correlation of activation across cortical columns. The initial conjecture that spatially sharpened response may induce a larger difference between the mean of primary column response and the adjacent column response was not true. Although many studies point out the peril of noise correlation in coding efficiency (Zohary et al., 1994; Abbott and Dayan, 1999; Middleton et al, 2012; Adibi et al 2013), it should be noted that noise correlation can

have different effects on coding efficiency, depending on the relationship between the average responses (Averbeck et al., 2006). For neurons sharing functional feature selectivity, such as those in the same column, a stimulus evokes similar average responses in the units recorded. That is, the average responses to two separate stimuli would both be located along the unity line. As a result, when the response clusters are more elongated due to higher noise correlation, they would become more overlapped (see Averbeck et al., 2006, Figure 1). In contrast, in the context of the spatial discriminability here, the functional units recorded are two adjacent columns, where a stimulus evokes dissimilar average responses, with the primary barrel having the stronger average response. In this scenario, increased noise correlation making the response clusters more elongated results in an increase in the separability of the responses.

For any given recording technique, the ideal observer analysis using information theory provides us with the optimal information that is available in the neural activity on a trial-to-trial basis. Combined with animal task performance, we can speculate what decoding strategy the brain may use to produce the observed behavior.

5.3 The diverse mechanisms regulating the brain state

A variety of processes are known to influence the brain state, varying in circuitry mechanisms, time scale, and specificity. Exemplified in this thesis are the effect of sensory adaptation on brain state through thalamic mechanisms and intrinsic de-synchronized/synchronized and UP/DOWN states that result in the dynamic regulation of detectability and discriminability of the stimulus. In the literature, top-down behavior processes such as wakefulness and intra-cortical processes have also demonstrated modulatory effects on brain state and sensory-evoked response, some of which have been found to also involve bottom-up feed forward processes (Castro-Alamancos, 2004;

Crochet and Petersen, 2006; Harris and Thiele, 2011; Poulet and Petersen, 2008; Poulet et al., 2012; Zagha and McCormick, 2014; Zagha et al., 2013). Active whisking for example, has been shown to suppress low frequency power in cortical LFP and desynchronize the cortex (Poulet et al., 2012). Active whisking is considered an internally generated process, as whisking does not depend on the afferent infraorbital nerve (Fee et al., 1997; Poulet et al., 2012). However, the modulatory effects of whisking on the cortex are not only associated with tonic firing of the thalamus but also abolished with the inactivation of the thalamus (Poulet et al., 2012). The similar effects on the state of S1 by the stimulation of vM1 however, are independent of the thalamus (Zagha et al., 2013), suggesting diverse and dynamic circuitries involved in brain state regulation.

The time scale of action and spatial specificity in brain state regulation is also diverse. Neuromodulators have been shown to play a major role in brain state modulation. For instance, norepinephrine has been shown to be critical in wakefulness (Constantinople and Bruno, 2011). Acetylcholine induces high frequency fluctuations in the cortex, facilitates wakefulness, and can also depolarize thalamic cells (Williams et al., 1994; Steriade et al., 1990; McCormick, 1992). In comparison to fast mechanisms such as thalamocortical short-term synaptic depression (sub-second time scale, Chung et al., 2002), neuromodulators act on a much longer time scale (seconds or longer) and have more diffuse and long-range projections (Williams et al., 1994; Steriade et al., 1990; McCormick, 1992; Castro-Alamancos and Oldford, 2002). While adaptation in the rat whisker system has been shown to be column-specific (Katz et al., 2006), neuromodulators typically have a much wider and longer projection range and can affect a larger, even multiple cortical areas (Harris and Thiele, 2011). Low-frequency fluctuation and rhythms have also been shown to affect a larger cortical area, and can be part of a travelling wave (Buzsaki and Draguhn, 2004; Csicsvari et al., 2003; Ferezou et al., 2006, 2007; Harris and Thiele, 2011; Luczak et al., 2007; Petersen et al., 2003b;

Steriade, 2001). The diverse time scale and spatial specificity of multiple modulating mechanisms could help the animal cope with different demands placed on the sensory system depending on the task – whereas distinguishing tactile features may require only local changes to enhance tactile sensation on a fast moment-to-moment basis, other tasks such as locating a prey require full alertness that may require long lasting global changes and coordination among multiple sensory and motor areas.

5.4 The interaction of modulating processes

Given the diverse processes regulating brain state, one may expect that multiple processes may co-exist temporally and interact with each other either in the same area or across different areas. It has been shown that in the alert state where the TC synapse is already depressed, the efficacy of adaptation is reduced (Castro-Alamancos, 2004). This seems to suggest that when multiple processes share a common mechanism, in this case TC synapse depression, there is likely a limited physiological capacity for that mechanism. Thus, it may appear that these processes may be mutually reducing each other's efficacy. However, the efficacy of adaptation is typically measured with an average response ratio in S1. It is unclear whether other changes known to be important for sensory encoding, such as variability and correlation are also reduced.

As previously mentioned, many different mechanisms are involved in each process. In the context of concurrent alertness and sensory adaptation, the alertness was produced by stimulating the brain stem reticular formation to trigger the release of acetylcholine (Castro-Alamancos and Oldford, 2002; Steriade et al., 1990; Williams et al., 1994), or by wakefulness, which requires norepinephrine and most likely involves acetylcholine as well (Constantinople and Bruno, 2011), while sensory adaptation acts on a faster time scale in a column-specific manner that likely does not involve neuromodulatory

mechanisms. It is more likely the case that although in the presence of alertness, the efficacy of adaptation is reduced in terms of the response size in S1, the two processes still have complementary mechanisms and effects that may support different tasks.

5.5 The nature of brain state

It is starting to emerge in the literature that brain state is likely a high-dimensional continuum. The frequency of fluctuation in EEG was originally thought to change only between sleep and wakefulness (Steriade et al., 1993). More recent studies have shown this change in EEG or LFP activity exists on a finer gradient and broader spectrum. For example, low-frequency fluctuations also exist in quiet wakefulness, and active behavior beyond wakefulness, such as mobility and active whisking (Castro-Alamancos, 2004; Crochet and Petersen, 2006; Poulet and Petersen, 2008; Poulet et al., 2012; Sachidhanandam et al., 2013; Zagha and McCormick, 2014). Results in frequency and velocity specific adaptation in Chapter 3 also support the continuous modulation of brain state and its graded effect on stimulus encoding. However, there are still large distinctions between certain behaviors, such as transitioning from being asleep to being awake. Thus, a more likely nature of brain state is a continuum but with distinct transitions.

There is a broadly consistent picture in the literature that associates many consistent cortical dynamics features together under the umbrella of one brain state – the de-synchronized state is often associated with alertness, thalamic tonic firing, cortical suppression and desynchronization (Castro-Alamancos, 2004; Crochet and Petersen, 2006; Curto et al., 2009; Poulet and Petersen, 2008; Poulet et al., 2012). However, more evidence also starts to point to more complex and dynamic effects. For example, attention suppresses low-frequency fluctuation, but could either increase or decrease gamma power

(Chalk et al., 2010; Fries et al., 2001; Harris and Thiele, 2011; Khayat et al., 2010). The stimulation of vM1 produces high-frequency activation, but does not require the thalamus (Zagha et al., 2013). Therefore, brain state does not simply encompasses a fixed list of cortical dynamics and corresponding behavior, but rather dynamically evokes different mechanisms and processes depending on the task placed on the sensory system.

Although the results in this thesis focus on the effect of brain state on sensory evoked response in S1, the brain state is not only the spontaneous activity in S1. It encompasses diverse processes that can act on different temporal and spatial scales. The characteristics of S1 activity not only determine how the stimulus is encoded, but is also shaped by, and interact with the processes that reflect behavior, cognition, integration with other sensory modalities, and motor control. This interaction may also in turn regulate brain state. While S1 is in a certain state, its feedback to the thalamus or to M1 could determine what modulation effects the thalamus or M1 should provide the S1 next. This effect could certainly be state-dependent. Thus brain state can be either stabilized or switched by feedback mechanisms, possibly depending on the demand of the task.

5.6 Future work

As previously discussed, the brain states under anesthesia investigated here are likely a small range on the spectrum of brain state continuum. To better elucidate the mechanisms and functions of cortical dynamics, following this thesis, the experiments should be done in awake and behaving animals to investigate the effect of wakefulness and various behavior on brain state and sensory evoked activity. Voltage sensitive fluorescent protein encoded in adeno associated virus (AAV) can be injected into S1 of rats (Jin et al., 2012) that can later be trained on head-fixation. We can then observe the spatiotemporal activation of the S1 both spontaneously and sensory-evoked in the awake and head-fixed

animal. Cre-dependent animals can be utilized so that the activity of excitatory cells and inhibitory cells can be separately observed.

The animals could be trained on a sensory task to answer the question of whether the perception is the same when the S1 exhibits the same sensory-evoked activity but the brain state is modulated by different mechanisms. In other words, does the animal have a separate awareness and interpretation of brain state separate from sensory perception? For example, the stimulus can be delivered when the thalamus is depolarized, or when the animal is whisking, or when vM1 stimulation is delivered, and the manipulation is adjusted accordingly to produce the same characteristic spontaneous S1 activity and sensory-evoked activity. The animal is then required to indicate the presence and a feature of the stimulus, which would elucidate whether the mechanism by which the state change was implemented affect the behavioral perceptibility of the stimulus feature, or the mechanisms are redundant such that the feature encoding remains unchanged.

Finally, the role of cortical control of state, specifically S1 feedback to other areas such as the thalamus and M1, needs to be investigated. Does S1 control its own state via feedback mechanisms? For example, does S1 signal the thalamus to switch to hyperpolarization if it has been in high-frequency fluctuation for a certain period of time, or does it signal it to keep depolarized so that it can maintain the high-frequency fluctuation? Does this signal perhaps depend on other neuromodulatory effects or behavior?

Answers to these questions could help us tease apart the complex mechanisms that govern brain state and provide insight into the nature of cortical variability, which ultimately determines the variability in the animal's perception and behavior.

REFERENCES

Abbott LF, Dayan P. (1999). The effect of correlated variability on the accuracy of a population code. Neural Comput 11:91–101.

Adams, N., Lozsadi, D.A., and Guillery, R.W. (1997). Complexities in the thalamocortical and corticothalamic pathways. Eur. J. Neurosci. 9, 204–209.

Adibi, M., McDonald, J.S., Clifford, C.W.G., and Arabzadeh, E. (2013). Adaptation improves neural coding efficiency despite increasing correlations in variability. J. Neurosci. 33, 2108–2120.

Ahissar, E., Sosnik, R., and Haidarliu, S. (2000). Transformation from temporal to rate coding in a somatosensory thalamocortical pathway. Nature 406, 302–306.

Albrecht, D., Farrar, S., and Hamilton, D. (1984). Spatial contrast adaptation characteristics of neurones recorded in the cat's visual cortex. J. Physiol.

Alonso, J.M., Usrey, W.M., and Reid, R.C. (1996). Precisely correlated firing in cells of the lateral geniculate nucleus. Nature 383, 815–819.

Andermann, M.L., Ritt, J., Neimark, M.A., and Moore, C.I. (2004). Neural correlates of vibrissa resonance; band-pass and somatotopic representation of high-frequency stimuli. Neuron 42, 451–463.

Anderson, J., Lampl, I., Reichova, I., Carandini, M., and Ferster, D. (2000). Stimulus dependence of two-state fluctuations of membrane potential in cat visual cortex. Nat. Neurosci. 3, 617–621.

Arabzadeh, E., Panzeri, S., and Diamond, M.E. (2004). Whisker vibration information carried by rat barrel cortex neurons. J. Neurosci. 24, 6011–6020.

Arabzadeh, E., Zorzin, E., and Diamond, M.E. (2005). Neuronal encoding of texture in the whisker sensory pathway. PLoS Biol. 3, e17.

Arieli, A., Sterkin, A., Grinvald, A., and Aertsen, A. (1996). Dynamics of ongoing activity: explanation of the large variability in evoked cortical responses. Science 273, 1868–1871.

Averbeck, B.B., Latham, P.E., and Pouget, A. (2006). Neural correlations, population coding and computation. Nat. Rev. Neurosci. 7, 358–366.

Barlow, H. (1961). Possible principles underlying the transformation of sensory messages. Sens. Commun.

Berg, R.W., and Kleinfeld, D. (2003). Rhythmic whisking by rat: retraction as well as protraction of the vibrissae is under active muscular control. J. Neurophysiol. 89, 104–117.

Bermejo, R., Vyas, A., and Zeigler, H.P. (2002). Topography of rodent whisking--I. Two-dimensional monitoring of whisker movements. Somatosens. Mot. Res. 19, 341–346.

Boloori, A. R., and Stanley, G. B. (2006). The dynamics of spatiotemporal response integration in the somatosensory cortex of the vibrissa system. The Journal of neuroscience, 26(14), 3767-3782.

Boly, M., Balteau, E., Schnakers, C., Degueldre, C., Moonen, G., Luxen, A., Phillips, C., and Peigneux, P. (2007). Baseline brain activity fluctuations predict somatosensory perception in humans. PNAS, 104(29), 12187-12192.

Börgers, C., Epstein, S., & Kopell, N. J. (2008). Gamma oscillations mediate stimulus competition and attentional selection in a cortical network model. PNAS, 105(46), 18023-18028.

Brecht, M., Preilowski, B., and Merzenich, M.M. (1997). Functional architecture of the mystacial vibrissae. Behav. Brain Res. 84, 81–97.

Brown, E., Lydic, R., and Schiff, N. (2010). General Anesthesia, Sleep, and Coma. N Engl J Med 363, 2638–2650.

Brumberg, J.C., Pinto, D.J., and Simons, D.J. (1996). Spatial gradients and inhibitory summation in the rat whisker barrel system. J. Neurophysiol. 76, 130–140.

Bruno, R.M. (2011). Synchrony in sensation. Curr. Opin. Neurobiol. 21, 701–708.

Bruno, R.M., Khatri, V., Land, P.W., and Simons, D.J. (2003). Thalamocortical angular tuning domains within individual barrels of rat somatosensory cortex. J. Neurosci. 23, 9565–9574.

Buonomano, D. V, and Maass, W. (2009). State-dependent computations: spatiotemporal processing in cortical networks. Nat. Rev. Neurosci. 10, 113–125.

Butts, D. a, Weng, C., Jin, J., Yeh, C.-I., Lesica, N. a, Alonso, J.-M., and Stanley, G.B. (2007). Temporal precision in the neural code and the timescales of natural vision. Nature 449, 92–95.

Buzsaki, G., and Draguhn, A. (2004). Neuronal Oscillations in Cortical Networks. 304, 1926–1930.

Cardin, J. a, Carlén, M., Meletis, K., Knoblich, U., Zhang, F., Deisseroth, K., Tsai, L.-H., and Moore, C.I. (2009). Driving fast-spiking cells induces gamma rhythm and controls sensory responses. Nature 459, 663–667.

Carpenter R. (2004). Contrast, Probability, and Saccadic Latency: Evidence for Independence of Detection and Decision. Current Biology 14: 1576-1580.

Carvell, G.E., and Simons, D.J. (1990). Biometric analyses of vibrissal tactile discrimination in the rat. J. Neurosci.

Castro-Alamancos, M. a (2002). Role of thalamocortical sensory suppression during arousal: focusing sensory inputs in neocortex. J. Neurosci. 22, 9651–9655.

Castro-Alamancos, M. a (2004). Absence of rapid sensory adaptation in neocortex during information processing states. Neuron 41, 455–464.

Castro-Alamancos, M. a, and Oldford, E. (2002). Cortical sensory suppression during arousal is due to the activity-dependent depression of thalamocortical synapses. J. Physiol. 541, 319–331.

Castro-Alamancos, M. a., and Gulati, T. (2014). Neuromodulators Produce Distinct Activated States in Neocortex. J. Neurosci. 34, 12353–12367.

Chalk, M., Herrero, J.L., Gieselmann, M. a, Delicato, L.S., Gotthardt, S., and Thiele, A. (2010). Attention reduces stimulus-driven gamma frequency oscillations and spike field coherence in V1. Neuron 66, 114–125.

Chen, Y., Geisler, W. S., and Seidemann, E. (2006). Optimal decoding of correlated neural population responses in the primate visual cortex. Nature neuroscience, 9(11), 1412-1420.

Chen Y, Geisler WS, and Seidemann E. (2008). Optimal temporal decoding of neural population responses in a reaction-time visual detection task. Journal of neurophysiology 99: 1366.

Chen, Y., Martinez-Conde, S., Macknik, S.L., Bereshpolova, Y., Swadlow, H. a, and Alonso, J.-M. (2008). Task difficulty modulates the activity of specific neuronal populations in primary visual cortex. Nat. Neurosci. 11, 974–982.

Chung, S., Li, X., and Nelson, S.B. (2002). Short-term depression at thalamocortical synapses contributes to rapid adaptation of cortical sensory responses in vivo. Neuron 34, 437–446.

Clement, E. a, Richard, A., Thwaites, M., Ailon, J., Peters, S., and Dickson, C.T. (2008). Cyclic and sleep-like spontaneous alternations of brain state under urethane anaesthesia. PLoS One 3, e2004.

Clifford, C.W.G., Webster, M. a, Stanley, G.B., Stocker, A. a, Kohn, A., Sharpee, T.O., and Schwartz, O. (2007). Visual adaptation: neural, psychological and computational aspects. Vision Res. 47, 3125–3131.

Cohen, M.R., and Maunsell, J.H.R. (2009). Attention improves performance primarily by reducing interneuronal correlations. Nat. Neurosci. 12, 1594–1600.

Constantinople, C.M., and Bruno, R.M. (2011). Effects and mechanisms of wakefulness on local cortical networks. Neuron 69, 1061–1068.

Cook EP, and Maunsell JHR. (2002). Dynamics of neuronal responses in macaque MT and VIP during motion detection. Nature Neuroscience 5: 985-994.

Crick, F. (1984). Function of the thalamic reticular complex : The searchlight hypothesis Neurobiology : Crick. 81, 4586–4590.

Crochet, S., and Petersen, C.C.H. (2006). Correlating whisker behavior with membrane potential in barrel cortex of awake mice. Nat. Neurosci. 9, 608–610.

Csicsvari, J., Jamieson, B., Arbor, A., and Leung, C.A. (2003). Mechanisms of Gamma Oscillations in the Hippocampus of the Behaving Rat. 37, 311–322.

Curtis, J.C., and Kleinfeld, D. (2009). Phase-to-rate transformations encode touch in cortical neurons of a scanning sensorimotor system. Nat. Neurosci. 12, 492–501.

Curto, C., Sakata, S., Marguet, S., Itskov, V., and Harris, K.D. (2009). A simple model of cortical dynamics explains variability and state dependence of sensory responses in urethane-anesthetized auditory cortex. J. Neurosci. 29, 10600–10612.

Desbordes, G., Jin, J., Weng, C., Lesica, N.A., Stanley, G.B., and Alonso, J. (2008). Timing precision in population coding of natural scenes in the early visual system. PLoS Biology 6, e324.

Diamond, M.E., and Arabzadeh, E. (2012). Whisker sensory system - From receptor to decision. Prog. Neurobiol.

Duda, R., Hart, P., and Stork, D. (2001). Pattern Classification and Scene Analysis 2nd ed. (New York: Wiley).

Ecker, A.S., Berens, P., Cotton, R.J., Subramaniyan, M., Denfield, G.H., Cadwell, C.R., Smirnakis, S.M., Bethge, M., and Tolias, A.S. (2014). State dependence of noise correlations in macaque primary visual cortex. Neuron 82, 235–248.

Efron, B., & Tibshirani, R. J. (1993). An introduction to the bootstrap. Chapman & Hall. New York, 436.

Ego-Stengel, V., Mello e Souza, T., Jacob, V., and Shulz, D.E. (2005). Spatiotemporal characteristics of neuronal sensory integration in the barrel cortex of the rat. J. Neurophysiol. 93, 1450–1467.

Engel, A. K., Fries, P., & Singer, W. (2001). Dynamic predictions: oscillations and synchrony in top–down processing. Nature Reviews Neuroscience, 2(10), 704-716.

Fairhall, A.L., Lewen, G.D., Bialek, W., and de Ruyter Van Steveninck, R.R. (2001). Efficiency and ambiguity in an adaptive neural code. Nature 412, 787–792.

Fanselow, E.E., and Nicolelis, M. a (1999). Behavioral modulation of tactile responses in the rat somatosensory system. J. Neurosci. 19, 7603–7616.

Fanselow, E.E., Sameshima, K., Baccala, L. a, and Nicolelis, M. a (2001). Thalamic bursting in rats during different awake behavioral states. Proc. Natl. Acad. Sci. U. S. A. 98, 15330–15335.

Fee, M.S., Mitra, P.P., and Kleinfeld, D. (1997). Central versus peripheral determinants of patterned spike activity in rat vibrissa cortex during whisking. J. Neurophysiol. 78, 1144–1149.

Ferezou, I., Bolea, S., and Petersen, C.C.H. (2006). Visualizing the cortical representation of whisker touch: voltage-sensitive dye imaging in freely moving mice. Neuron 50, 617–629.

Ferezou, I., Haiss, F., Gentet, L.J., Aronoff, R., Weber, B., and Petersen, C.C.H. (2007). Spatiotemporal dynamics of cortical sensorimotor integration in behaving mice. Neuron 56, 907–923.

Freeman, W.J., Rogers, L.J., Holmes, M.D., and Silbergeld, D.L. (2000). Spatial spectral analysis of human electrocorticograms including the alpha and gamma bands. J. Neurosci. Methods 95, 111–121.

Fridman GY, Blair HT, Blaisdell AP, and Judy JW (2010). Perceived intensity of somatosensory cortical electrical stimulation. Experimental brain research 203: 499-515.

Fries, P., Reynolds, J.H., Rorie, A.E., and Desimone, R. (2001). Modulation of Oscillatory Neuronal Synchronization by Selective Visual Attention. 291, 1560–1564.

Ganmor, E., Katz, Y., and Lampl, I. (2010). Intensity-dependent adaptation of cortical and thalamic neurons is controlled by brainstem circuits of the sensory pathway. Neuron 66, 273–286.

Gawne, T.J. and Richmond, B.J. (1993). How independent are the messages carried by adjacent inferior temporal cortical-neurons. J. Neurosci. 13, 2758–2771.

Gentet, L.J., Avermann, M., Matyas, F., Staiger, J.F., and Petersen, C.C.H. (2010). Membrane potential dynamics of GABAergic neurons in the barrel cortex of behaving mice. Neuron 65, 422–435.

Gilbert, C.D., and Li, W. (2013). Top-down influences on visual processing. Nat. Rev. Neurosci. 14, 350–363.

Goble, A., and Hollins, M. (1993). Vibrotactile adaptation enhances amplitude discrimination. J. Acoust. Soc. Am. 93, 771–780.

Goodale, M.A., and Milner, A.D. (1992). Separate visual pathways for perception and action. Trends Neurosci 15, 20-25.

Gold JI, and Shadlen MN. (2001). Neural computations that underlie decisions about sensory stimuli. Trends in Cognitive Sciences 5: 10-16.

Gold JI, and Shadlen MN. (2007). The neural basis of decision making. Annu Rev Neurosci 30: 535- 574.

Greenberg, D.S., Houweling, A.R., and Kerr, J.N.D. (2008). Population imaging of ongoing neuronal activity in the visual cortex of awake rats. Nat. Neurosci. 11, 749–751.

Grinvald, A., and Hildesheim, R. (2004). VSDI: a new era in functional imaging of cortical dynamics. Nat. Rev. Neurosci. 5, 874–885.

Harris, K.D., and Thiele, A. (2011). Cortical state and attention. Nat. Rev. Neurosci. 12, 509–523.

Harvey, M.A., Bermejo, R., and Zeigler, H.P. (2001). Discriminative whisking in the head-fixed rat: optoelectronic monitoring during tactile detection and discrimination tasks. Somat Mot Res 18: 211–222.

Hasenstaub, A., Sachdev, R.N.S., and McCormick, D. a (2007). State changes rapidly modulate cortical neuronal responsiveness. J. Neurosci. 27, 9607–9622.

Haslinger, R., Ulbert, I., Moore, C.I., Brown, E.N., and Devor, a (2006). Analysis of LFP phase predicts sensory response of barrel cortex. J. Neurophysiol. 96, 1658–1663.

He, B. (2013). Spontaneous and Task-Evoked Brain Activity Negatively Interact. J. Neurosci. 33, 1–11.

Heiss, J.E., Katz, Y., Ganmor, E., and Lampl, I. (2008). Shift in the balance between excitation and inhibition during sensory adaptation of S1 neurons. J. Neurosci. 28, 13320–13330.

Hentschke, H., Haiss, F., and Schwarz, C. (2006). Central signals rapidly switch tactile processing in rat barrel cortex during whisker movements. Cereb. Cortex 16, 1142–1156.

Higley, M.J., and Contreras, D. (2006). Balanced excitation and inhibition determine spike timing during frequency adaptation. J. Neurosci. 26, 448–457.

Higley, M.J., and Contreras, D. (2007). Frequency adaptation modulates spatial integration of sensory responses in the rat whisker system. J. Neurophysiol. 97, 3819–3824.

Hirata, A., and Castro-Alamancos, M. A. (2010). Neocortex Network Activation and Deactivation States Controlled by the Thalamus. J. Neurophysiol. 103, 1147–1157.

Houweling, A.R., and Brecht, M. (2008). Behavioural report of single neuron stimulation in somatosensory cortex. Nature 451, 65–68.

Huber, D., Petreanu, L., Ghitani, N., Ranade, S., Hromádka, T., Mainen, Z., and Svoboda, K. (2008). Sparse optical microstimulation in barrel cortex drives learned behaviour in freely moving mice. Nature 451, 61–64.

Huk AC, and Shadlen MN. (2005). Neural activity in macaque parietal cortex reflects temporal integration of visual motion signals during perceptual decision making. The Journal of neuroscience 25: 10420.

Hutson, K.A., and Masterton, R.B. (1986). The sensory contribution of a single vibrissa's cortical barrel. J. Neurophysiol. 56, 1196–1223.

Jin, L., Han, Z., Platisa, J., Wooltorton, J.R. a, Cohen, L.B., and Pieribone, V. a (2012). Single action potentials and subthreshold electrical events imaged in neurons with a fluorescent protein voltage probe. Neuron 75, 779–785.

Katz, Y., Heiss, J.E., and Lampl, I. (2006). Cross-whisker adaptation of neurons in the rat barrel cortex. J. Neurosci. 26, 13363–13372.

Khatri, V., Hartings, J. a, and Simons, D.J. (2004). Adaptation in thalamic barreloid and cortical barrel neurons to periodic whisker deflections varying in frequency and velocity. J. Neurophysiol. 92, 3244–3254.

Khatri, V., Bruno, R.M., and Simons, D.J. (2009). Stimulus-specific and stimulus-nonspecific firing synchrony and its modulation by sensory adaptation in the whisker-to-barrel pathway. J. Neurophysiol. 101, 2328–2338.

Khayat, P.S., Niebergall, R., and Martinez-Trujillo, J.C. (2010). Frequency-dependent attentional modulation of local field potential signals in macaque area MT. J. Neurosci. 30, 7037–7048.

Kleinfeld, D., and Delaney, K.R. (1996). Distributed representation of vibrissa movement in the upper layers of somatosensory cortex revealed with voltage-sensitive dyes. J. Comp. Neurol. 375, 89–108.

Kleinfeld, D., Ahissar, E., and Diamond, M.E. (2006). Active sensation: insights from the rodent vibrissa sensorimotor system. Curr. Opin. Neurobiol. 16, 435–444.

Klimesch, W. (1999). EEG alpha and theta oscillations reflect cognitive and memory performance: a review and analysis. Brain Res. Rev. 29, 169–195.

Kohn, A., and Whitsel, B.L. (2002). Sensory cortical dynamics. Behav. Brain Res. 135, 119–126.

Kohn, A., Zandvakili, A., and Smith, M. A. (2009). Correlations and brain states: from electrophysiology to functional imaging. Curr. Opin. Neurobiol. 19, 434–438.

Kopell, N., Ermentrout, G.B., Whittington, M.A., and Traub, R.D. (1999). Gamma rhythms and beta rhythms have different synchronization properties.

Krupa, D.J., Matell, M.S., Brisben, a J., Oliveira, L.M., and Nicolelis, M. a (2001). Behavioral properties of the trigeminal somatosensory system in rats performing whisker-dependent tactile discriminations. J. Neurosci. 21, 5752–5763.

Kyriazi, T., Simons, J., Kyriazi, H., and Simons, D. (1993). Thalamocortical Response Transformations in Simulated Whisker Barrels. J. Neurosci. 13.

LaMotte, R.H., and Mountcastle, V.B. (1979). Disorders in somesthesis following lesions of parietal lobe. J. Neurophysiol. 42, 400–419.

Lampl, I., Reichova, I., & Ferster, D. (1999). Synchronous membrane potential fluctuations in neurons of the cat visual cortex. Neuron, 22(2), 361-374.

Lee, D., Port, N.L., Kruse,W., and Georgopoulos, A.P. (1998). Variability and correlated noise in the discharge of neurons in motor and parietal areas of the primate cortex. J. Neurosci. 18, 1161–1170.

Lee, C.J., and Whitsel, B.L. (1992). Mechanisms underlying somatosensory cortical dynamics: I. In vivo studies. Cereb. Cortex 2, 81–106.

Leiser, S.C., and Moxon, K. a (2007). Responses of trigeminal ganglion neurons during natural whisking behaviors in the awake rat. Neuron 53, 117–133.

Lesica, N. a, and Stanley, G.B. (2004). Encoding of natural scene movies by tonic and burst spikes in the lateral geniculate nucleus. J. Neurosci. 24, 10731–10740.

Lesica, N. a, Weng, C., Jin, J., Yeh, C.-I., Alonso, J.-M., and Stanley, G.B. (2006). Dynamic encoding of natural luminance sequences by LGN bursts. PLoS Biol. 4, e209.

Lesica, N. a, Jin, J., Weng, C., Yeh, C.-I., Butts, D. a, Stanley, G.B., and Alonso, J.-M. (2007). Adaptation to stimulus contrast and correlations during natural visual stimulation. Neuron 55, 479–491.

Li, C.-Y.T., Poo, M.-M., and Dan, Y. (2009). Burst spiking of a single cortical neuron modifies global brain state. Science 324(5927), 643-646.

Lippert, M.T., Takagaki, K., Xu, W., Huang, X., and Wu, J.-Y. (2007). Methods for voltage-sensitive dye imaging of rat cortical activity with high signal-to-noise ratio. J. Neurophysiol. 98, 502–512.

Lottem, E., and Azouz, R. (2011). A unifying framework underlying mechanotransduction in the somatosensory system. J. Neurosci. 31, 8520–8532.

Luczak, A., Barthó, P., Marguet, S.L., Buzsáki, G., and Harris, K.D. (2007). Sequential structure of neocortical spontaneous activity in vivo. Proc. Natl. Acad. Sci. U. S. A. 104, 347–352.

Luczak, A., Bartho, P., and Harris, K.D. (2013). Gating of sensory input by spontaneous cortical activity. J. Neurosci. 33, 1684–1695.

Lustig, B. R., Friedman, R. M., Winberry, J. E., Ebner, F. F., & Roe, A. W. (2013). Voltage-sensitive dye imaging reveals shifting spatiotemporal spread of whisker-induced activity in rat barrel cortex. Journal of neurophysiology, 109(9), 2382-2392.

Macmillan, N., and Creelman, C. (2004). Detection theory: A user's guide (Psychology Press).

Maravall, M., Petersen, R.S., Fairhall, A.L., Arabzadeh, E., and Diamond, M.E. (2007). Shifts in coding properties and maintenance of information transmission during adaptation in barrel cortex. PLoS Biol. 5, e19.

Marple Jr, S. L. (1999). Computing the discrete-time "analytic" signal via FFT. Signal Processing, IEEE Transactions on, 47(9), 2600-2603.

Mazurek ME, Roitman JD, Ditterich J, and Shadlen MN. (2003). A role for neural integrators in perceptual decision making. Cerebral Cortex 13: 1257.

McCormick, D. A, McGinley, M.J., and Salkoff, D.B. (2015). Brain state dependent activity in the cortex and thalamus. Curr. Opin. Neurobiol. 31, 133–140.

Middleton, J. W., Omar, C., Doiron, B., & Simons, D. J. (2012). Neural correlation is stimulus modulated by feedforward inhibitory circuitry. The Journal of Neuroscience, 32(2), 506-518.

Millard, D. C., Wang, Q., Gollnick, C. A., & Stanley, G. B. (2013). System identification of the nonlinear dynamics in the thalamocortical circuit in response to patterned thalamic microstimulation in vivo. Journal of neural engineering, 10(6), 066011.

Moore, C.I. (2004). Frequency-dependent processing in the vibrissa sensory system. J. Neurophysiol. 91, 2390–2399.

Moore, C.I., Nelson, S.B., and Sur, M. (1999). Dynamics of neuronal processing in rat somatosensory cortex. Trends Neurosci. 22, 513–520.

Moruzzi, G., and Magoun, H.W. (1949). Brain stem reticular formation and activation of the EEG. Electroencephalogr. Clin. Neurophysiol. 1, 455–473.

Mountcastle, V. (1968). Neural mechanisms in somesthesia. In Medical Physiology Vol. II, pp. 1372–1423.

Nicolelis, M.A.L., and Fanselow, E.E. (2002). Thalamcortical optimization of tactile processing according to behavioral. 5, 517–524.

Niell, C.M., and Stryker, M.P. (2010). Modulation of visual responses by behavioral state in mouse visual cortex. Neuron 65, 472–479.

O'Connor, D.H., Clack, N.G., Huber, D., Komiyama, T., Myers, E.W., and Svoboda, K. (2010). Vibrissa-based object localization in head-fixed mice. J. Neurosci. 30, 1947–1967.

Okun, M., Naim, A., and Lampl, I. (2010). The subthreshold relation between cortical local field potential and neuronal firing unveiled by intracellular recordings in awake rats. J. Neurosci. 30, 4440–4448.

Ollerenshaw, D.R., Bari, B. a, Millard, D.C., Orr, L.E., Wang, Q., and Stanley, G.B. (2012). Detection of tactile inputs in the rat vibrissa pathway. J. Neurophysiol. 108, 479–490.

Ollerenshaw, D.R., Zheng, H.J.V., Millard, D.C., Wang, Q., and Stanley, G.B. (2014). The Adaptive Trade-Off between Detection and Discrimination in Cortical Representations and Behavior. Neuron 81, 1152–1164.

Otazu, G.H., Tai, L.-H., Yang, Y., and Zador, A.M. (2009). Engaging in an auditory task suppresses responses in auditory cortex. Nat. Neurosci. 12, 646–654.

Paxinos, G., and Watson, C. (2007). The rat brain in stereotaxic coordinates (San Diego, CA: Academic).

Petersen, C.C.H. (2007). The functional organization of the barrel cortex. Neuron 56, 339–355.

Petersen, C.C.H., Grinvald, A., and Sakmann, B. (2003a). Spatiotemporal dynamics of sensory responses in layer 2/3 of rat barrel cortex measured in vivo by voltage-sensitive dye imaging combined with whole-cell voltage recordings and neuron reconstructions. J. Neurosci. 23, 1298–1309.

Petersen, C.C.H., Hahn, T.T.G., Mehta, M., Grinvald, A., and Sakmann, B. (2003b). Interaction of sensory responses with spontaneous depolarization in layer 2/3 barrel cortex. Proc. Natl. Acad. Sci. U. S. A. 100, 13638–13643.

Petersen, R.S., Panzeri, S., and Diamond, M.E. (2001). Population coding of stimulus location in rat somatosensory cortex. Neuron 32, 503–514.

Pinto, D.J., Brumberg, J.C., and Simons, D.J. (2000). Circuit dynamics and coding strategies in rodent somatosensory cortex. Journal of Neurophysiology 83, 1158–1166.

Pouget, a, Deneve, S., Ducom, J.C., and Latham, P.E. (1999). Narrow versus wide tuning curves: What's best for a population code? Neural Comput. 11, 85–90.

Poulet, J.F. a, and Petersen, C.C.H. (2008). Internal brain state regulates membrane potential synchrony in barrel cortex of behaving mice. Nature 454, 881–885.

Poulet, J.F. a, Fernandez, L.M.J., Crochet, S., and Petersen, C.C.H. (2012). Thalamic control of cortical states. Nat. Neurosci. 15, 370–372.

Puig, M.V., Watakabe, A., Ushimaru, M., Yamamori, T., and Kawaguchi, Y. (2010). Serotonin modulates fast-spiking interneuron and synchronous activity in the rat prefrontal cortex through 5-HT1A and 5-HT2A receptors. J. Neurosci. 30, 2211–2222.

Ramirez, A., Pnevmatikakis, E. a, Merel, J., Paninski, L., Miller, K.D., and Bruno, R.M. (2014). Spatiotemporal receptive fields of barrel cortex revealed by reverse correlation of synaptic input. Nat. Neurosci. 17, 866–875.

Ritt, J.T., Andermann, M.L., and Moore, C.I. (2008). Embodied information processing: vibrissa mechanics and texture features shape micromotions in actively sensing rats. Neuron 57, 599–613.

Roitman JD, and Shadlen MN. (2002). Response of neurons in the lateral intraparietal area during a combined visual discrimination reaction time task. The Journal of neuroscience 22: 9475.

Romo, R., Hernández, A., Zainos, A., and Salinas, E. (1998). Somatosensory Discrimination based on cortical microstimulation. Lett. to Nat. 392, 387–390.

Romo, R., Hernández, A., Zainos, A., Brody, C.D., and Lemus, L. (2000). Sensing without touching: psychophysical performance based on cortical microstimulation. Neuron 26, 273–278.

Romo, R., Hernandez, A., Zainos, A., and Salinas, E. (2003). Correlated neuronal discharges that increase coding efficiency during perceptual discrimination. Neuron 38, 649–657.

Roy, S. a, and Alloway, K.D. (2001). Coincidence detection or temporal integration? What the neurons in somatosensory cortex are doing. J. Neurosci. 21, 2462–2473.

Sachdev, R.N.S., Ebner, F.F., Wilson, C.J., Robert, N.S., Ebner, F.F., and Wilson, C.J. (2004). Effect of Subthreshold Up and Down States on the Whisker-Evoked Response in Somatosensory Cortex. 3511–3521.

Sachidhanandam, S., Sreenivasan, V., Kyriakatos, A., Kremer, Y., and Petersen, C.C.H. (2013). Membrane potential correlates of sensory perception in mouse barrel cortex. Nat. Neurosci. 16, 1671–1677.

Schall JD, and Thompson KG. (1999). Neural selection and control of visually guided eye movements. Annual Review of Neuroscience 22: 241-259.

Schneidman, E., Berry, M.J., Segev, R., and Bialek, W. (2006). Weak pairwise correlations imply strongly correlated network states in a neural population. Nature 440:1007-1012.

Scholvinck, M.L., Saleem, a. B., Benucci, a., Harris, K.D., and Carandini, M. (2015). Cortical State Determines Global Variability and Correlations in Visual Cortex. J. Neurosci. 35, 170–178.

Sclar, G., Lennie, P., and DePriest, D. (1989). Contrast adaptation in striate cortex of macaque. Vision Res.

Semba, K., & Komisaruk, B. R. (1984). Neural substrates of two different rhythmical vibrissal movements in the rat. Neuroscience, 12(3), 761-774.

Sherman, S.M. (2001a). A wake-up call from the thalamus. Nat. Neurosci. 4, 344–346.

Sherman, S.M. (2001b). Tonic and burst firing: dual modes of thalamocortical relay. Trends in Neurosciences 24, 122–126.

Sheth, B., Moore, C.I., and Sur, M. (1998). Temporal modulation of spatial borders in rat barrel cortex. J. Neurophysiol. 464–470.

Shoham, D., Glaser, D. E., Arieli, A., Kenet, T., Wijnbergen, C., Toledo, Y., Hildesheim, R., and Grinvald, A. (1999). Imaging cortical dynamics at high spatial and temporal resolution with novel blue voltage-sensitive dyes. Neuron, 24(4), 791-802.

Simons, D.J. (1978). Response properties of vibrissa units in rat SI somatosensory neocortex. J. Neurophysiol. 41, 798–820.

Simons, D.J., and Carvell, G.E. (1989). Thalamocortical response transformation in the rat vibrissa/barrel system. J. Neurophysiol. 61, 311–330.

Simons, D.J., Carvell, G.E., Hershey, A.E., and Bryant, D.P. (1992). Responses of barrel cortex neurons in awake rats and effects of urethane anesthesia. Exp. Brain Res. 91, 259–272.

Simons, S.B., Tannan, V., Chiu, J., Favorov, O. V, Whitsel, B.L., and Tommerdahl, M. (2005). Amplitude-dependency of response of SI cortex to flutter stimulation. BMC Neurosci. 6, 43.

Smith PL, and Ratcliff R. Psychology and neurobiology of simple decisions (2004). TRENDS in Neurosciences 27: 161-168.

Stanley, G.B. (2013). Reading and writing the neural code. Nat. Publ. Gr. 16, 259–263.

Stanley, G.B., Jin, J., Wang, Y., Desbordes, G., Wang, Q., Black, M.J., and Alonso, J.-M. (2012). Visual orientation and directional selectivity through thalamic synchrony. J. Neurosci. 32, 9073–9088.

Steriade, M. (2001). Impact of Network Activities on Neuronal Properties in Corticothalamic Systems.

Steriade, McCormick, and Sejnowski (1993). Thalamocortical Oscillations in the Sleeping and Aroused Brain.

Steriade, M., Par, D., and Oakson, G. (1990). Neuronal Activities in Brain-Stem Cholinergic Nuclei Related Activation Processes in Thalamocortical Systems to Tonic. 2541–2559.

Stüttgen, M.C., Rüter, J., and Schwarz, C. (2006). Two psychophysical channels of whisker deflection in rats align with two neuronal classes of primary afferents. J. Neurosci. 26, 7933–7941.

Stüttgen, M.C., and Schwarz, C. (2008). Psychophysical and neurometric detection performance under stimulus uncertainty. Nat. Neurosci. 11, 1091–1099.

Stüttgen MC, and Schwarz C. (2010). Integration of vibrotactile signals for whisker-related perception in rats is governed by short time constants: comparison of neurometric and psychometric detection performance. The Journal of neuroscience 30: 2060.

Swadlow, H. A, and Gusev, a G. (2001). The impact of "bursting" thalamic impulses at a neocortical synapse. Nat. Neurosci. 4, 402–408.

Tannan, V., Whitsel, B.L., and Tommerdahl, M.A. (2006). Vibrotactile adaptation enhances spatial localization. Brain Res. 1102, 109–116.

Temereanca, S., Brown, E.N., and Simons, D.J. (2008). Rapid changes in thalamic firing synchrony during repetitive whisker stimulation. J. Neurosci. 28, 11153–11164.

Tommerdahl, M., Favorov, O., and Whitsel, B.L. (2002). Optical imaging of intrinsic signals in somatosensory cortex. Behav. Brain Res. 135, 83–91.

Usrey, W.M., Alonso, J.M., and Reid, R.C. (2000). Synaptic interactions between thalamic inputs to simple cells in cat visual cortex. J. Neurosci. 20, 5461–5467.

Le Van Quyen, M., Foucher, J., Lachaux, J.-P., Rodriguez, E., Lutz, A., Martinerie, J., and Varela, F.J. (2001). Comparison of Hilbert transform and wavelet methods for the analysis of neuronal synchrony. J. Neurosci. Methods 111, 83–98.

Vierck, C.J., and Jones, M.B. (1970). Influences of low and high frequency oscillation upon spatio-tactile resolution. Physiol. Behav. 5, 1431–1435.

Von Békésy, G. (1967). Sensory inhibition. (Princeton University Press).

Von Heimendahl, M., Itskov, P.M., Arabzadeh, E., and Diamond, M.E. (2007). Neuronal activity in rat barrel cortex underlying texture discrimination. PLoS Biol. 5, e305.

Wang, Q., Webber, R.M., and Stanley, G.B. (2010). Thalamic synchrony and the adaptive gating of information flow to cortex. Nat. Neurosci. 13, 1534–1541.

Wang, Q., Millard, D.C., Zheng, H.J. V, and Stanley, G.B. (2012). Voltage-sensitive dye imaging reveals improved topographic activation of cortex in response to manipulation of thalamic microstimulation parameters. J. Neural Eng. 9, 059601.

Wark, B., Lundstrom, B.N., and Fairhall, A. (2007). Sensory adaptation. Curr. Opin. Neurobiol. 17, 423–429.

Warren, D.J., Fernandez, E., and Normann, R. a. (2001). High-resolution two-dimensional spatial mapping of cat striate cortex using a 100-microelectrode array. Neuroscience 105, 19–31.

Webber, R. M., and Stanley, G. B. (2004). Nonlinear encoding of tactile patterns in the barrel cortex. Journal of neurophysiology, 91(5), 2010-2022.

Webber, R.M., and Stanley, G.B. (2006). Transient and steady-state dynamics of cortical adaptation. J. Neurophysiol. 95, 2923–2932.

Williams, J., Comisarow, J., Day, J., Fibiger, C., and Reiner, P. (1994). State-Dependent Release of Acetylcholine Measured by in viva Microdialysis in Rat Thalamus. J. Neurosci. 14, 5236–5242.

Wolfe, J., Hill, D.N., Pahlavan, S., Drew, P.J., Kleinfeld, D., and Feldman, D.E. (2008). Texture coding in the rat whisker system: slip-stick versus differential resonance. PLoS Biol. 6, e215.

Zagha, E., and McCormick, D. a (2014). Neural control of brain state. Curr. Opin. Neurobiol. 29, 178–186.

Zagha, E., Casale, A.E., Sachdev, R.N.S., McGinley, M.J., and McCormick, D. A. (2013). Motor cortex feedback influences sensory processing by modulating network state. Neuron 79, 567–578.

Zohary, E., Shadlen, M.N. and Newsome, W.T. Correlated neuronal discharge rate and its implications for psychophysical performance. Nature 370, 140–143, 1994.